DEVELOPMENT OF FRAGILITY CURVES FOR SEISMIC VULNERABILITY ASSESSMENT OF HIGH-RISE R/C BUILDINGS WITH ADDED VISCOUS DAMPERS

by

Esra Mete Güneyisi

B.S. in Civil Engineering, Boğaziçi University, 2000

M.S. in Civil Engineering, Boğaziçi University, 2002

Submitted to the Institute for Graduate Studies in
Science and Engineering in partial fulfillment of
the requirements for the degree of
Doctor of Philosophy

Graduate Program in Civil Engineering

Boğaziçi University

2007

To

Our Little Baby

ACKNOWLEDGEMENTS

I would like to express my most sincere gratitude to my thesis supervisor Prof. Dr. Gülay Altay for her invaluable guidance, gracious support, motivation and for the influence she has had on my professional growth. Her breadth of experience, professionalism and integrity as a researcher will always be a source of inspiration for me.

My sincere gratitude is also due to my thesis examining committee, Prof. Dr. M. Cengiz Dökmeci, Asst. Prof. Dr. Kutay Orakçal, Prof. Dr. Turan Özturan and Prof. Dr. Nesrin Yardımcı for their time, comments and useful suggestions.

The support provided by the European Union as a part of the sixth framework project namely; "Earthquake Protection of Historical Buildings by Reversible Mixed Technologies"; (PROHITECH) under Contract No. INCO-CT-2004-509119 is also gratefully appreciated. I also deeply appreciates for the financial support of TUBITAK (The Scientific and Technical Research Council of Turkey)-BAYG.

I am also thankful to Prof. Dr. Ellena Dumova-Jovanoska, St.Cyril and Methodius University-Skopje, Faculty of Civil Engineering, for her help and suggestions regarding the use of IDARC structural analysis program.

I would also like to thank my friends Bilge Alıcıoğlu, Cenk Güngör, Yavuz Tokmak for their helpful supports and friendship.

I am grateful to my parents and sister for all their generous love and support during these years. Thanks for always being there for me.

Finally, I would like to thank my dearest Erhan without whose continued encouragement and support the completion of this research would not have been possible.

ABSTRACT

DEVELOPMENT OF FRAGILITY CURVES FOR SEISMIC VULNERABILITY ASSESSMENT OF HIGH-RISE R/C BUILDINGS WITH ADDED VISCOUS DAMPERS

The fragility curves are used to represent the probabilities that the structural damages, under various level of seismic excitation, exceed specified damage states by means of earthquake intensity-damage relations. This, in turn, can be utilized for prioritizing retrofit, pre-earthquake planning, and loss estimation tools such as cost-benefit analysis. Therefore, the fragility analysis is also particularly useful in regions of moderate and high seismicity, such as İstanbul. In this study, a twelve storey non-ductile R/C office building, which represents the typical properties of the high rise office buildings located in Mecidiyeköy region, was selected and fragility curves were developed for the economic loss estimation as well as a basis for assigning retrofit prioritization for the R/C office buildings in Mecidiyeköy region. For the purpose of seismic retrofitting, external passive fluid viscous damper systems were designed to provide the structure with different effective damping ratios (ζ) of 10, 15 and 20 per cent; and the improvement of the system reliability achieved through the use of the dampers was assessed through fragility, risk and cost-benefit analysis. In order to be able to compare the innovative technique applied with the conventional retrofitting techniques, the building was also retrofitted by shear walls. In the fragility analysis, a set of 240 artificially generated earthquake ground motions compatible with the design spectrum selected to represent the variability in ground motion were developed to study nonlinear dynamic responses of the structures before and after retrofit. Fragility curves represented by lognormal distribution functions were constructed as a function of peak ground acceleration, spectral acceleration and displacement. By combining fragility analysis results with the seismic hazard risk of the region, the effectiveness of viscous damper systems and shear walls in the retrofit of the high rise R/C building is further investigated based on economic point of view by performing seismic risk analysis and cost-benefit analysis.

ÖZET

VİSKOZ SÖNDÜRÜCÜ SİSTEMLERLE GÜÇLENDİRİLMİŞ YÜKSEK KATLI BETONARME BİNALARIN DEPREM HASSASİYETİNİN HASAR OLASILIK EĞRİLERİ OLUŞTURULARAK DEĞERLENDİRİLMESİ

Hasar olasılık eğrileri, değişik deprem ivmeleri altında oluşabilecek yapısal hasar olasılıkların deprem şiddeti-hasar ilişkisi olarak belirlenmesinde kullanılmaktadır. Hasar olasılık eğrileri, gerçekte, öncelikli güçlendirmenin belirlenmesi, deprem öncesi planlama yapılması, maliyet-yarar analizi gibi deprem öncesi planlama sırasında kayıp ve zarar tahmininde yararlanılmaktadır. Olasılık analizinin uygulanması, özellikle yönetimlerin deprem öncesi planlama ve güçlendirme çalışmaları yaptıkları İstanbul gibi orta ve yüksek derece deprem bölgelerinde yararlı olmaktadır. Bu çalışmada, Mecidiyeköyde bulunan ofis binalarının tipik özelliklerini taşıyan on iki katlı sünek olmayan betonarme ofis binası seçildi ve hasar olasılık eğrileri bu bina göz önüne alınarak oluşturuldu. Mevcut binanın güçlendirilmesinde, pasif viskoz söndürücü sistemler binanın etkili sönümleme oranı (ζ) yüzde 10, 15 ve 20 olacak şekilde tasarımı yapıldı ve pasif viskoz söndürücü sistem kullanımının binanın güvenirliğinde sağladığı iyileşme, öncelikle hasar olasılık eğrileri oluşturularak, daha sonra da risk ve maliyet-yarar analizi yapılarak değerlendirildi. Kullanılan yeni güçlendirme tekniğinin, geleneksel güçlendirme teknikleriyle karşılaştırılabilmesi için bina ayrıca betonarme perdelerle de güçlendirildi. Hasar olasılık analizinde, deprem hareketlerindeki değişkenliği gösterebilecek tasarım spektrumu ile uyumlu üretilen 240 yapay deprem ivmesi, binanın güçlendirme öncesi ve sonrası non-lineer dinamik davranışının belirlenmesinde kullanıldı. Log-normal dağılıma sahip olasılık eğrileri maksimum yer ivmesi, spektral ivme ve yer değiştirmeye bağlı olarak oluşturuldu. Sonuç olarak, olasılık analiz sonuçları bölge için belirlenmiş olan hasar riski ile birleştirilerek, viskoz söndürücü sistemlerin ve perde duvar eklenmesinin etkisi, yapısal performansın değerlendirilmesine ek olarak ekonomik açıdan da mevcut ve güçlendirilmiş binalar için deprem riski ve maliyet–yarar analizleri yapılarak incelendi.

TABLE OF CONTENTS

LIST OF FIGURES

LIST OF TABLES

LIST OF SYMBOLS/ABBREVIATIONS

a	One of function parameter
$A(t)$	Envelope function
A_0	Amplitude of first cosine wave in the simulation formula
A_n	Amplitude of the *n*-th cosine wave in the simulation formula
b	One of function parameter
c	Decay parameter for envelope function
C	Damping coefficient of the damper
c_{corr}	Correction coefficient
C_{cr}	Critical damping coefficient,
C_z	Direct cost of retrofitting case *z*
[C]	Viscous matrix of the structure
CD^{con}	Building content losses
CD^{eco}	Loss of proprietors' income and rental costs
CD^{fat}	Cost of human fatality
CD^{rel}	Relocation expenses
CD^{rep}	Building repair and replacement cost
CD_k	Cost in present dollar value of k^{th} damage limit state
CD_k^{con}	Building content losses for the k^{th} damage state
CD_k^{eco}	Loss of proprietors' income and rental costs for the k^{th} damage state
CD_k^{fat}	Cost of human fatality for the k^{th} damage state
CD_k^{rel}	Relocation expenses for the k^{th} damage state
CD_k^{rep}	Building repair and replacement cost for the k^{th} damage state
CF_1	Coefficient for actions determined at the stage of maximum drift
CF_2	Coefficient for actions determined at the stage of maximum velocity
d	Discount rate
EDB_z	Expected discount benefit for retrofitting case *z*

EDC_z	Expected discount cost for retrofitting case *z*
$f(n)$	Natural vibration frequency
$f(PGA)$	Probability density function of PGA
$f(t)$	Acceleration time history
$f_0(t)$	Function obtained from stationary stochastic process with zero mean
F_D	Damper force
F_i	Story shear of ith floor
F_i^{old}	Force at floor "i" in the previous loading step
$f^{(i)}(t)$	Sample function of the simulated stochastic process
ΔF_i	The increment in the force distribution
$\{\Delta F\}$	Vector with the increment in lateral forces
$\{\Delta F_{err}\}$	Vector with the unbalanced forces
K	Stiffness
$[K]$	Stiffness matrix,
$[K_t]$	Tangent structural stiffness
$\{L_h\}$	Allocation vectors for the horizontal ground accelerations
m	Mass
m_i	Mass of storey i
$[m]$	Lumped mass matrix
[M]	Lumped mass matrix of the structure
n	Index of cosines in the simulation formula
N	Total number of cosines in the simulation formula
P	Force response of the damper system
P_0	Amplitude of the force response of the damper
p_f	Probability of meeting or exceeding a specific damage state
$P(\geq D)$	Annual probability of exceedance of damage state D
$P(\geq D \mid PGA)$	Probability of exceedance of damage D conditional upon PGA

$P\left(D_k \middle\| PGA\right)$	Probability of only kth damage occurring for a PGA value
$P_{exc}\left(D,T\right)$	Exceedance probability based on time
$\left\{\Delta P_v\right\}$	Restoring forces from viscous dampers
R^2	Pearson correlation coefficient
$R\left(\tau\right)$	Autocorrelation function
$S_{capacity}$	Structural capacity
S_{demand}	Structural demand
$S\left(w\right)$	Two sided power spectral density function
$SRSA(w)$	Computed response spectrum
t	Time
T_0	Initial period
t_1	Rise times of the ground motion,
t_2	Decay times of the ground motion
T_n	Natural period of the SDOF system
T_A , T_B	Characteristic periods of the spectrum
Δt	Time step
$TRSA(w)$	Prescribed target response spectrum,
u	Displacement
u_0	Amplitude of the displacement
u_j	Relative displacement of damper j
$\dot{u}$	Velocity
$\dot{u}_0$	Velocity response spectrum,
$\ddot{u}_0$	Acceleration response spectrum
$u\left(t,T_n,\zeta\right)$	Displacement time histories
$\dot{u}\left(t,T_n,\zeta\right)$	Velocity time histories
$\ddot{u}\left(t,T_n,\zeta\right)$	Acceleration time histories of the SDOF system
$\left\{\Delta u\right\}$	Incremental vectors of displacement
$\left\{\Delta \dot{u}\right\}$	Incremental vectors of velocity

$\{\Delta \ddot{u}\}$	Incremental vectors of acceleration
V_b	Base shear of the structure
w	Excitation frequency
w_0	Nature frequency
W_D	The energy dissipated by the damper
W_i	Weight of the i^{th} storey
W_j	Energy dissipated by the j^{th} damper of the system
W_k	Elastic strain energy of the frame
W_s	Elastic strain energy of the SDOF system
w_u	Upper cut-off frequency
X	Lognormal distributed ground motion index
$\Delta \ddot{x}_{gh}$	Increment in the horizontal ground accelerations
z	Retrofitting case number
α	Damper exponential for linear and nonlinear damper behavior
β	Standard deviation
γ	A parameter of the Newmark method
δ	Phase angle
Δ_i	Story drift of the i^{th} floor
ε	Mean
ζ	Damping ratio
ζ_0	Inherent damping ratio
ζ_d	Damping ratio contributed by the damper
ζ_{eff}	Effective damping ratio
θ_j	Inclined angle of damper j
κ	A parameter of the Newmark method
$\lambda(PGA)$	Mean annual rate of occurrence of PGA
μ	Median value of ground motion index

$\sum$	Sum
ϕ_i	First mode displacement at floor i
ϕ_{rj}	Relative horizontal displacement of damper j
$\phi_1,\ \phi_2,.....\phi_{N-1}$	Independent random phase angles in the interval [0,2π]
$\phi_0^i,\ \phi_1^i,.....\phi_{N-1}^i$	Phase angles at the i^{th} realizations
Φ	Standard normal cumulative distribution function,
Φ_{i1}	Value of the first mode shape at story i
$\Phi(\geq D \mid PGA)$	Standard normal cumulative distribution function of damage state D
$[\Phi_1]$	First mode shape of the system

1D	One dimensional
2D	Two dimensional
BCR	Benefit cost ratio
CBA	Cost Benefit Analysis
EDB	Expected discounted benefits
EDC	Expected discounted costs
MPa	Megapascal
PFVD	Passive fluid viscous damper
PGA	Peak ground acceleration
R/C	Reinforced concrete
S_a	Spectral acceleration
S_d	Spectral displacement
SDOF	Single degree of freedom
US	United States
USA	United States of America

1. INTRODUCTION

The need to predict the seismic vulnerability of existing buildings has led to increased interest on research dealing with the development of seismic vulnerability assessment techniques. A number of procedures have been proposed in the literature, which can generally be classified into two categories.

First category that consists the simplest and quickest ways, called walk-down survey or street survey, requires only superficial data collected from a brief inspection of the building. The number of stories, vertical and plan irregularities, location of the building, age of the building, its structural system and apparent material and workmanship quality are typical parameters that are used. FEMA 154 (1988), FEMA 310 (1998) and Japanese system of assessment fall into this category. The purpose of rapid evaluation techniques is to identify or rank highly vulnerable buildings that deserve further investigation.

The in-depth evaluation of the buildings through sophisticated structural analyses or investigation falls into the second category of vulnerability assessment. The comprehensive information on the geometrical properties of the components, mechanical properties of the materials, and detailing of the components are obtained from the structural drawings and as-built features of the building. The vulnerability of a certain structure or a whole category of structures is defined in the form of earthquake intensity-damage relationship. These relationships yield the probability distribution of the occurrence of damage for a given earthquake intensity and are most frequently presented in the form of damage probability matrices (damage indices) and fragility curves.

1.1. Performance Evaluation through Fragility (Vulnerability) Analysis

In performing a seismic risk analysis of a structural system, it is imperative to identify seismic vulnerability of component structures associated with various states of damage. The development of vulnerability information in the form of fragility curves is a widely practiced approach when the information is to be developed accounting for a multitude of uncertain sources involved, for example, in estimation of seismic hazard,

structural characteristics, soil-structure interaction. Vulnerability (Fragility) curves relate the probability of exceedance of multiple damage states to a parameter of ground motion severity and can therefore be regarded as a graphical representation of seismic risk. Existing vulnerability curves can be classified into the four generic groups of empirical, judgmental, analytical and hybrid according to whether the damage data used in their generation derives mainly from observed post earthquake surveys, expert opinion, analytical simulations, or combinations of these, respectively. Each data source has associated advantages and disadvantages.

1.1.1. Empirical Fragility Curves

In the last decade several important accelerograms have been recorded during different earthquakes and observed structural and non-structural damage has been well documented. This information gives a unique opportunity to explore the possibility of finding a reliable parameter for measuring seismic damage. Such a parameter should consider not only typical characteristics of earthquake ground motions but also characteristics representative of structures. Empirical curves use the building damage distributions reported in post-earthquake surveys as their statistical basis. The observational source is the most realistic as all practical details of the exposed stock are taken into consideration alongside soil–structure interaction effects, topography, site, path and source characteristics. However, the same aspects that render observational data the most realistic are responsible for the severe limitation in their application potential. The empirical ground motion–damage relationships developed for European countries are typically based on very few damage surveys carried out for single locations or earthquake events (Orsini, 1999). No distinction between buildings of different materials, heights or seismic design provisions is commonly made. Consequently the curves are highly specific to a particular seismo-tectonic, geotechnical and built-environment. A wider scope of application is possible if the performance of different structural systems is considered and if a large quantity of reliable empirical data, covering a wide range of ground motions is used for the curve derivation. In practice, this is only achievable through the combination of data from different earthquakes and locations. However, due to the infrequency of large magnitude earthquake events near densely populated areas, the observational data used for the curve generation tend to be scarce and highly clustered in the low-damage, low ground-

motion severity range. This leads to large uncertainties being associated with their use in large magnitude events. To allow an accurate determination of the ground motion and for the reported damage distribution to be representative of the variation in seismic resistance of the buildings, empirical vulnerability curves should use post-earthquake surveys carried out for large populations of buildings of similar construction, over areas of uniform soil conditions in close proximity to ground motion recording stations. Errors in building damage classification (especially for the lighter damage states) are introduced in the statistics at source due to the typically rapid execution of post earthquake surveys by engineers of varied experience and the use of poorly defined damage scales. Moreover, damage due to multiple earthquakes may be aggregated and attributed to a single event or buildings damaged as a consequence of phenomena other than ground shaking (e.g. ground subsidence, landslides, flooding and fire) included in the data. These errors cannot be removed via manipulation of the damage statistics and lead to a large data scatter even in cases where a single event and limited survey area are considered (Orsini, 1999). The low level of refinement in terms of both structure and damage classification that typifies post-earthquake survey statistics therefore poses a real hindrance to the combination of damage data for building populations of different composition.

In the study of Rossetto and Elnashai (2003), the empirical fragility curves for reinforced concrete building populations in Europe are derived based on a data bank of 99 post-earthquake damage distributions observed in 19 earthquakes and concerning a total of 340 000 reinforced concrete structures.

1.1.2. Judgmental Fragility Curves

Judgment-based curves are not associated with the same problems regarding the quantity and quality of building damage statistics that typify empirical relationships mentioned above. Expert panels of civil engineers with experience in the field of earthquake engineering are asked to make estimates of the probable damage distribution within building populations when subjected to earthquakes of different intensities. Probability distribution functions are fit to the expert predictions to represent the range of damage estimates at each intensity level. The probability of a specified damage state is derived from the resulting distributions and plotted against the corresponding ground-

motion level to obtain a set of vulnerability curves, and associated uncertainty bounds. Since the experts can be asked to provide damage estimates for any number of structural types, the curves can be easily made to include all the factors affecting the seismic response of different structures. Consequently expert opinion is the predominant source used by most current rehabilitation codes in the United States of America for the generation of damage probability matrices and vulnerability curves (ATC 13, 1985; ATC 40, 1996). The reliability of judgment-based curves is questionable, however, due to their dependence on the individual experience of the experts consulted. It is practically impossible to evaluate of the degree of conservatism associated with the judgment-based source, and inherent in the expert vulnerability predictions is a consideration of local structural types, typical configurations, detailing and materials.

1.1.3. Hybrid Fragility Curves

Hybrid vulnerability curves attempt to compensate for the scarcity of observational data, subjectivity of judgmental data and modeling deficiencies of analytical procedures by combining data from the different sources. Existing examples of hybrid curves typically involve the modification of analytical or judgment-based relationships with observational data. In most cases the data deriving from the additional sources are, however, very limited in quantity and scope. The curves proposed in ATC 13 (1985) and ATC 40 (1996), though based heavily on expert opinion, also incorporate limited observational data from the San Fernando earthquake (1971) and Northridge earthquake (1994), respectively. In some cases, these data are further supplemented with experimental test results. The latter source has gained importance in recent years as the testing of large and reasonably realistic structures has become more frequent. However, due to the cost and time required for full-scale testing and since small-scale testing is non-definitive on similitude grounds, a very limited number of parameters can be investigated and parametric variations are not possible. Experimental data are therefore currently only used for verification purposes, rather than as an additional source of building damage statistics. Singhal and Kiremidjian (1997) also adopt a Bayesian technique to update analytical curves for low-rise frames with observational damage data from a tagging survey of only 84 buildings affected by the Northridge earthquake. Observations taken from a single earthquake event will cover only

a small range of ground motions. Hence, it is concluded that the consideration of multiple data sources is necessary for the correct determination of vulnerability curve reliability.

1.1.4. Analytical Fragility Curves

Analytical vulnerability curves adopt damage distributions simulated from the analyses of structural models under increasing earthquake loads as their statistical basis. Analyses can result in a reduced bias and increased reliability of the vulnerability estimate for different structures compared to expert opinion. Despite this, few analytical vulnerability curves for reinforced concrete buildings have been generated in the past due to the substantial computational effort involved and limitations in modeling capabilities. Architectural finishes can not be accounted for, detailed modeling of infill walls remains a challenge, elaborate soil models cannot be accommodated alongside elaborate structural models and rocking and uplifting of structures poses serious numerical modeling difficulties. Many existing analysis environments also have difficulties converging when structures are subjected to large demands, and numerical collapse may precede structural failure. However, recent developments have lead to the inclusion of a number of response features, such as shear-flexure–axial interaction, soil–structure interaction, interactive confinement on concrete members and reinforcing bar buckling, into analytical methods. Furthermore, new analysis techniques and solution procedures have been established that enable the generation of damage data for large and complex structures at very high speeds. Hence analytical approaches to vulnerability curve generation are becoming ever more attractive in terms of the ease and efficiency by which data can be generated, but have not yet been fully exploited to the limits of their potential.

Most existing analytical vulnerability relationships have been derived for structures in America. A variety of analysis procedures have been followed, ranging from the elastic analysis of equivalent single degree of freedom systems (Mosalam *et al*., 1997), to non-linear time history analyses of 3D models of R/C structures (Singhal and Kiremidjian, 1997). The choices made for the analysis method, structural idealization, seismic hazard and damage models strongly influence the derived curves and have been seen to cause significant discrepancies in seismic risk assessments made by different authorities for the same location, structure type and seismicity (Priestley, 1998).

1.2. Problem Description

The vulnerability of reinforced concrete construction to earthquake ground motion was clearly apparent during the 1999 İzmit Earthquake and its aftermath, where the property losses reached 20 billion US$ and fatalities exceeded 18,000 (USGS, 2000). These failures highlight the impact of the deficiencies in current reinforced concrete (R/C) building practices aimed at mitigating risk from the earthquake hazards. Most of these buildings, date back to 1960s and 1970s, were built before the advent of the seismic codes according to the almost nominal seismic design regulations of that time with forces equal to small ratio of the weight and with non-ductile detailing. In the recent studies, the probability of being subjected to a strong ground shaking in Istanbul during the first thirty years of the century is estimated as 47-77 per cent (Hubert-Ferrari *et al*., 2000; Parsons *et al*., 2000). The threat of a devastating earthquake in İstanbul has pointed out the urgent need to develop a comprehensive risk analysis and disaster management system for İstanbul (Aleskerov *et al.*, 2005). Therefore, it is obvious that there is a significant need to perform adequate seismic assessment of R/C buildings in Istanbul and to investigate possible retrofitting measures prior to future seismic events.

Conventional retrofitting measures used for seismic mitigation usually include the addition of existing walls or foundations and strengthening of frames. However, most of these techniques often led to inconvenient consequences such as heavy demolition, reconstruction and occupant relocation. Therefore, in recent years, in commercial buildings, instead of these environmentally hostile, intrusive approach associated with conventional techniques, the use of innovative retrofitting measures such as incorporation of passive energy dissipation systems is preferred (Soong and Dargush, 1997).

One of the most important elements in assessment of seismic damage in the buildings and evaluation the effects of retrofitting decisions is so called fragility curve. The fragility curves are recently used to represent the probabilities of structural damage due to earthquakes as a function of ground motion indices e.g. peak ground acceleration (PGA), spectral acceleration (S_a), or spectral displacement (S_d). While fragility curves for the structures in their retrofitted conditions are imperative, the development of these curves requires careful consideration for their reliable and responsible integration in a seismic risk

assessment. The characterization of the earthquake ground motion and the identification of the different degrees of structural damage have a vital role in developing seismic fragility curves for any structure.

Assessment of the probable seismic damage in the buildings and design of possible retrofitting measures are not alone sufficient, the decision to invest in retrofitting measures that can protect property and life against possible seismic damage is primarily an economic decision. In addition to the fragility analysis, it should therefore be taken in the framework of the cost-benefit analysis (CBA) to show if the benefits to life and property protected through retrofitting measures exceeds the cost of the measure.

In the literature, there are several studies regarding the seismic hazard assessment of the residential buildings located in İstanbul (Erdik and Aydınoğlu, 2002; Smyth *et al*., 2004; Kırçıl and Polat, 2006). Those studies generally deal with the seismic behavior of original buildings before and/or after retrofit by conventional strengthening techniques. However, an application of fragility analysis method to high rise R/C office building with innovative strengthening techniques such as additional viscous damping through a device placed as a brace have not been attempted in the literature. Moreover, the seismic fragility analysis is relatively new concept, especially for the evaluation of effectiveness of the retrofitting strategies. Among the retrofitting strategies, the application of the passive fluid viscous damper systems in retrofitting is one of the innovative techniques. Therefore, this study provides a comprehensive research on the seismic behavior of typical high rise office buildings in Mecidiyeköy region with the goal of evaluating the effectiveness of fluid viscous damper systems in seismic retrofitting through seismic fragility analysis, seismic risk analysis and cost-benefit analysis.

1.3. Objectives of Research

The aim of this study is to develop fragility curves for comparative seismic vulnerability analysis of existing R/C office buildings before and after retrofitting by innovative strengthening techniques such as additional viscous dampers. The approach was applied to an existing twelve-storey office building representative of buildings built in 1970s in İstanbul, designed according to the former version (1975) of the Turkish seismic

design code (ABYYHY, 1975). For retrofitting strategies, similar type of viscous dampers was used and designed according to FEMA 273 (1997) and FEMA 274 (1997) to provide the structure with three different effective damping ratios (ζ) of 10, 15, and 20 per cent. In order to be able to compare effectiveness of the innovative technique with conventional one, the building was also retrofitted by using shear walls.

For this purpose, because of the limited number of real time histories for İstanbul region, firstly, a set of 240 artificially generated earthquake accelerations compatible with the design spectrum selected to represent the variability in ground motion was developed using MATLAB program. Secondly, structures under consideration were represented by analytical models, which include the nonlinear behavior of the appropriate components. Thirdly, the response of the existing and retrofitted structures under different earthquake excitations was defined performing nonlinear time history analysis. For the needs of this investigation, a nonlinear structural analysis program, IDARC-2D Version 6.1, was utilized. This choice was made because this program is mainly intended for analysis of damage due to dynamic loads. Keeping in mind that most of the seismic loading parameters are characterized by a single numerical value such as in this case PGA, S_a and S_d, single-value indicators have also been selected to represent the structural damage. For this, fourthly, type of damage response convenient for the structural type was selected and threshold damage limits were determined. Then, using a probabilistic seismic demand model obtained by regression analysis on the simulated damage data, the individual fragility curves for each damage state and for each building were developed. Finally, in addition to fragility analysis, by using risk analysis and CBA approaches, the developed fragility curves were combined with information about the probability of earthquake occurrence in space and time, to compare the benefits obtained in terms of avoided damage or collapse with the cost of the retrofitting measures.

It has been expected that the research provides an insight into the seismic reliability of high-rise R/C buildings retrofitted by innovative strengthening techniques such as additional viscous dampers. The results obtained from seismic fragility analysis are also expected to provide some useful information for seismic risk and loss assessment of such buildings before and after retrofit, and intend a new contribution to the current information in the literature.

1.4. Outline of the Thesis

Chapter 2 provides a description of the representative building selected as a case study. As retrofitting measures, passive viscous fluid damper systems were selected. The viscous damper systems were designed differently in order to provide the structure different effective damping ratios. The building was also retrofitted by using shear walls in order to be able to see the effectiveness of passive viscous damper systems in comparison to conventional techniques commonly used. Therefore, in this chapter, the details on modeling of the original structure and damper systems are provided and also the reasoning behind the selection of these systems and the basic design philosophy are presented.

In the development of fragility curves, artificially generated acceleration records are required. For this, in Chapter 3, the generation of artificial earthquake accelerations based on Spectral Representation Based Simulation methodology is defined and explained. Within the scope of this thesis, a total of 240 synthetic seismic ground motion time histories were generated between 0 and 1 PGA by using MATLAB program.

In Chapter 4, the seismic assessment of the vulnerability of the reinforced concrete buildings, and the retrofitted buildings with passive viscous damper systems and shear walls through fragility analysis are presented. The details for the selection of seismic damage response parameters, the determination of damage limit states, and the development of seismic fragility curves in terms of PGA, S_a and S_d (as demand measures) are given. Discussion of the results based on reliability analysis is also represented.

Since the decision to invest in retrofitting measures that can protect property and life against possible seismic damage is primarily an economic decision, in Chapter 5 the seismic risk analyses of the existing and the retrofitted buildings are determined and the retrofitting measures applied are further investigated through cost-benefit analysis.

Finally, in Chapter 6 the summary and conclusion based on results of this study is presented. Moreover, the description of the future research is given in Chapter 7.

2. CASE STUDY: SELECTION OF REPRESENTATIVE STRUCTURE & APPLICATION OF PFVD SYSTEMS FOR RETROFITTING

In this study, the high rise office buildings, which were built in 1970s, have been considered. For this purpose, an office building representing the typical properties of the buildings in Mecidiyeköy region was selected.

Seismic retrofit of existing structures is one method to reduce the risk to vulnerable structures. Recently, a significant amount of research has been devoted to the study of various retrofit techniques to enhance the seismic performance of R/C structures (Pincheira and Jirsa, 1995; Elnashai and Pinho, 1998; Bruno and Valente, 2002; Perera *et al*., 2004; Güneyisi and Altay, 2005). However, conventional retrofitting measures usually include the addition of existing walls or foundations and strengthening of frames which often led to inconvenient consequences such as heavy demolition, reconstruction and occupant relocation. Since for this kind of commercial buildings, the use of innovative techniques such as incorporation of passive viscous damper systems are more convenient; the seismic performance of the existing structure was improved by application of passive fluid viscous damper (PFVD) systems. In order to compare the effectiveness of PFVD systems with a well known retrofitting measure the structure retrofitted by shear walls was also investigated.

2.1. Description of the Sample Building

An actual building located in Mecidiyeköy region, a suburb of Istanbul, was selected as a sample office building, since it is deemed to be highly representative of the many office buildings in and around Istanbul. The building, which is shown in Figure 2.1, is a typical R/C twelve-story building founded on Z2-type soil (relatively stiff soil) according to the description in the current Turkish seismic design code. It was designed according to the 1975 version of the Turkish seismic design code (ABYYHY, 1975) which prescribes much smaller seismic loads than the current code and lacks some important consideration

with respect to ductile detailing. Figure 2.2 shows the layout, elevation and plan of the building. The main structural system of the building consists of moment resisting R/C frames in two directions; there are shear walls only through the peripheral of the elevator. The typical floor area is 989 m^2 and the storey height is 2.75 m. The concrete of the structure has a characteristic yield limit of 16 MPa while the corresponding Young's Modulus is 27000 MPa. The characteristic yield strength of the reinforcement is 220 MPa. These values represent the common practice in the late 1970s for this kind of office buildings.

Figure 2.1. Photograph of the existing high-rise office building

2.2. Seismic Performance of the Building According to Current Turkish Seismic Code

The existing building was modeled by using ETABS Nonlinear Version 7.20 Structural Analysis Program in order to investigate the seismic performance according to current Turkish Seismic Code. The load patterns were determined according to TS 498 (1997). The building was assumed to carry dead load of 6.1 kN/m^2 and live load of 2

kN/m^2 applied as uniform distributed load at each floor slab and distributed to the beams around the slab with slab tributary areas.

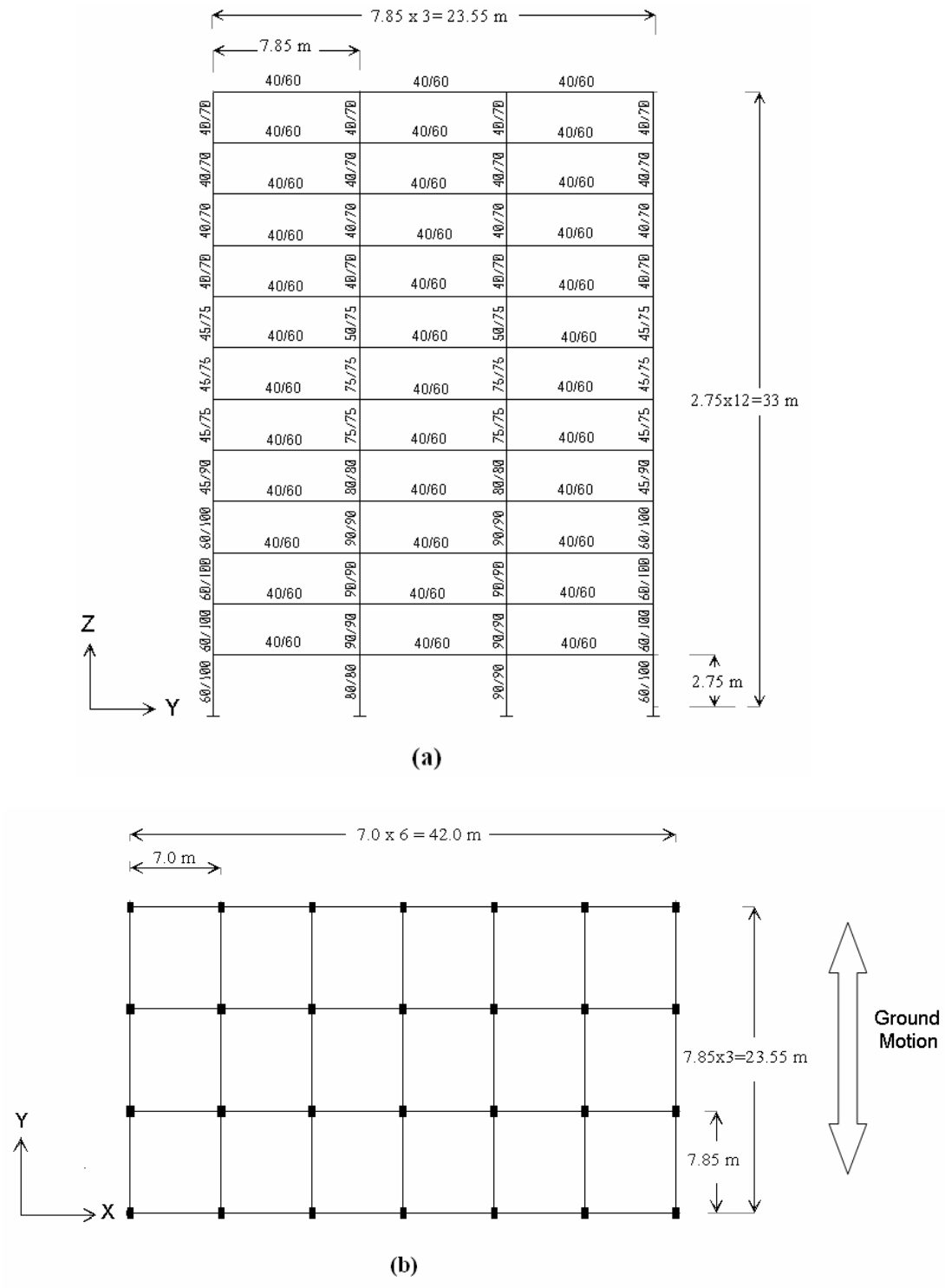

Figure 2.2. A layout for a) elevation, b) floor plan of the existing building

Mode superposition method defined in the Turkish Earthquake Code (ABYYHY, 1998) was used for seismic analysis. In this method, maximum internal forces and displacements are determined by the statistical combination of maximum contributions obtained from each of the sufficient number of natural vibration modes considered. The parameters required for seismic loads such as building importance factor, live load participation factor, effective ground acceleration coefficient, local site class, were taken as 1.0, 0.3, 0.4 and Z2, respectively. The elastic and inelastic design spectrum defined in Turkish Earthquake Code is given in Figure 2.3.

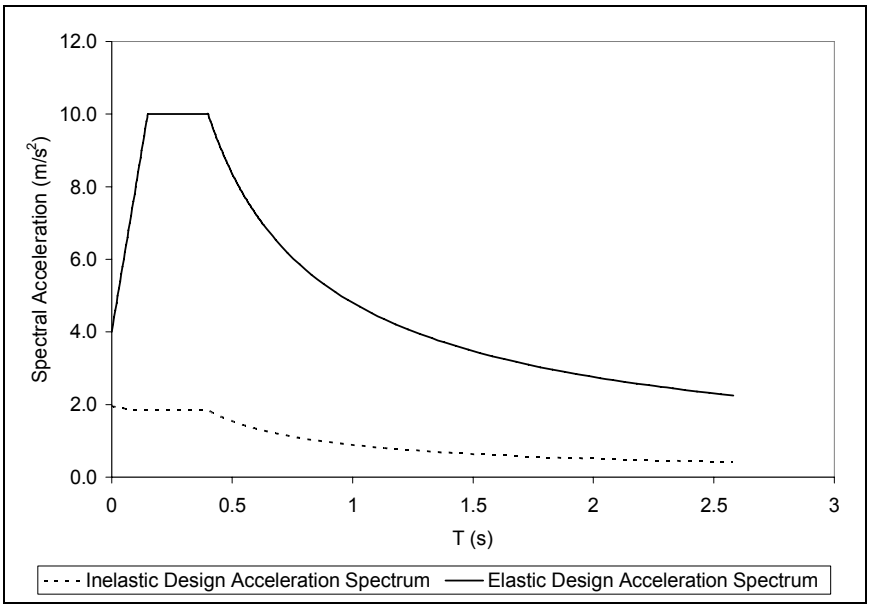

Figure 2.3. Elastic and inelastic design acceleration spectrum according to Turkish Earthquake Code

2.3. Analytical Models for Nonlinear Static and Time History Analysis

For nonlinear static and time history analysis, models able to represent the selected structural types and also the dampers in a sufficiently reliable way, both in terms of stiffness and resistance, have been implemented by using IDARC 6.1 structural analysis program. This choice was made because this program allows for direct input of section dimensions and reinforcement details, from which the program generates the moment-curvature relationships of every member. Within this program, there is a possibility to define several different parameters of damage. Another important feature of the program is

the ability to specify a variety of hysteretic behavior patterns using certain control parameters, to model stiffness deterioration, strength degradation, and pinching, slip or crack closing behavior. In the analytical models, frame structures with rigid or semi-rigid connections made of beams, columns, shear walls, connecting beams, and damping braces (fluid viscous) can be defined. Furthermore, the validity of the analytical models performed with IDARC has been demonstrated by a number of studies (Kunnath *et al*., 1992; Bracci *et al.*, 1992a; 1992b; 1992c; Li and Reinhorn, 1995; Reinhorn *et al.*, 1995), and this program was used in various studies in the literature for inelastic, nonlinear dynamic analysis of R/C structures (Dumova-Javonoska, 2000; Ghobarah *et al.*, 2000; Elenas and Meskouris, 2001; Kırçıl and Polat, 2006). The regularity of the representative building in terms of mass and stiffness in both plan and elevation enables a 2-D analysis to be used when assessing seismic response. The building is modeled as a 2-D planar frame with lumped masses and the hysteretic behavior of the beams and columns has been specified at both ends of each member using a three parameter Park model. This hysteretic model incorporates stiffness degradation, strength deterioration, non-symmetric response, slip-lock and a trilinear monotonic envelope as shown in Figure 2.4. The nominal values of the parameters (α, β, and γ, such as 12, 0.01 and 0.4) suggested by the authors for non-ductile buildings were used to consider the effect of stiffness degradation, strength deterioration and pinching (Reinhorn *et al*., 2006).

Nonlinear static and nonlinear time history analysis is carried out using the Newmark-β integration method with a sufficiently small time step to ensure accuracy of the results, and to avoid the problem of non-balanced forces transferred from one interval to another.

2.4. Nonlinear Static (Pushover) Analysis of the Existing Building

Building structures are often designed using results from elastic analysis, although inelastic behavior is observed well during the design earthquake. To estimate the actual response of the structure when some of the elements behave in the inelastic range, inelastic nonlinear structural analysis is required. Therefore, in order to further investigate the seismic response of the building pushover analysis was conducted.

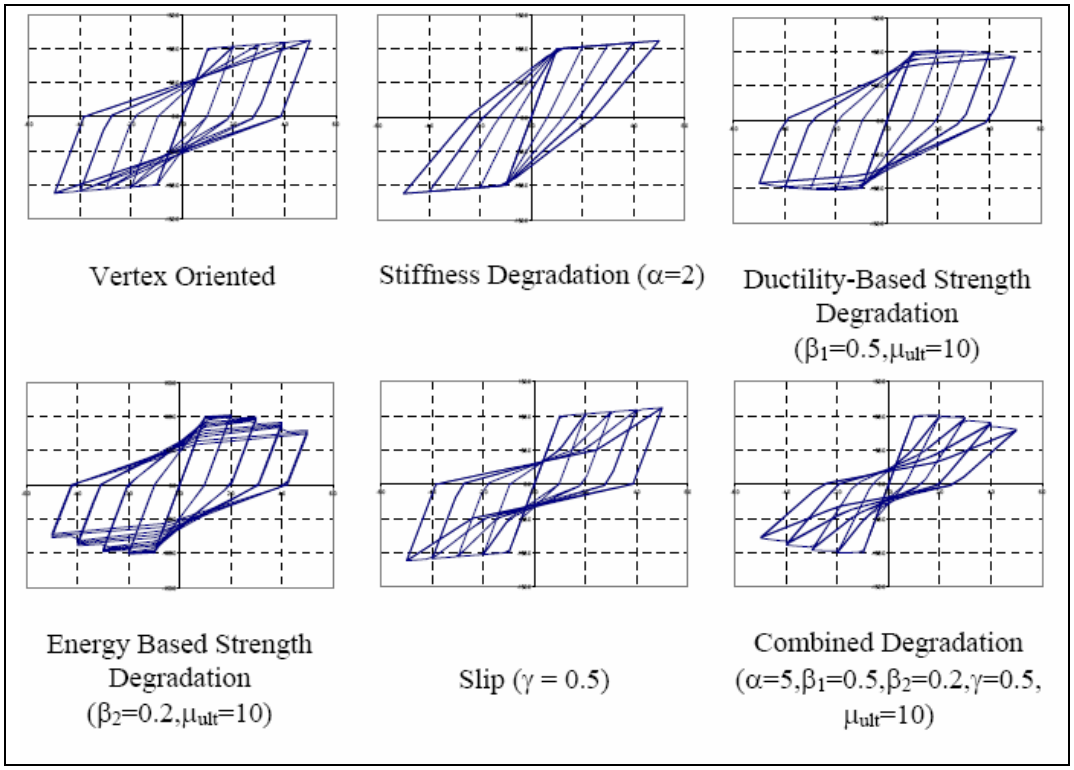

Figure 2.4. Hysteretic models that can be defined in the IDARC Structural Analysis Program

Pushover analysis is a static, nonlinear procedure in which the magnitude of the structural loading is incrementally increased in accordance with a certain predefined pattern until failure criteria is reached. With the increase in the magnitude of the loading weak links and the failure modes of the structure are found. The nonlinear pushover analysis, or collapse mode analysis, is a simple and efficient technique to predict the seismic response of structures prior to a full dynamic analysis. Strength and deformation capacity of the components (columns and beams) of the structures play the main role in determination of the overall capacity of the structure.

A pushover analysis can establish the sequence of component yielding, the potential ductility capacity, and the adequacy of the building lateral strength. The pushover analysis performs an incremental analysis of the structure subjected to a distribution of lateral forces. The system of equations solved during the analysis procedure is:

$$[K_t]\{\Delta u\} = \{\Delta F\} + c_{corr}\{\Delta F_{err}\} \tag{2.1}$$

where $[K_t]$ is the tangent structural stiffness; $\{\Delta u\}$ is the vector with the increment of lateral displacements; $\{\Delta F\}$ is the vector with the increment in lateral forces; c_{corr} is a correction coefficient (usually taken as one); and $\{\Delta F_{err}\}$ is the vector with the unbalanced forces in the structure (Valles *et al*., 1996).

The pushover analysis may be carried out using force control or displacement control. In this study, analysis were carried out as force controlled which means that the structure is subjected to an incremental distribution of lateral forces and the incremental displacement are calculated. Since the deformed profile is not known, and an estimate of the lateral distribution of forces can be made, therefore force control is commonly used in the literature. The maximum force distribution can be specified as uniform, inverted triangular, generalized power or modal adaptive distributions. From these, modal adaptive force distribution was selected in the pushover analysis.

The modal adaptive distribution differs significantly from other loading conditions in that the story force increments are not constant. A constant distribution throughout the incremental analysis will force the structure to respond in a certain form. Often the distribution of forces is selected considering force distributions during an elastic response; however, it is clear that when the structure enters the inelastic range, the elastic distribution of forces may not be applicable anymore. If the pushover forces are not modified to account for the new stiffness distribution, the structure is forced to respond in a way that may considerably differ in form what an earthquake may impose to the structure.

The modal adaptive distribution is developed to capture the changes in the distribution of lateral forces. Instead of a polynomial distribution, the mode-shapes of the structure are considered. Since the inelastic response of the structure will change the stiffness matrix, the mode shapes will also be affected, and a distribution proportional to the mode shapes will capture this change. If the fundamental mode is considered, the increment in the force distribution is calculated according to:

$$\Delta F_i = \frac{W_i \Phi_{i1}}{\sum_{i=1}^{N} W_i \Phi_{i1}} V_b - F_i^{old} \tag{2.2}$$

where Φ_{i1} is the value of the first mode shape at story "i", V_b is the new base shear of the structure, and F_i^{old} is the force at floor "i" in the previous loading step (Valles *et al*., 1996).

2.5. Evaluation of Results of Linear and Nonlinear Static Analysis

After the nonlinear static analysis of the existing building was performed through IDARC computer program in both x and y directions, the capacity curves related to base shear to weight ratio versus roof displacement to building height are obtained. Figure 2.5 illustrates the capacity curves of the existing building in x and y directions, respectively. As it is seen from the figure, the existing building has more stiffness and higher load carrying capacity in the x direction than in the y direction.

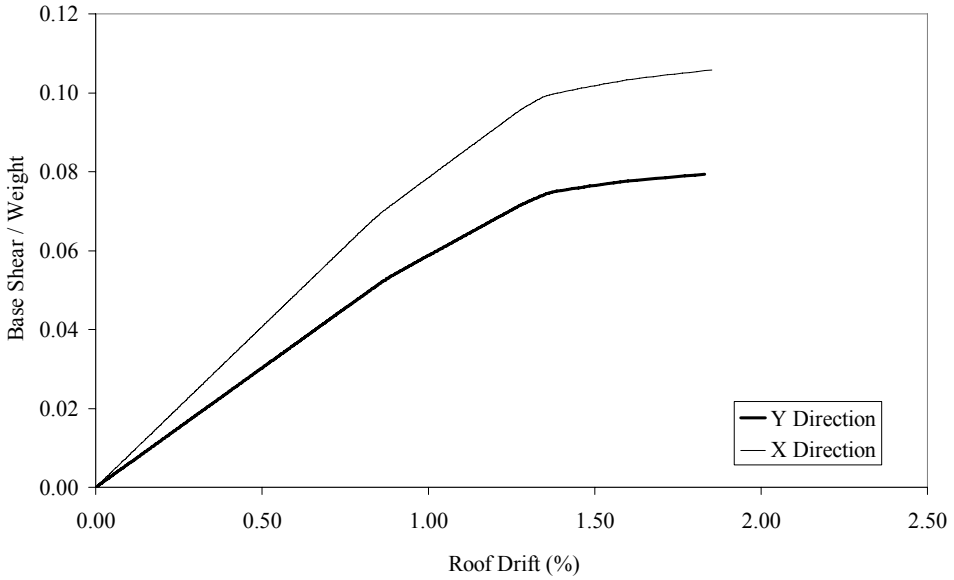

Figure 2.5. Capacity curve of the existing building in x and y direction

From the result of the nonlinear static analysis, it is observed that the weak axis of the structure is the y axis. In the further analysis for the construction of the fragility curves,

the direction of the earthquake is always assumed to be parallel to the weak axis of the structure, i.e., only the y-z plane frames were considered, as indicated in Figure 2.2. This is a worst-case scenario and the fragility analysis results should therefore be interpreted as an upper bound on the risk in that sense.

At the end of the linear analysis, the inter-storey drift ratios, column capacities under seismic loads, irregularities of the building such as torsional irregularity, inter-storey stiffness and strength irregularities were investigated. It is seen that the inter-storey drift ratios are less than or equal to the limit defined in the code as 3.5 per cent and there is only torsional irregularity, which is in the limit only to increase the eccentricities. However, the column demand capacity ratios under earthquake loading exceeds up to 4.3 times. From the results of the seismic performance evaluated according to the Turkish Earthquake Code, it is seen that the building does not meet minimum requirements up to the current building code and may suffer severe damage during a seismic event. Therefore, the existing building must be retrofitted in order to increase its seismic performance.

Two main rehabilitation approaches have been developed to upgrade the seismic performance of existing undamaged structures before being subjected to an earthquake. These are: a) as conventional approaches: adding new structural elements such as shear walls, or selective strengthening of deficient structural elements such as the use of concrete and steel jackets and fiber reinforced polymers; b) as innovative approaches, using base isolation or passive energy dissipation systems. The retrofitting of the building requires an appreciation for the technical, economic and social aspects of the issue in hand. Changes in construction technologies and innovation in retrofit technologies present added challenge in selecting a technically, economically and socially acceptable solution. Currently the most widely used system for providing earthquake resistance without significant accompanying damage is that of seismic isolation. However, not all structures are suited for this form of protection and there is an associated cost and difficulty in construction. Another alternative that is beginning to receive more attention involves the use of passive energy dissipating elements within the structure (Butterworth, 1999). In order to be able to compare the use of innovative and conventional strengthening techniques, for strengthening the existing building, as conventional strengthening approach addition of shear walls and as innovative approach addition of viscous damper systems were selected.

Therefore, in the present study, the existing building was retrofitted by passive control devices such as fluid viscous damper systems, which provide different levels of effective damping (ζ) to the structure such as 10, 15, and 20 per cent. These retrofitted buildings are investigated in comparison to the existing building and the retrofitted building by conventional strengthening technique (shear walls), through fragility analysis.

2.6. Application of Passive Fluid Viscous Damper Systems for Retrofitting

2.6.1. Fluid Viscous Dampers

Viscous dampers can absorb almost all the earthquake energy, leaving the structure intact and ready for immediate use after an event. A fluid viscous damper dissipates energy by pushing fluid through an orifice, producing a damping pressure which creates a force. Viscous dampers provide forces which are 90 degrees out of phase with the displacement driven forces in the structure. This force is proportional to the relative velocity between the ends of the damper. The ideal force output of a viscous damper can be expressed as follows:

$$F_D = C\left|\dot{u}\right|^{\alpha} \operatorname{sgn}\left(\dot{u}\right) \tag{2.3}$$

where F_D is the damper force, C is an arbitrary constant, (C remains constant over the full range of velocities) $\dot{u}$ is velocity, α is an exponent that can range from 0.3 to 1.95 (α remains constant over the full range of velocities). From the equation, it is obvious that the damper force only varies with velocity, there is no spring constant. For a given velocity, the force will be the same at any point in the stroke. Therefore, since dampers provide no restoring force, the structure itself must resist all static lateral loads.

A typical viscous damper and installation of viscous damper in a frame are shown in Figure 2.6 and Figure 2.7, respectively. As seen from the Figure 2.6, a central piston strokes through a fluid-filled chamber and as the piston moves, it pushes fluid through orifices around and through the piston head. Fluid velocity is very high in this region so the upstream pressure energy converts almost entirely to kinetic energy. When the fluid

subsequently expands into the full volume on the other side of the piston head it slows down and loses its kinetic energy into turbulence. There is very little pressure on the downstream side of the piston head compared with the full pressure on the upstream side of the piston head. This difference in pressures produces a large force that resists the motion of the damper. Viscous dampers, when correctly designed and fabricated, have zero leakage and require no accumulator or external liquid storage device to keep them full of fluid. They have nearly perfect sealing. In a correctly designed and fabricated viscous damper there is nothing to wear out or deteriorate over time so there is no practical limit on expected life. All materials in the damper including the working fluid must be nontoxic and nonflammable. In most cases silicone-based fluids are used to insure proper fluid performance and stability.

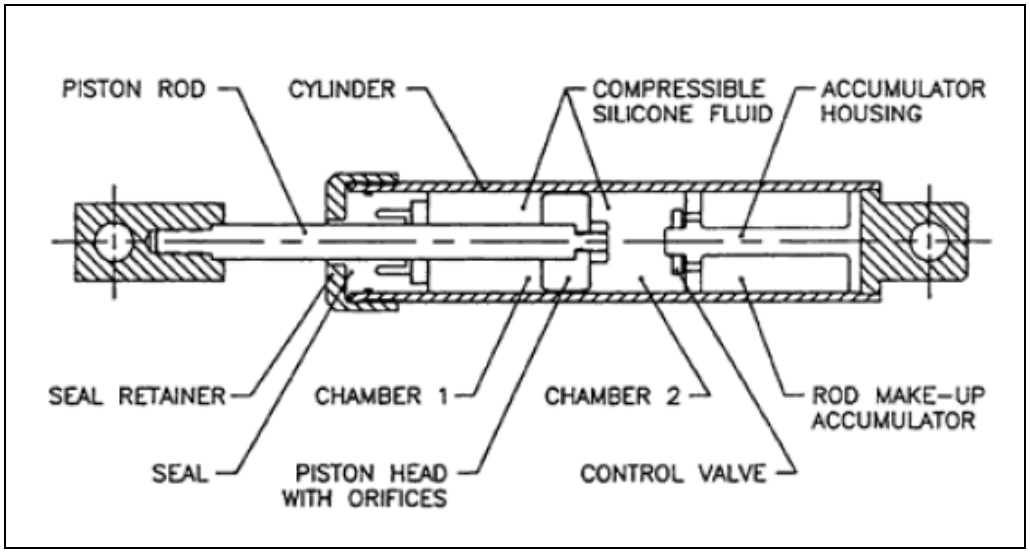

Figure 2.6. Typical Viscous Damper (Lee and Taylor, 2001)

Viscous dampers add energy dissipation to a structure, which significantly reduces response to earthquakes, blasts, induced gusts and other shock and vibration inputs. A value of 30 per cent of the critical effective damping value is a practical upper limit for combined viscous and structural damping. Around 25 per cent of this is viscous damping and the remaining five per cent is structural damping. The addition of viscous dampers does not change the period of the structure. This is because viscous damping is 90 degrees out of phase with the structural forces (Christis and Chrysostomou, 2005).

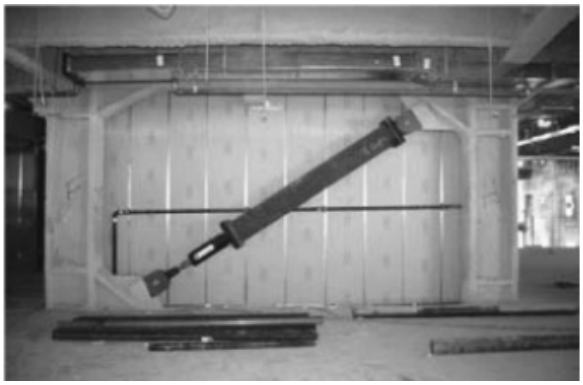

Figure 2.7. Installation of fluid viscous damper (Uriz and Whittaker, 2001)

It is theoretically possible to provide enough viscous damping to completely prevent plastic hinging. This provides a totally linear structure. Economically, it is best to retain some plastic hinging since this results in the least overall cost. Viscous dampers still limit inter-storey drift sufficiently to provide immediate occupancy after a worst-case event. They also limit and control the degree of plastic hinging and greatly reduce base shear and inter-storey shear.

Figure 2.8 shows a plot of force against velocity for several values of α, the damping exponent. A value of α=1 is the curve for linear damping, in which the damper force is proportional to velocity. This figure demonstrates the efficiency of nonlinear dampers in minimizing high velocity shocks. It is obvious that for a small relative velocity, the damper with a α value less than one, can give a larger damping force than the other two types of dampers.

The hysteresis loop for a linear damper is a pure ellipse, as shown in Figure 2.9. α=0.3 is the lowest damping exponent normally possible and it is seen from the figure that the hysteresis curve for this value of α is almost in rectangular shape. Structural dampers always use α value between 0.3 and 1.0, as any value above 1.0 produces very poor performance.

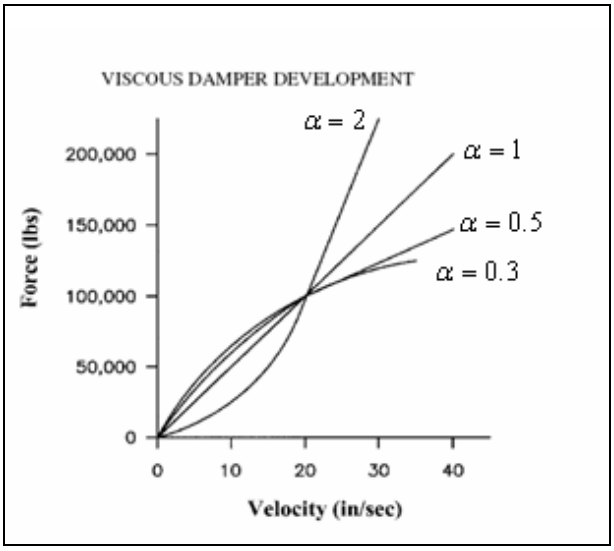

Figure 2.8. Plot of force against velocity for several values of the damping exponent, α (Lee and Taylor, 2001)

Linear damping (α=1) is easy to analyze and can be handled by most software packages. Also, linear damping is unlikely to excite higher modes in a structure. Another advantage of linear damping is that there is very little interaction between damping forces and structural forces in a building. Structural forces peak when damping forces are zero. Damping forces peak when structural forces are zero. Between these points there is a gradual transfer of force as shown in Figure 2.9. Nonlinear damping with a low exponent shows a much more rectangular hysteresis curve and the damping forces tend more to superimpose on the structural forces. In addition, nonlinear damping can possibly excite higher modes in a structure (Martinez-Rodrigo and Romero, 2003).

2.6.2. Design of Passive Viscous Dampers Providing Different Levels of Effective Damping

Among the advantages of viscous devices we can underline: stable hysteresis loop; shock transmission function; industrial products subjected to experimental tests; high stability and durability; ease of implementation; limited sensitivity to environmental condition changes. PFVD systems can be used especially in buildings and turn out very effective in retrofit interventions and refurbishment of monumental and frame buildings, since it provides reduction of structural response under seismic actions; reduction of inter-

storey drift; reduction of damage in structural elements due to energy dissipation. Among the disadvantages of viscous damper systems it can be said that the PFVD systems can not be applicable to all kinds of buildings; the buildings must have sufficient structural quality, that can resist the structural overloading either in the beam or the column elements. Furthermore, viscous devices are one of the more expensive among all the energy dissipation systems, but they give more reliability. Their application has been showed a great convenience in the case of strategic and monumental buildings.

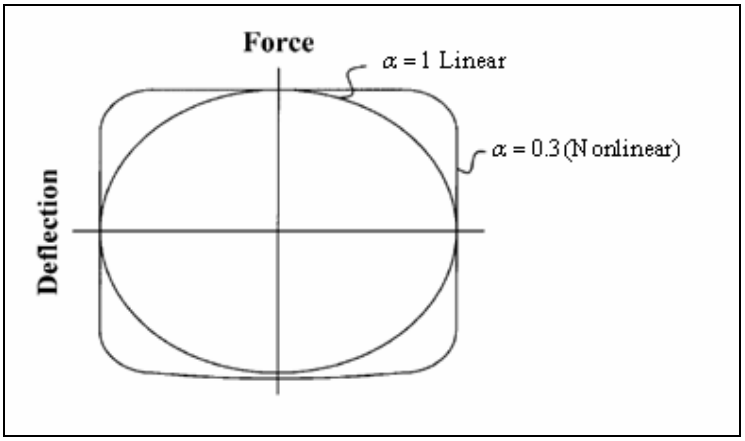

Figure 2.9. Hysteresis loops for linear and nonlinear dampers for two values of the damping exponent, α (Lee and Taylor, 2001)

For these reasons, in this study fluid viscous dampers (Taylor Devices Co.) (Constantinou and Symans, 1992) are considered in improving the seismic behavior of the existing building. Although these dampers can be constructed as linear or nonlinear functions of velocity; the configuration of dampers that can be represented by a linear relation within the expected range of operations without stiffening characteristics are considered.

The viscous dampers are added to all stories at the same locations. The locations of the viscous damper systems on the story plan are given in Figure 2.10.

The seismic design of the viscous fluid devices is done according to FEMA 273 (1997) and FEMA 274 (1997) in order to provide various levels of effective damping ratio to the structure such as 10, 15 and 20 per cent effective damping.

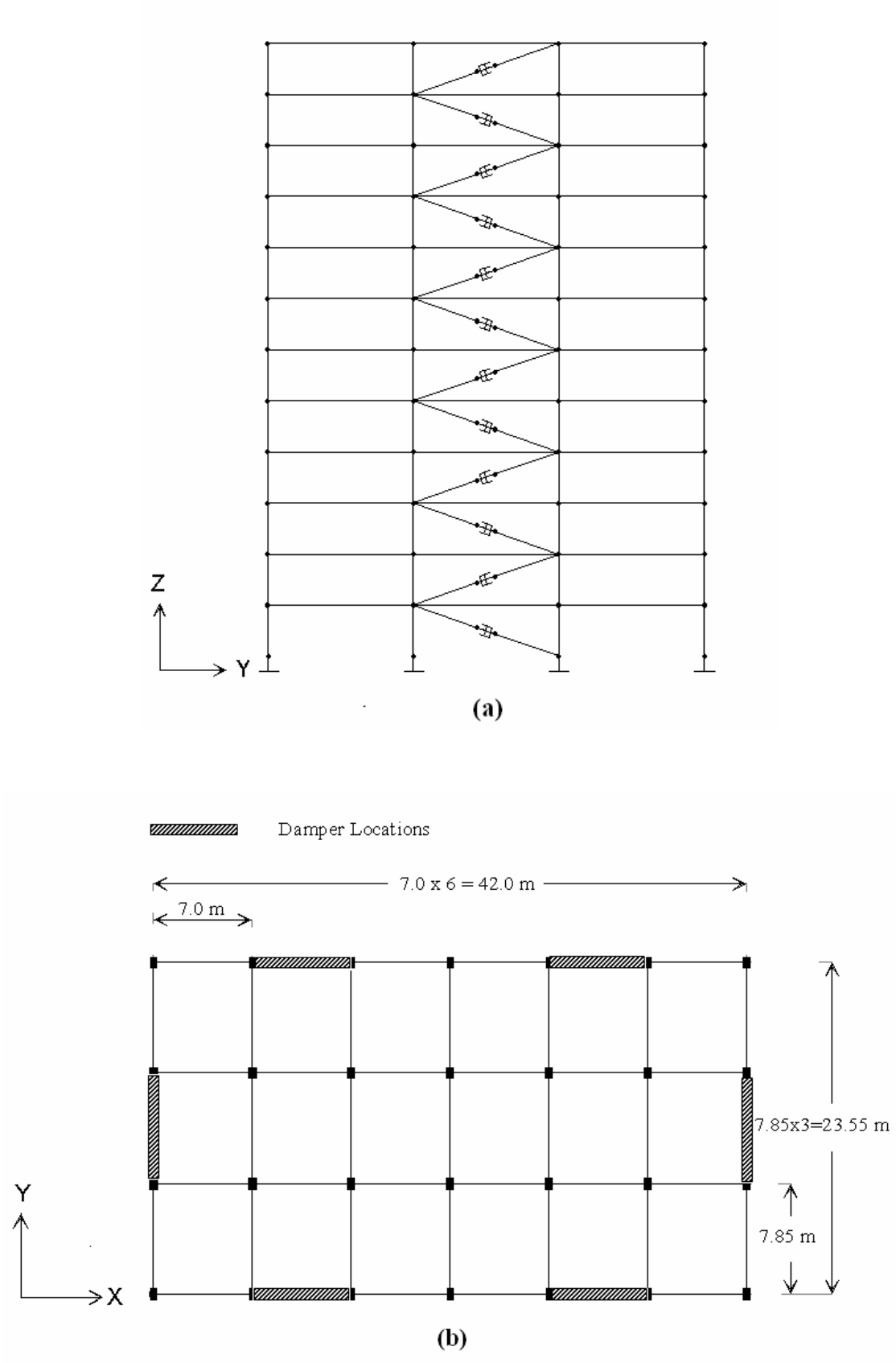

Figure 2.10. Location of PFVD system: a) elevation, b) floor plan view

For the design of the viscous dampers, a single degree of freedom system equipped with a linear viscous damper under an imposed sinusoidal displacement time history is considered according to FEMA 273(1997) and FEMA 274 (1997).

$$u = u_0 \sin wt \tag{2.4}$$

where u is the displacement of the system and the damper; u_0 is the amplitude of the displacement, and the w is the excitation frequency. The measured force response is

$$P = P_0 \sin\left(wt + \delta\right) \tag{2.5}$$

where P is the force response of the system, P_0 is the amplitude of the force, and δ is the phase angle. The energy dissipated by the damper W_D is

$$W_D = \oint F_D du \tag{2.6}$$

where F_D is the damper force which equals to $C\dot{u}$; C is the damping coefficient of the damper, and $\dot{u}$ is the velocity of the system and the damper. Therefore; the energy dissipated by the damper becomes:

$$W_D = \oint C\dot{u}du = \int_0^{2\pi/w} C\dot{u}^2 dt = Cu_0^2 w^2 \int_0^{2\pi} \cos^2 wt \; d\left(wt\right) = \pi C u_0^2 w \tag{2.7}$$

Recognizing that the damping ratio contributed by the damper can be expressed as $\zeta_d = C/C_{cr}$, it is obtained

$$W_D = \pi C u_0^2 w = \pi \zeta_d C_{cr} u_0^2 w = 2\pi \zeta_d \sqrt{Km} u_0^2 w = 2\pi \zeta_d K u_0^2 \frac{w}{w_0} = 2\pi \zeta_d W_S \frac{w}{w_0} \tag{2.8}$$

where C_{cr}, K, m, w_0, and W_s are respectively the critical damping coefficient, stiffness, mass and nature frequency and elastic strain energy of the system. The damping ratio attributed to the damper can be expressed as:

$$\zeta_d = \frac{W_D}{2\pi W_S}\frac{w_0}{w} \tag{2.9}$$

where W_D and W_S are illustrated in Figure 2.11. Under earthquake excitations, w is essentially equal to w_0, and then, damping ratio attributed by the damper becomes:

$$\zeta_d = \frac{W_D}{2\pi W_S} \tag{2.10}$$

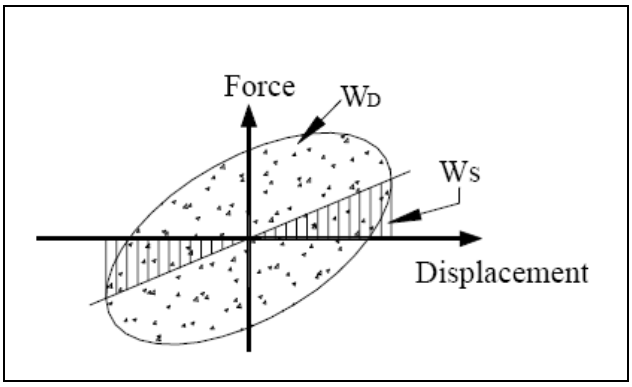

Figure 2.11. Definition of energy dissipated W_D in a cycle of harmonic motion and maximum strain energy W_S of a SDOF system with PFVD

The total effective damping ratio of the system ζ_{eff}, is defined as,

$$\zeta_{eff} = \zeta_0 + \zeta_d \tag{2.11}$$

where ζ_0 is the inherent damping ratio of the MDOF system without dampers, and ζ_d is the viscous damping ratio attributed to the added dampers. In this study the inherent

damping ratio of the system is assumed to be five per cent. Extended from the concept of a SDOF system, the equation shown below is used by FEMA 273 to represent ζ_d :

$$\zeta_d = \frac{\sum W_j}{2\pi W_k} \tag{2.12}$$

where $\sum W_j$ is the sum of the energy dissipated by the j[th] damper of the system in one cycle; and W_k is the elastic strain energy of the frame. W_k is equal to $\sum F_i \Delta_i$ where F_i is the story shear and Δ_i is the story drift of the i[th] floor. Now, the energy dissipated by the viscous dampers can be expressed as :

$$\sum_j W_j = \sum_j \pi C_j u_j^2 w_0 = \frac{2\pi^2}{T} \sum_j C_j u_j^2 \tag{2.13}$$

where u_j is the relative displacement of the damper j between the ends.

Experimental evidence has shown that if the damping ratio of a structure is increased the higher mode responses of the structure will be suppressed. As a consequence, only the first mode of a MDOF system is usually considered in the simplified procedure of practical applications. Using the modal strain energy method, the energy dissipated by the dampers and the elastic strain energy provided by the primary frame can be rewritten as:

$$\sum_j W_j = \frac{2\pi^2}{T} \sum C_j \phi_{rj}^2 \cos^2 \theta_j \tag{2.14}$$

$$W_K = \Phi_1^T [K] \Phi_1 = \Phi_1^T W^2 [m] \Phi_1 = \sum_i w^2 m_i \phi_i^2 = \frac{4\pi^2}{T^2} \sum_i m_i \phi_i^2 \tag{2.15}$$

where $[K]$, $[m]$, $[\Phi_1]$ are respectively the stiffness matrix, the lumped mass matrix and the first mode shape of the system; ϕ_{rj} is the relative horizontal displacement of damper j corresponding to the first mode shape; ϕ_i is the first mode displacement at floor i ; m_i is the

mass of floor i ; and θ_j is the inclined angle of damper j . Substituting (2.12), (2.13), (2.14) and (2.15) into (2.11), the effective damping ratio of a structure with linear viscous dampers given by :

$$\zeta_{eff} = \zeta_0 + \frac{\frac{2\pi^2}{T}\sum_j C_j \theta_{rj}^2 \cos^2\theta_j}{2\pi \frac{4\pi^2}{T^2}\sum m_i \phi_i^2} = \zeta_0 + \frac{T\sum_j C_j \theta_{rj}^2 \cos^2\theta_j}{4\pi \sum m_i \phi_i^2} \tag{2.16}$$

Corresponding to a desired added damping ratio, there is no substantial procedure suggested by design codes for distributing C values over the whole building. Therefore, during the design of the dampers, distributing the C values equally in each floor is preferred.

Since the force of viscous dampers and the displacement response of the frame are out of phase, it is difficult to determine the internal force of each member of the frame through the static procedure. Therefore, when the rehabilitation of buildings is executed with velocity dependent devices, FEMA 273 suggests engineers to check the actions for components of the buildings in the following three stages of deformation such as: stage of maximum drift, stage of maximum velocity and zero drift, and stage of maximum acceleration.

Furthermore, FEMA 273 recommends a procedure to calculate the member force at the instant of the maximum acceleration. The procedure indicates that design actions in components should be determined as the sum of “actions determined at the stage of maximum drift” times CF_1 and “actions determined at the stage of maximum velocity” times CF_2, where

$$CF_1 = \cos\left[\tan^{-1}\left(2\zeta_{eff}\right)\right] \tag{2.17}$$

$$CF_2 = \sin\left[\tan^{-1}\left(2\zeta_{eff}\right)\right] \tag{2.18}$$

in which ζ_{eff} is given by:

$$\zeta_{eff} = \zeta_0 + \frac{\frac{2\pi^2}{T}\sum_j C_j \theta_{rj}^2 \cos^2\theta_j}{2\pi\frac{4\pi^2}{T^2}\sum m_i \phi_i^2} = \zeta_0 + \frac{T\sum_j C_j \theta_{rj}^2 \cos^2\theta_j}{4\pi\sum m_i \phi_i^2} \qquad (2.19)$$

The passive fluid viscous damper properties obtained for each case of effective damping is summarized in Table 2.1. For all three cases, the damper systems were considered to withstand a lateral load equal to at least twice its own weight concomitant to the maximum axial load. The existing structural elements connected to the passive devices were also strengthened to bear their reaction force. Therefore, for all three retrofitting cases, the structural properties of dampers to provide 10, 15 and 20 per cent critical damping without overloading either the beam or the column structural elements were designed.

Table 2.1. Properties of the dampers designed for various effective damping ratios

Retrofitting cases	Total effective damping ratio	Damping constant C (kNs/m)
Case-1	ζ_{eff}=10 %	362
Case-2	ζ_{eff}=15 %	725
Case-3	ζ_{eff}=20 %	1087

2.7. Application of Shear Walls for Retrofitting

Shear walls, because of their great stiffness and lateral strength, provide the most significant part of the earthquake resistance of the building structure. Therefore, addition of shear walls into the existing structure is one of the conventional methods used to enhance the reinforced concrete buildings performance against seismic forces.

The shear walls are added to the same location with the viscous damper systems throughout the height of the building. The thickness of the shear walls were selected as 25 cm through out the building. In the retrofitting measure applied, the quality of concrete

used is C25 and the reinforcement used is S420. The retrofit of the existing structure by using shear walls was designed and checked according to the Turkish earthquake code.

3. GROUND MOTION MODELLING

A significant step in fragility analysis is the selection of representative set of earthquake motions that represent the variability in earthquakes. Using a set of actual ground motion records would be preferred. However, many of the available records are not well identified as per the soil classification at the site. In addition, many of the available records are not free field time history but rather modified by the response of the structure. Therefore, the number of available and usable earthquake records is not large enough to obtain sufficiently accurate results (Ghobarah *et al.*, 2000). For these reasons, in this study, artificially generated ground motions are used in the analysis.

The seismic model selected to generate artificial waves will significantly influence the analysis and the success of the seismic analysis depends on how well the artificial seismic waves represent the main characteristics of the seismic ground motion. In the literature, there are two approaches for modeling earthquake strong motion, one is Deterministic (Kinematics) Modeling Approach (Aki, 1968; Aki and Richards, 1980; Atkinson and Somerville, 1994; Beresnev and Atkinson, 1997; Irikura and Kamae, 1994; Bolt, 1995), and the other one is Stochastic Engineering Approach (Shinozuka and Yang, 1971; Soong and Grigoriu, 1993; Shinozuka and Jan, 1972; Grigoriu, 1995; Shinozuka and Deodatis, 1991; Deodatis, 1996).

In this study, 240 synthetic seismic ground motion time histories were generated between 0 and 1 PGA by using the Spectral Representation Based Simulation methodology based on Stochastic Engineering Approach which is suggested by Deodatis (1996) and later modified by Saxena *et al*. (2000).

3.1. Simulation of Seismic Ground Motion Compatible with Prescribed Response Spectra

In order to model earthquake ground motion; acceleration, velocity or displacement time histories can be generated at several locations on the ground surface according to power spectral density functions. The only negative aspect of this approach is that it is

often preferable to work with time histories that are compatible with prescribed response spectra, rather than prescribed power spectral density functions. An obvious reason for this preference is that it is much easier and more reliable to find a response spectrum specified for a given location, rather than a power spectral density function. In order to address this issue Deodatis (1996) introduces an iterative scheme based on the proposed simulation algorithm, to generate seismic ground motion time histories that are compatible with prescribed response spectra, include the wave propagation effect, and have a specified duration of strong ground motion.

The spectral representation method is used first to generate ergodic, stationary ground motion time histories that are compatible with a prescribed velocity of wave propagation, but not with the prescribed response spectra. These ground motion time histories are modeled as a stationary stochastic vector process (with arbitrarily defined spectral density functions at the beginning of the iterative scheme involved in the methodology). After multiplying the generated stationary time histories by appropriate envelope functions to introduce non-stationary, the resulting non-stationary time histories are used to compute the corresponding response spectra. These computed response spectra are then compared with the prescribed response spectra, and if they do not match, the power spectral density functions are upgraded and new stationary time histories according to the upgraded power spectral density function is generated and then it is multiplied with envelope function to introduce non-stationary. This upgrading procedure is repeated many times until the time history becomes compatible with the prescribed response spectrum to the desired degree.

A recent problem of the original algorithm recognized by Saxena *et al*. (2000), is that although at the end of the iterations the generated time histories closely reflect the prescribed response spectra, the upgrading of the spectral density functions at each iteration makes them eventually functions of the random phase angles used in the beginning of the iterative scheme to generate the first set of the underlying stationary time histories. These random phase angles enter the spectral density functions through the computed response spectra from the corresponding non-stationary time histories. The aforementioned problem arises because the amplitudes of the spectral density functions become random as the iterations proceed. In order to deal with this problem, the following

two modifications are introduced to the original methodology: a) Only sample functions that take a relatively small number of iterations to converge are kept b) The upgraded power spectral density function is smoothed by a simple rectangular window at each iteration. The modified iterative algorithm used in this study is shown in Figure 3.1.

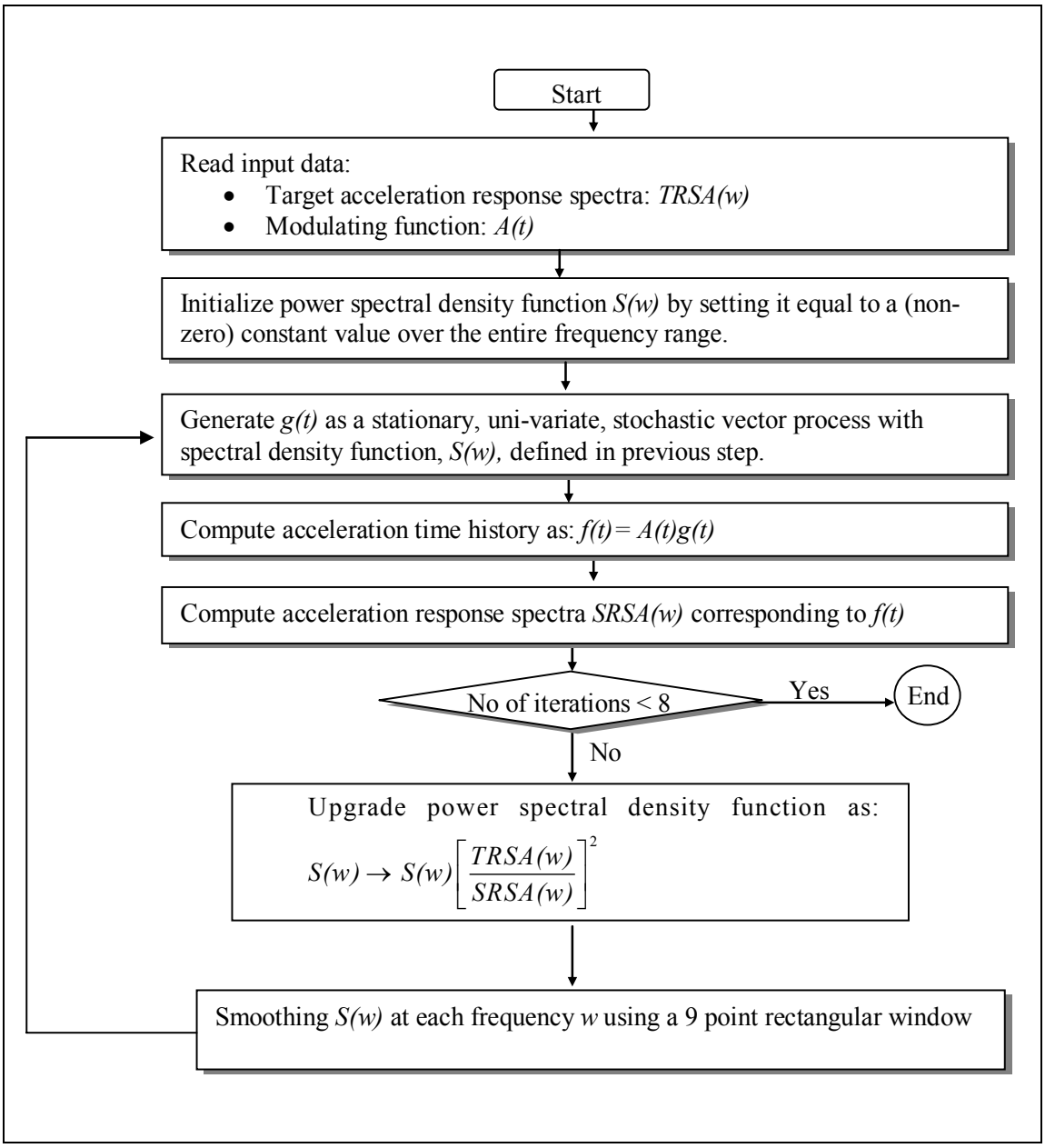

Figure 3.1. Iterative scheme to simulate response spectrum compatible acceleration time history

Within the scope of this thesis, by applying the algorithm of which the details are given below, a total of 240 synthetic seismic ground motion time histories between zero and one PGA were generated by using MATLAB code.

3.1.1. Simulation of Stationary Stochastic Process

Consider a 1D stationary stochastic process $f_0(t)$ with mean value equal to zero, autocorrelation function $R(\tau)$ and two sided power spectral density function $S(w)$. In the following, distinction will be made between the stochastic process $f_0(t)$ and its simulation $f(t)$ (Shinozuka and Deodatis, 1991).

In the stochastic process, $f_0(t)$ can be simulated by the following series as $N \to \infty$:

$$f(t) = \sqrt{2} \sum_{n=0}^{N-1} A_n \cos(w_n t + \phi_n) \tag{3.1}$$

where

$$A_n = (2\, S(w_n) \Delta w)^{1/2}, \quad n = 0,1,2,...,N\text{-}1 \tag{3.2}$$

$$w_n = n\Delta w, \quad n = 0,1,2,...,N\text{-}1 \tag{3.3}$$

$$w = w_u / N \tag{3.4}$$

$$A_0 = 0 \quad or \quad S(w_0 = 0) = 0 \tag{3.5}$$

In the above equations w_u represents an upper cut-off frequency beyond which the power spectral density function $S(w)$ may be assumed to be zero for either mathematical or physical reasons. As such, w_u is a fixed value and hence $\Delta w \to 0$ as $N \to \infty$ so that $N\Delta w = w_u$. The following criterion is usually used to estimate the value of w_u:

$$\int_0^{w_u} S(w)\,dw = (1-\varepsilon)\int_0^{\infty} S(w)\,dw \tag{3.6}$$

where $\varepsilon << 1$ *(e.g.* $\varepsilon = 0.01, 0.001$*).*

The $\phi_1, \phi_2, \phi_3, \ldots\ldots\ldots\phi_{N-1}$, are independent random phase angles distributed uniformly over the interval $[0,2\pi]$.

Under the condition of (3.5), it is easy to show that the simulated stochastic process $f(t)$ obtained by (3.1) is periodic with period T_0 :

$$T_0 = 2\pi / \Delta w \tag{3.7}$$

Equation (3.7) indicates that the smaller Δw, or equivalently the larger N under a specified upper cut-off frequency value, the longer the period of the simulated stochastic process.

A sample function $f^{(i)}(t)$ of the simulated stochastic process $f(t)$ can be obtained by replacing the sequence of random phase angles $\phi_0, \phi_1, \phi_2, \ldots, \phi_{N-1}$ with their respective i-th realizations $\phi^{(i)}_0, \phi^{(i)}_1, \phi^{(i)}_2, \ldots, \phi^{(i)}_{N-1}$:

$$f^{(i)}(t) = \sqrt{2}\sum_{n=0}^{N-1} A_n \cos(w_n t + \phi_n^{(i)}) \tag{3.8}$$

The condition given in (3.5) is necessary (and must be forced if $S(0) \neq 0$) to guarantee that the temporal average and the temporal autocorrelation function of any sample function $f^{(i)}(t)$ are identical to the corresponding targets, $\varepsilon[f_0(t)] = 0$ and $R_{fofo}(\tau)$, respectively.

At this point it should be noted that when generating sample functions of the simulated stochastic process according to (3.8), the time step Δt separating the generated values of $f^{(i)}(t)$ in the time domain has to obey the following condition:

$$\Delta t \le 2\pi / 2w_u \tag{3.9}$$

The condition set on Δt in (3.9) is necessary in order to avoid aliasing according to sampling theorem (Bracewell, 1986).

The generated values of $f^i(t)$ according to (3.9) are bounded as follows:

$$f^{(i)}(t) \le \sqrt{2}\sum_{n=0}^{N-1} A_n = \sqrt{2}\sum_{n=0}^{N-1}\left(2S(w_n)\Delta w\right)^{1/2} \tag{3.10}$$

By using the condition in (3.10) for w_u=15×2π;

$$\Delta t \le 2\pi / 2(15\times 2\pi) \tag{3.11}$$

$$\Delta t \le 0.0333 \tag{3.12}$$

The time step was selected as Δt = 0.01 second whereas duration of the generated histories is 30 seconds.

3.1.2. Nonstationary Stochastic Process

To model the time varying intensity of a typical earthquake, the stationary acceleration time history generated is typically multiplied by a suitable envelope non-stationary function. A simple and realistic form for this envelope function $A(t)$, is defined in the studies of Jennings *et al.* (1968) and Sues *et al*. (1985).

$$A(t) = (t/t_1)^2 \qquad (0 < t < t_1) \tag{3.13}$$

$$A(t)=1 \quad (\ t_1 \ \le \ t \ \le \ t_2\ ) \tag{3.14}$$

$$A(t)=e^{-c(t-t_2)} \quad t<t_2 \tag{3.15}$$

where t_1 and t_2 are the rise and decay times of the ground motion, t_2-t_1 is the strong shaking duration and c is a decay parameter. The suggested values for these parameters are $t_1=1.5$ s and $c=0.18$. The shape of the envelope function is shown in Figure 3.2. A mean duration of the strong motion duration was derived from the results presented in previous studies (Moayyad and Mohraz, 1982; Vanmarcke and Lai, 1980). It is taken as 7 seconds for intermediate ground conditions (Sues *et al*., 1985) and therefore, the strong ground motion duration is considered deterministic in this analysis.

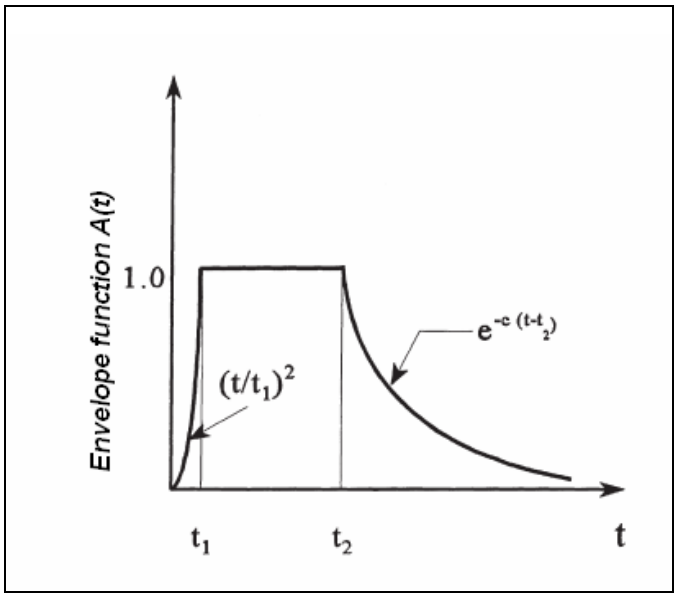

Figure 3.2. Envelope function for the generated ground motion.

3.1.3. Determination of Response Spectrum

A plot of the peak value of a response quantity as a function of natural vibration period T_n of the system, or a related parameter such as circular frequency w_n or cyclic frequency f_n, is called the response spectrum for that quantity. Each such plot is for single degree of freedom systems having a fixed damping ratio (ζ) and several such plots for

different values of ζ are included to cover the range of damping values encountered in the original structure. Whether the peak response is plotted against f_n or T_n is a matter of personal preference. Generally, using natural period rather than the natural frequency is preferred because the period of vibration is more familiar and intuitively appealing (Chopra, 2000).

A variety of response spectra can be defined depending on the response quantity that is plotted. Consider the following peak responses:

$$u_0(T_n,\zeta) \equiv \max \left| u(t,T_n,\zeta) \right| \tag{3.16}$$

$$\dot{u}_0(T_n,\zeta) \equiv \max \left| \dot{u}(t,T_n,\zeta) \right| \tag{3.17}$$

$$\ddot{u}_0(T_n,\zeta) \equiv \max \left| \ddot{u}(t,T_n,\zeta) \right| \tag{3.18}$$

where $u(t,T_n,\zeta)$, and $\dot{u}(t,T_n,\zeta)$, $\ddot{u}(t,T_n,\zeta)$ are displacement, velocity , and acceleration time histories of the SDOF system with duration of earthquake t, natural period T_n and damping ratio ζ . The deformation response spectrum is a plot of u_o against T_n for fixed ζ . A similar plot for $\dot{u}_0$ is the relative velocity response spectrum, and for $\ddot{u}_0$ it is called the acceleration response spectrum (Chopra, 2000).

Soil investigations based on appropriate site and laboratory tests are available for Mecidiyeköy region, and according to ABYYHY-98, it is observed that the soil satisfies Z2 local site class. Therefore, elastic acceleration response spectrum with spectrum characteristic periods of T_A= 0.15 and T_B=0.4 given for local site class Z2 in Turkish Seismic Code (ABBYHY, 1998) is used as shown in Figure 3.3.

3.1.4. Upgrading the Spectral Density Function

After multiplying the generated stationary time histories by appropriate envelope functions to introduce non-stationarity in the first simulation, the resulting non-stationary

time histories are used to compute the corresponding response spectra. These computed response spectra are then compared with the prescribed response spectra, and if they do not match as shown in Figure 3.4 , the diagonal terms of the cross-spectral density matrix of the underlying stationary stochastic vector process are upgraded according to the following formula:

$$S(w) = S(w)\left[\frac{TRSA(w)}{SRSA(w)}\right]^2 \tag{3.19}$$

where *S(w)* is the previous spectral density function of the stationary vector process, *TRSA* is the prescribed target response spectrum, and *SRSA* is the computed response spectrum from the corresponding non-stationary time history. In addition to this, at each iteration smoothing of the upgraded power spectral density functions by a nine point simple rectangular window is performed to decrease the number of iterations. The iterative scheme proceeds with the upgraded cross-spectral density matrix of the underlying stationary vector process, until the computed response spectra of the resulting non-stationary time histories match the corresponding target response spectra with an acceptable level of accuracy as shown in Figure 3.5. Such a convergence is achieved within a reasonable number of iterations which is limited to eight. At the end of eighth iteration, it is decided that the satisfactory convergence has been reached.

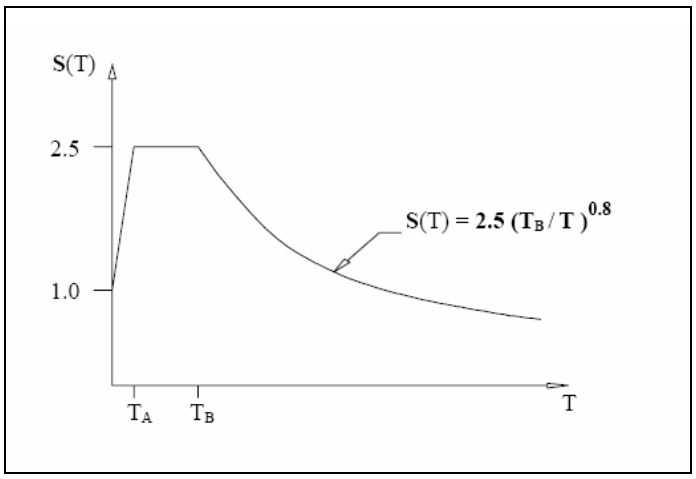

Figure 3.3. Elastic acceleration spectrum according to Turkish Seismic Code

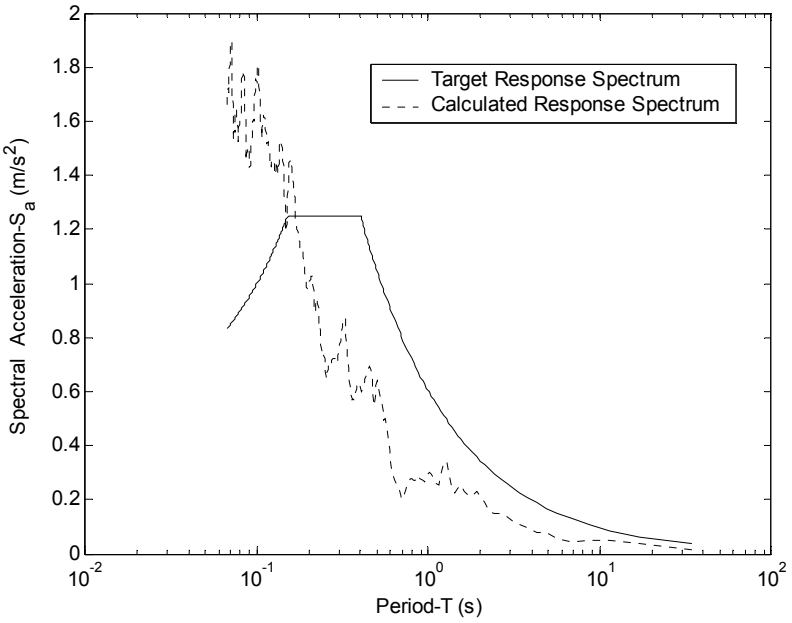

Figure 3.4. Comparison of the target response spectrum with the calculated spectrum before iterations

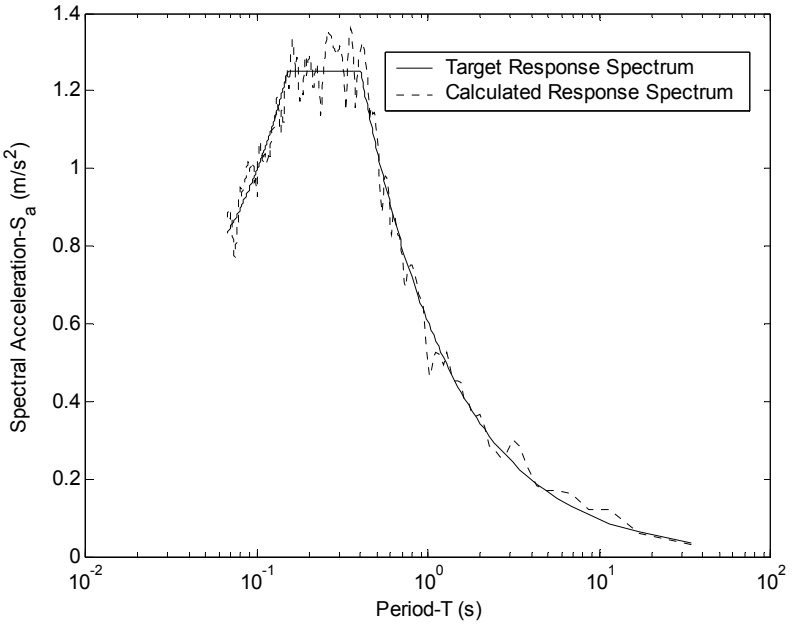

Figure 3.5. Comparison of the target response spectrum with the calculated spectrum after eighth iterations

4. DEVELOPMENT OF FRAGILITY CURVES

According to the literature, fragility curves can be developed from the seismic response data obtained from nonlinear time history analysis, nonlinear static analysis (Mander and Basoz, 1999; Shinozuka *et al*., 2000a) or elastic spectral analysis (Hwang *et al*., 2000). Although nonlinear time history analysis method has been identified as the most time consuming, among them the most rigorous method in the literature for developing analytical fragility curves is through the utilization of non-linear time history analysis for determining the seismic demand (Shinozuka *et al*., 2000b). The non-linear time history analysis method has been developed and adopted in various forms by Hwang *et al*. (2000), Saxena *et al*. (2000), Shinozuka *et al*. (2000b), Karim and Yamazaki (2003), Choi *et al*. (2004), Elnashai *et al*. (2004), Erberik and Elnashai (2004), and Mackie and Stojadinovic (2004).

In the current study, nonlinear time history analysis was carried out to provide the structural response for a given seismic excitation and a selected representative R/C frame structure before and after retrofit. For this purpose, firstly, a set of 240 synthetic earthquake motions compatible with the target response spectrum and equally scaled between 0 and 1 PGA was generated as given in previous chapter. Secondly, structures under consideration were represented by analytical models, which include the nonlinear behavior of the appropriate components. The main point of defining the earthquake intensity damage relationship in development of fragility curves is to anticipate the structural response to excitation with a given intensity. Therefore, thirdly there were two key clarifications to be made, one was the selection of an indicator of earthquake intensity, and the other was the selection of an indicator of response (i.e. damage parameter). As indicator of earthquake intensity, PGA, S_a, S_d and as indicator of seismic response inter-storey drift were chosen. Finally, using a probabilistic seismic demand model obtained by regression analysis on the simulated damage data, the individual fragility curves for each damage state and for each building were developed. Detail for every step is given hereafter.

4.1. Seismic Damage (Response) Parameters for Development of Fragility Curve

In the literature, there are various damage states and corresponding limit values in terms of different damage measures considered. For instance, for bridges, the Park–Ang damage index was preferred by Karim and Yamazaki (2000, 2001, 2003). Furthermore, Shinozuka *et al*. (2000a, 2000b) and Saxena *et al*. (2000) used the section ductility demand and corresponding limit values as a damage indicator of five damage states namely no, slight, moderate, extensive and complete collapse damage states. In the studies of Choi (2002) and Choi *et al*. (2004), both the ductility and deformation are used as the damage limit values of the bridge components: columns, steel fixed bearings, and steel expansion bearings. For building type structures, Kircher *et al*. (1997) and Smyth *et al*. (2004) specified four different damage levels: slight; moderate; major or extensive; and complete or collapse. Maximum inter-story drift ratio was accepted as the damage measure and each damage level has an assumed limit value of inter-story drift ratio. Dumova-Jovanoska (2000) used similar damage levels, however, the Park–Ang damage index was employed by her as a damage indicator.

In this study, for the seismic fragility analysis of typical high-rise R/C office building, four damage states, namely slight, moderate, major, and collapse in terms of average inter-storey drift ratio were taken into account since the behavior and the failure modes of such R/C moment resisting frame structures are governed by deformation. The damage state definitions used were based on the recommendations from the previous studies (Smyth *et al.*, 2004; Dumova-Jovanoska, 2000) and followed the qualitative descriptions of the damage levels as provided by HAZUS (1997), which are given below:

Slight Structural Damage: Flexural or shear type hairline cracks in some beams and columns near joints or within joints.

Moderate Structural Damage: Most beams and columns exhibit hairline cracks. In ductile frames some of the frame elements have reached yield capacity indicated by larger flexural cracks and some concrete spalling. Non-ductile frames may exhibit larger shear cracks and spalling.

Major Structural Damage: Some of the frame elements have reached their ultimate capacity indicated in ductile frames by large flexural cracks, spalled concrete and buckled main reinforcement; non-ductile frame elements may have suffered shear failures or bond failures at reinforcement splices, or broken ties or buckled main reinforcement in columns which may result in partial collapse.

Complete (Collapse) Structural Damage: Structure is collapsed or in imminent danger of collapse due to brittle failure of non-ductile frame elements or loss of frame stability.

Almost all damage levels used in previous studies are related to the assumed limit values of the considered damage measures. Those limit values are quantitative descriptions of the capacity of a member to undergo deformations, displacements, or other damage measures that associate the structural component with a descriptive damage state. Well defined and realistic limit values for damage states are of paramount significance since these values have direct effect on fragility curve parameters. The limit values given in Table 4.1 for the damage states are determined by using capacity curve obtained for the weak axis of the structure from the pushover analysis according to the procedures given in the guidelines of HAZUS. To determine damage limit values of the building, the local limit states of beam and column elements are obtained. The local limit states are considered in terms of the first crack, yield or failure monitored in any column or beam in the structure during the pushover analysis. Then, these local limit states of members are used to obtain the global limit state of the structure as defined in HAZUS. The slight damage limit is defined by the first structural component to yield on its load deformation curve. In the slight damage, also cracks in some columns and beams are observed. Moderate damage limit is defined on the capacity curve for which about five per cent of components have each reached yield point on their respective load deformation curves. Major damage limit is defined by a similar to moderate damage, except that about 25 per cent of components have each reached yield point and some have reached failure point on their load deformation curves. Major damage is likely to affect a number of components distributed throughout the building. Complete damage is defined on the capacity curve by an inter-storey drift value for which at least 50 per cent of structural components have reached failure, or the structure has lost its stability. The results of the pushover analysis together

with the structural damage limit values determined for each damage state according to HAZUS are shown in Figure 4.1.

Table 4.1. Inter-storey drift ratio at threshold of damage state

Inter-storey drift ratio (%)			
Slight	Moderate	Major	Collapse
0.465	0.845	1.372	1.955

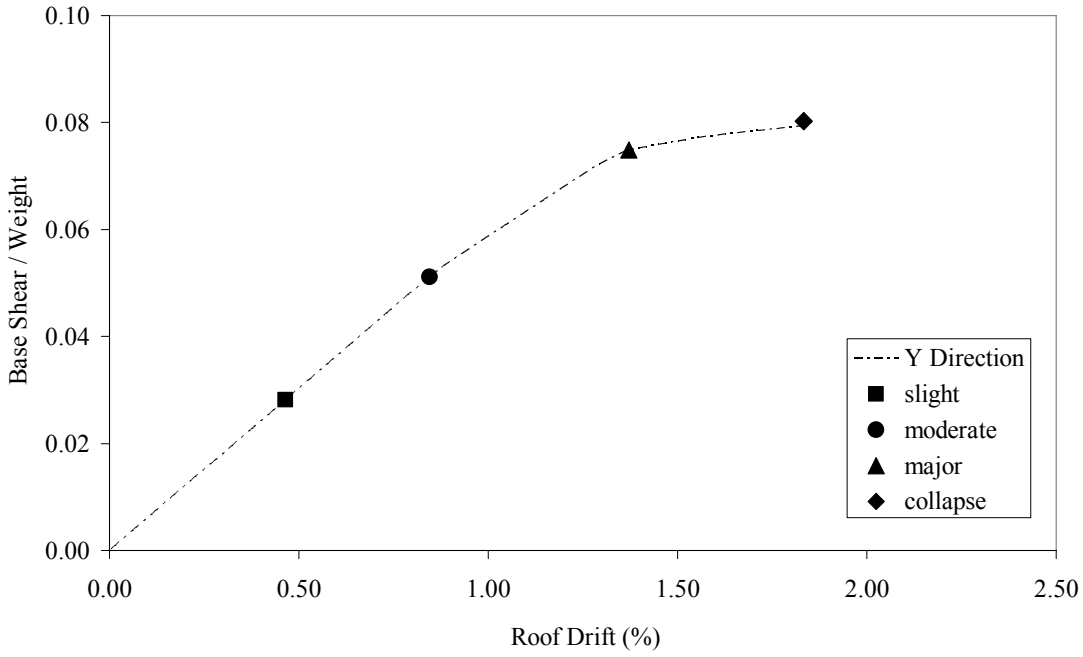

Figure 4.1. Demonstration of damage state limits on the capacity curve

4.2. Seismic Intensity Parameters for Development of Fragility Curves

There are various indicators of earthquake intensity such as spectral acceleration, peak ground acceleration, spectral intensity, Modified Mercalli intensity, spectral velocity etc. From these, in this study, peak ground acceleration (PGA), spectral acceleration (S_a) and spectral displacement (S_d), which were generally used in seismic loss assessment

programs, were chosen as the ground motion intensity measures for developing the fragility curves.

4.3. Nonlinear Time History Analysis

The seismic response of the existing and retrofitted structures for the fragility analysis was evaluated by means of nonlinear time history analyses. For nonlinear time history analysis, models that are able to represent the dampers and selected structural types in a sufficiently reliable way both in terms of stiffness and resistance, were implemented by using IDARC Version 6.1 Structural Analysis Program. The regularity of the representative building in terms of mass and stiffness in both plan and elevation enables a 2-D analysis to be used when assessing seismic response. The building was modeled as a 2-D planar frame with lumped masses and the hysteretic behavior of the beams and columns has been specified at both ends of each member using a three parameter Park model. This hysteretic model incorporates stiffness degradation, strength deterioration, non-symmetric response, slip-lock and a trilinear monotonic envelope. The nominal values of the parameters suggested by the authors were used to consider the effect of stiffness degradation and strength deterioration and pinching (Valles *et al*., 1996).

In the IDARC program, the nonlinear dynamic analysis is carried out using a combination of the Newmark-Beta integration method, and the pseudo-force method. The solution is carried out in incremental form, according to:

$$[M]\{\Delta\ddot{u}\}+[C]\{\Delta\dot{u}\}+[K_t]\{\Delta u\}=-[M]\{L_h\}\Delta\ddot{x}_{gh}-\{\Delta P_v\}+c_{corr}\{\Delta F_{err}\} \qquad (4.1)$$

where [M] is the lumped mass matrix of the structure; [C] is the viscous matrix of the structure; [K_t] is the tangent stiffness matrix; $\{\Delta u\}$, $\{\Delta\dot{u}\}$, and $\{\Delta\ddot{u}\}$ are the incremental vectors of displacement, velocity and acceleration in the structure, respectively; $\{L_h\}$ are the allocation vectors for the horizontal ground accelerations; $\Delta\ddot{x}_{gh}$ are the increment in the horizontal ground accelerations; $\{\Delta P_v\}$ are the restoring forces from viscous dampers, c_{corr}

is a correction coefficient; and $\{\Delta F_{err}\}$ is the vector with the unbalanced forces in the structure.

The solution of the incremental system is carried out using the Newmark-Beta algorithm, which assumes a linear variation of the acceleration as given in the equations:

$$\{\dot{u}\}_{t+\Delta t} = \{\dot{u}\}_t + \Delta t\left[(1-\gamma)\{\ddot{u}\}_t + \gamma\{\ddot{u}\}_{t+\Delta t}\right] \tag{4.2}$$

$$\{u\}_{t+\Delta t} = \{u\}_t + \Delta t\{\dot{u}\}_t + (\Delta t)^2\left[(0.5-\kappa)\{\ddot{u}\}_t + \kappa\{\ddot{u}\}_{t+\Delta t}\right] \tag{4.3}$$

where γ and κ are the parameters of the method.

The solution is performed incrementally assuming that the properties of the structure do not change during the time step of analysis. Since the stiffness of some elements is likely to change during the time step, the new configuration may not satisfy equilibrium (Valles *et al*., 1996).

The time step was selected small enough to ensure accuracy of the results, and to avoid the problem of non-balanced forces transferred from one interval to another. Therefore, nonlinear time history analysis was carried out using the Newmark-β integration method with a time step of 0.0001 s.

4.4. Generation of Fragility Curves

Recalling that a fragility curve offers the probability of meeting or exceeding a level of damage under an input ground motion intensity parameter given, we observe that the level of damage (damage state) can be related to the structural capacity and that the ground motion intensity relates to the structural demand. Thus, an appropriate model for assessing the fragility of a structural system is to determine the probability that the structural demand exceeds the structural capacity, as given in equation below;

$$p_f = P\left[\frac{S_{demand}}{S_{capacity}} \geq 1\right] \tag{4.4}$$

where p_f is the probability of meeting or exceeding a specific damage state, S_{demand} is the structural demand and $S_{capacity}$ is the structural capacity.

Fragility curves were expressed in the form of two-parameter lognormal distribution functions where the structural demand and capacity are assumed to be normally distributed. Based on this acknowledgement, the cumulative probability of the occurrence of damage, equal to or higher than damage level D, is expressed as:

$$P[\leq D] = \Phi\left[\frac{1}{\beta}\ln\left(\frac{X}{\mu}\right)\right] \tag{4.5}$$

where Φ is the standard normal cumulative distribution function, X is the lognormal distributed ground motion index (e.g., PGA, S_a, and S_d), and μ is the median value of ground motion index at which the building reaches the threshold of damage state D, defined using allowable drift ratios and β is the standard deviation of the natural logarithm of ground motion index of damage state.

4.5. Reliability Analysis and Discussion of Results

Although in the cost benefit analysis only the fragility curves in terms of PGA is necessary; since most of the seismic loss assessment tools use spectral acceleration and spectral displacement as indicator of seismic intensity, the fragility curves are developed also in terms of S_a and S_d for the existing building and the retrofitted cases.

The fragility curve parameters: the median and standard deviation of log-normally distributed ground motion indices for the existing and retrofitted buildings for each damage level under consideration are obtained by using MATLAB program as given in Table 4.2.

Table 4.2. Fragility curve parameters

Damage Level	Earthquake Parameter	Existing		Case-1		Case-2		Case-3		Case-4	
		μ	β	μ	β	μ	β	μ	β	μ	β
Slight	PGA	0.03	0.21	0.05	0.31	0.06	0.37	0.07	0.40	0.05	0.32
	S_a	0.04	0.25	0.06	0.37	0.07	0.45	0.08	0.49	0.08	0.38
	S_d	3.18	0.21	4.95	0.31	5.94	0.38	6.68	0.41	0.66	0.21
Moderate	PGA	0.09	0.25	0.14	0.23	0.17	0.31	0.19	0.37	0.17	0.28
	S_a	0.11	0.30	0.16	0.27	0.21	0.37	0.23	0.44	0.28	0.35
	S_d	9.26	0.25	13.76	0.23	17.62	0.31	19.42	0.37	2.00	0.26
Major	PGA	0.15	0.25	0.24	0.44	0.28	0.41	0.31	0.38	0.29	0.38
	S_a	0.18	0.30	0.28	0.52	0.34	0.49	0.39	0.46	0.52	0.38
	S_d	15.21	0.25	23.98	0.44	28.55	0.41	31.44	0.39	5.65	0.25
Collapse	PGA	0.22	0.27	0.34	0.40	0.40	0.43	0.42	0.33	0.41	0.33
	S_a	0.26	0.32	0.40	0.48	0.48	0.52	0.55	0.51	0.72	0.50
	S_d	22.01	0.27	34.01	0.41	40.32	0.43	44.65	0.43	12.52	0.24

The fragility curves developed for the existing and the retrofitted buildings by PFVD systems providing various effective damping ratios for four damage states and by shear walls are given in Figure 4.2 through Figure 4.16 in terms of peak ground acceleration, spectral acceleration and displacement.

These figures show that the fragility curves for the existing and retrofitted buildings having similar shapes, but with varying values for the different damage states. For all damage states, the physical improvement of the seismic vulnerability due to retrofitting becomes evident in terms of enhanced fragility curves shifting those associated with the existing building to the right when plotted as a function of peak ground acceleration, spectral acceleration and spectral displacement.

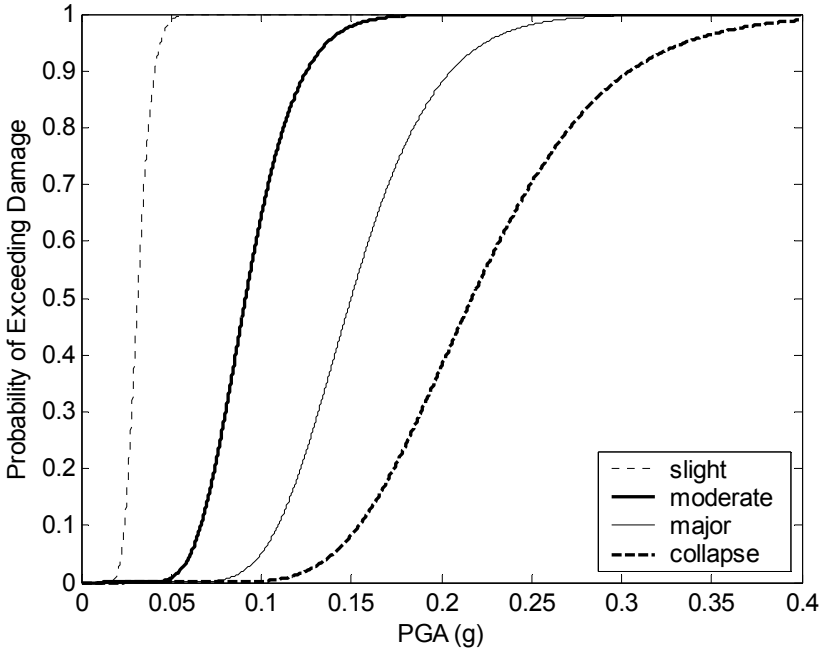

Figure 4.2. Fragility curves for slight, moderate, major, collapse damage levels of existing building in terms of PGA

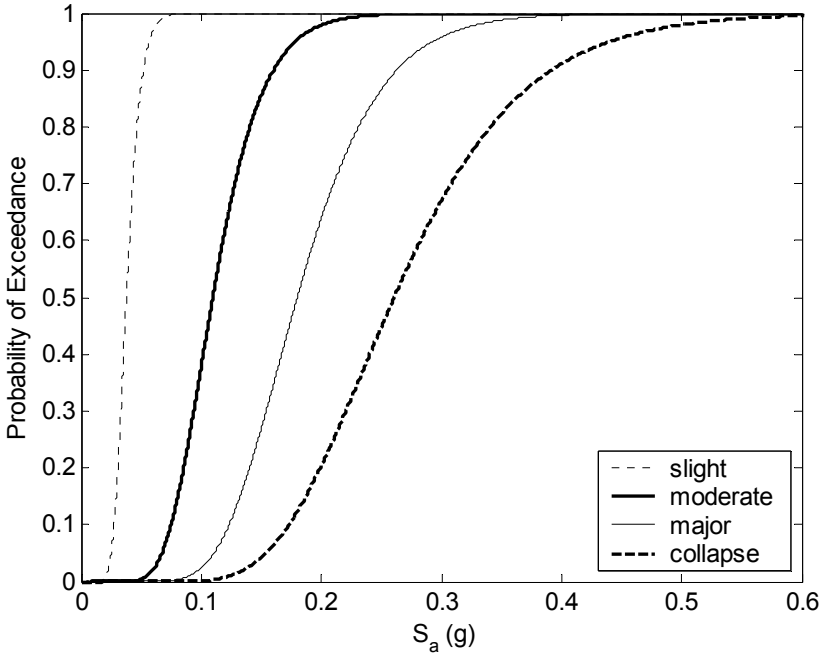

Figure 4.3. Fragility curves for slight, moderate, major, collapse damage levels of existing building in terms of S_a

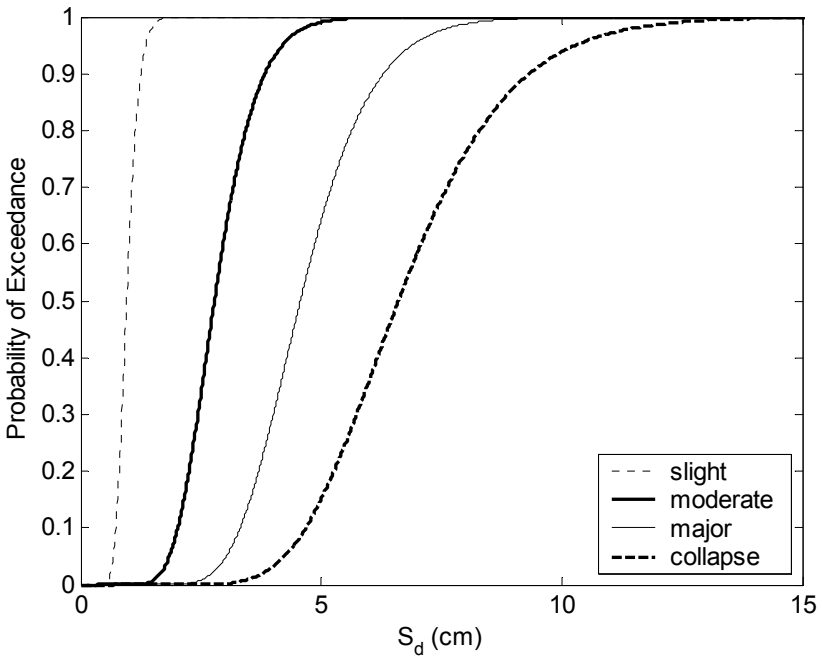

Figure 4.4. Fragility curves for slight, moderate, major, collapse damage levels of existing building in terms of S_d

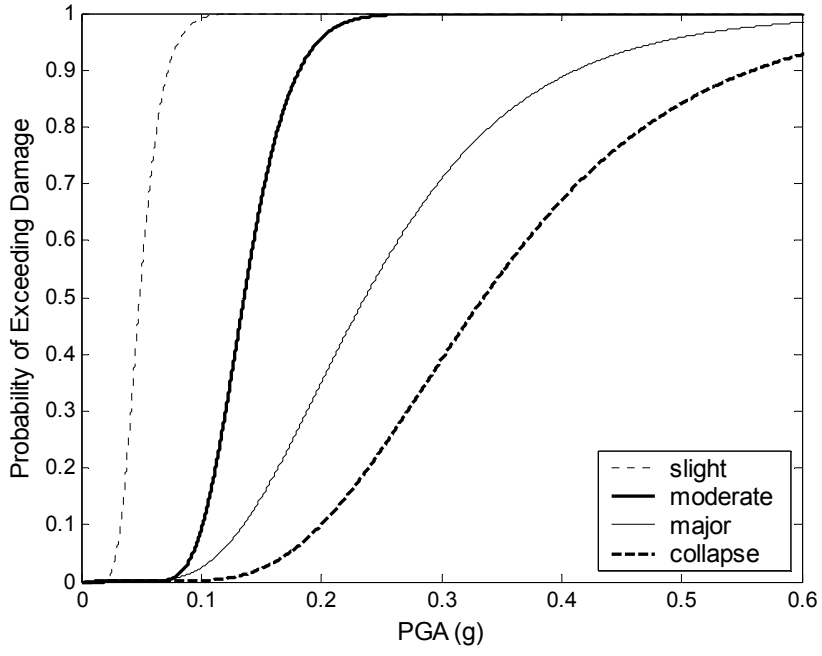

Figure 4.5. Fragility curves for slight, moderate, major, collapse damage levels of Case-1 retrofitted building with $\zeta_{eff} = 10\%$, in terms of PGA

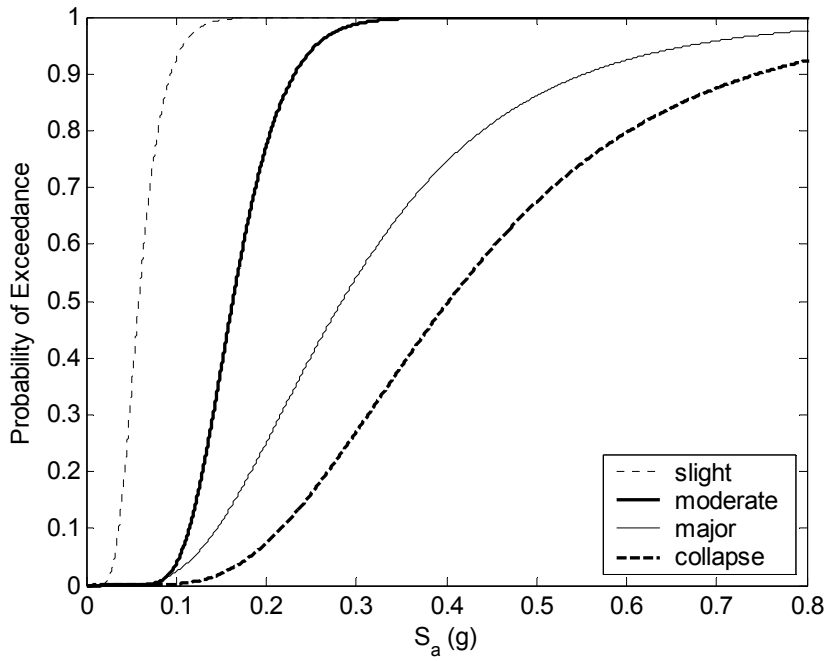

Figure 4.6. Fragility curves for slight, moderate, major, collapse damage levels of Case-1 retrofitted building with $\zeta_{eff} = 10\%$, in terms of S_a

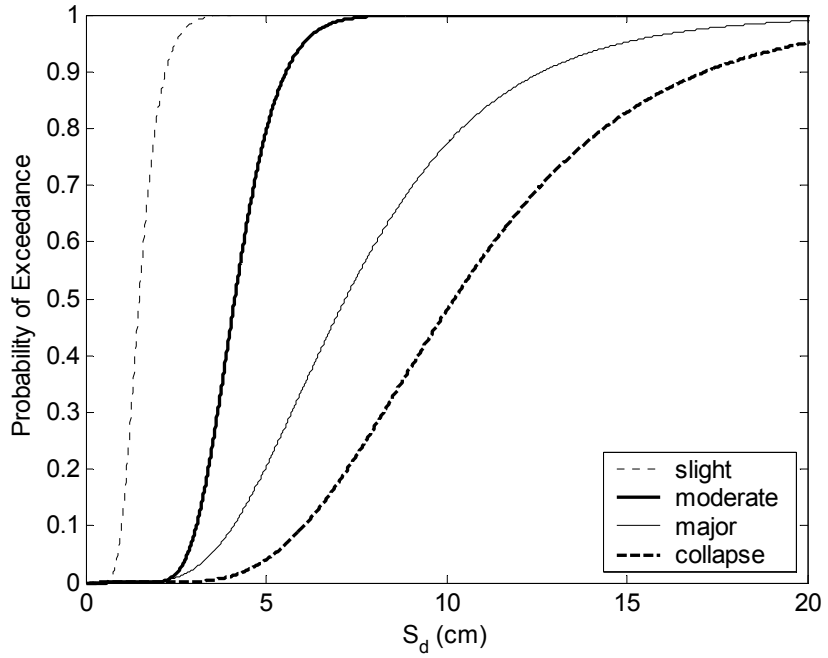

Figure 4.7. Fragility curves for slight, moderate, major, collapse damage levels of Case-1 retrofitted building with $\zeta_{eff} = 10\%$, in terms of S_d

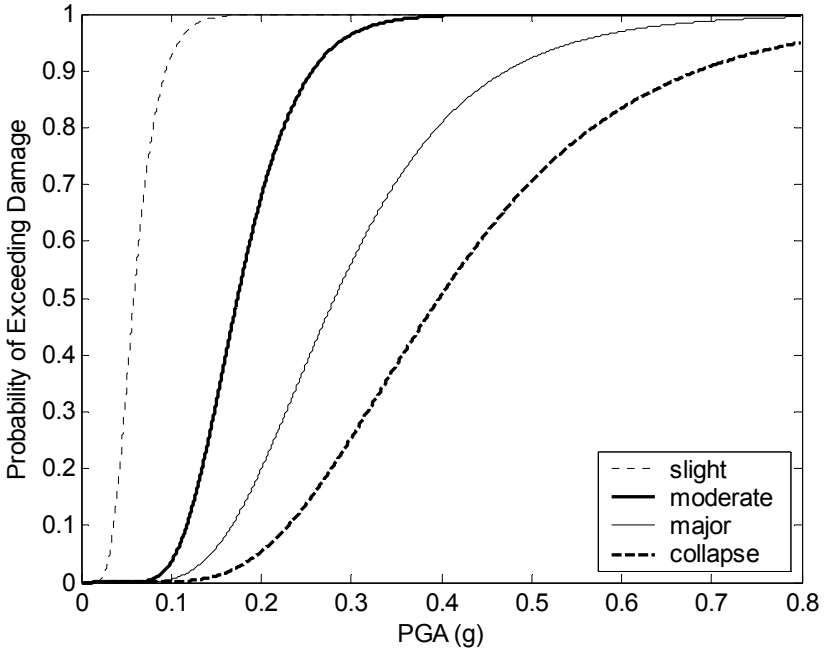

Figure 4.8. Fragility curves for slight, moderate, major, collapse damage levels of Case-2 retrofitted building with $\zeta_{eff} = 15\%$, in terms of PGA

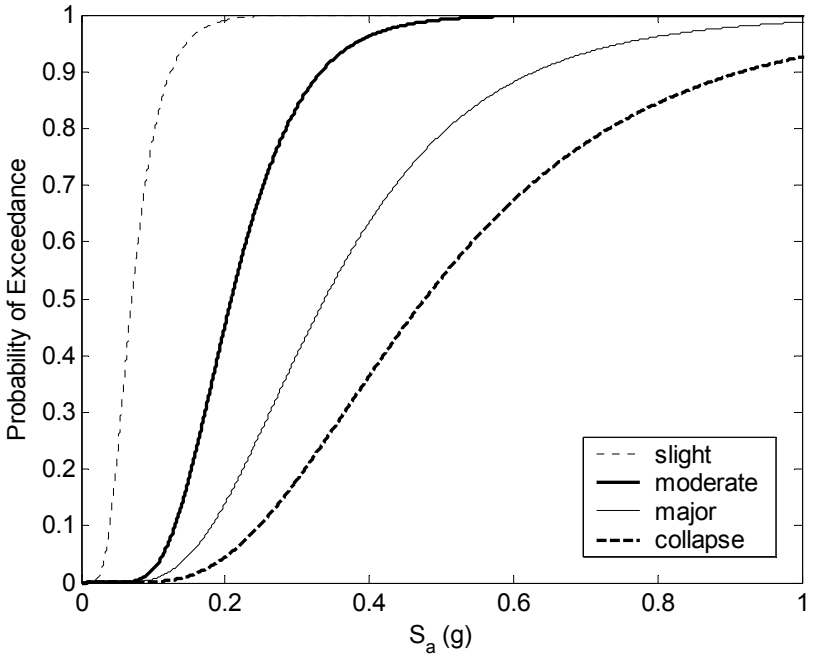

Figure 4.9. Fragility curves for slight, moderate, major, collapse damage levels of Case-2 retrofitted building with $\zeta_{eff} = 15\%$, in terms of S_a

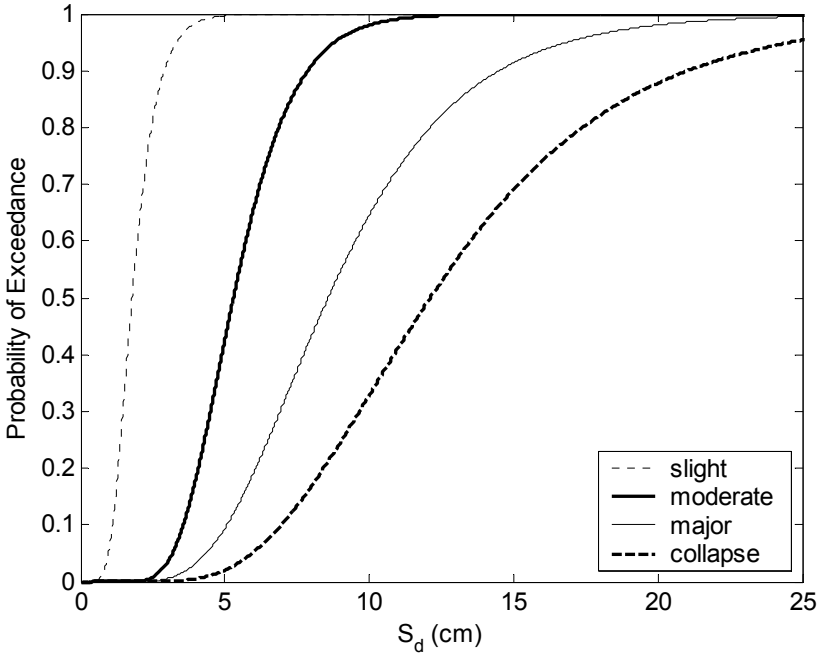

Figure 4.10. Fragility curves for slight, moderate, major, collapse damage levels of Case-2 retrofitted building with $\zeta_{eff} = 15\%$, in terms of S_d

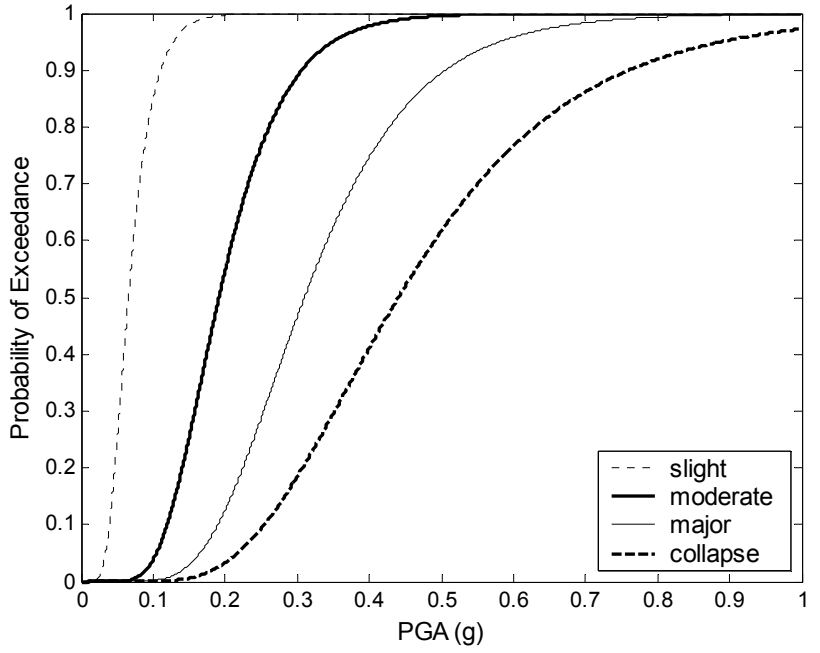

Figure 4.11. Fragility curves for slight, moderate, major, collapse damage levels of Case-3 retrofitted building with $\zeta_{eff} = 20\%$, in terms of PGA

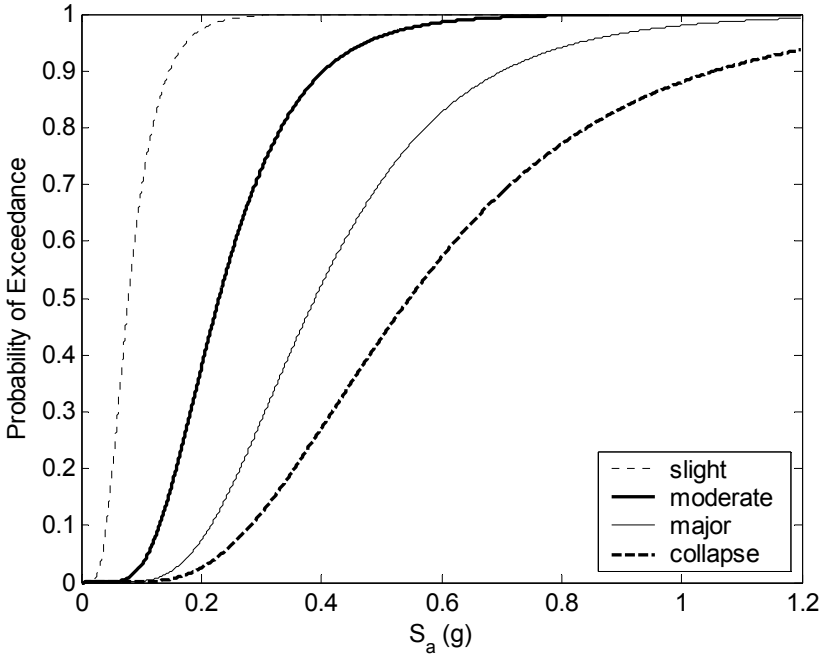

Figure 4.12. Fragility curves for slight, moderate, major, collapse damage levels of Case-3 retrofitted building with $\zeta_{eff} = 20\%$, in terms of S_a

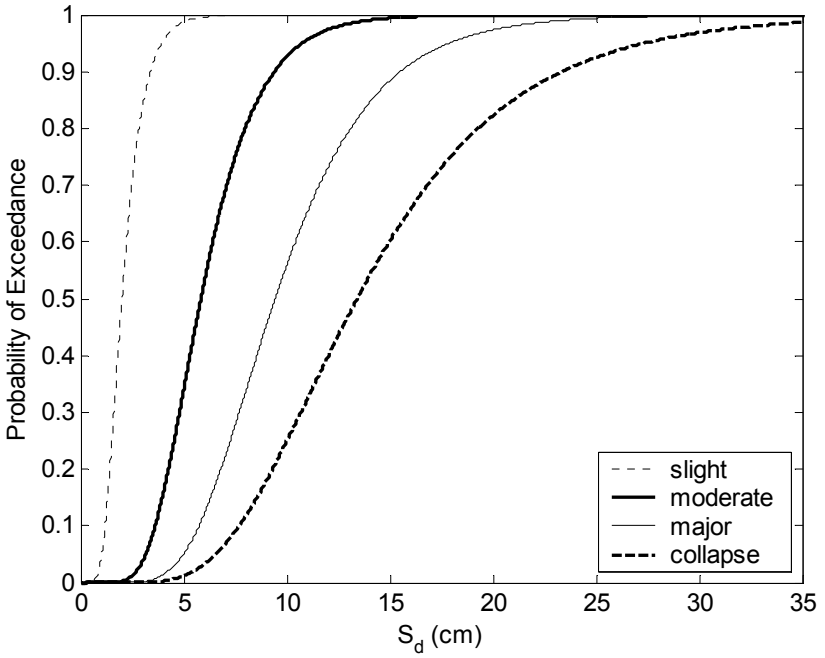

Figure 4.13. Fragility curves for slight, moderate, major, collapse damage levels of Case-3 retrofitted building with $\zeta_{eff} = 20\%$, in terms of S_d

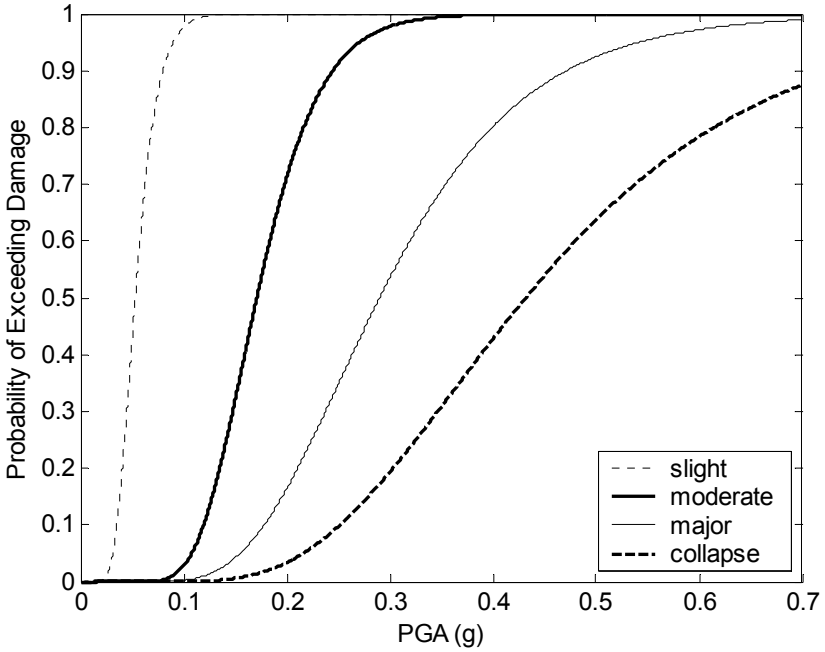

Figure 4.14. Fragility curves for slight, moderate, major, collapse damage levels of Case-4 retrofitted building by using shear walls, in terms of PGA

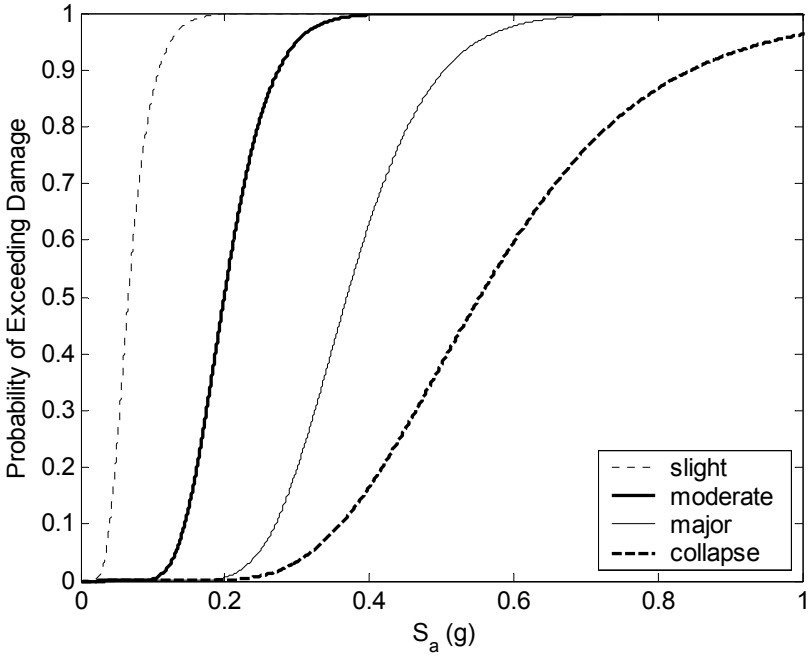

Figure 4.15. Fragility curves for slight, moderate, major, collapse damage levels of Case-4 retrofitted building by using shear walls, in terms of S_a

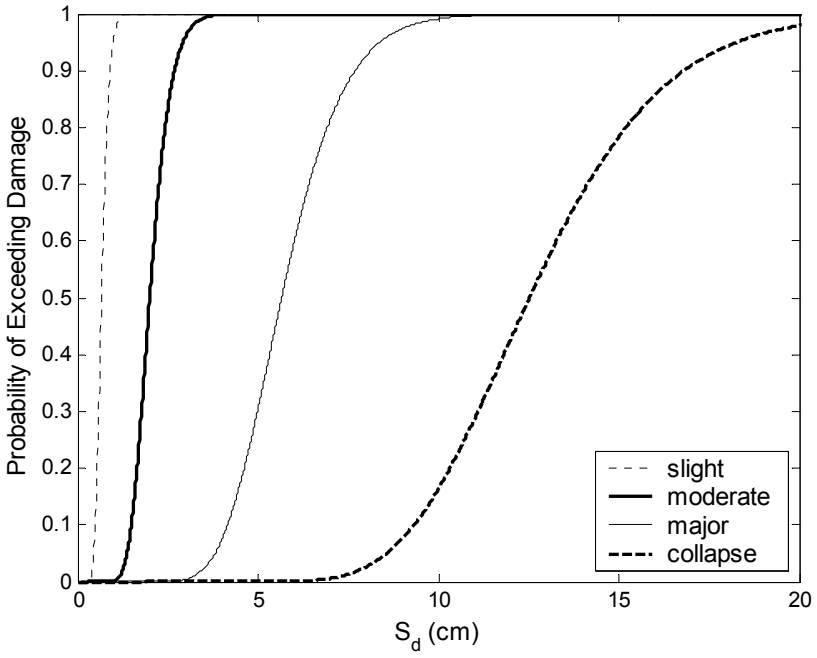

Figure 4.16. Fragility curves for slight, moderate, major, collapse damage levels of Case-4 retrofitted building by using shear walls, in terms of S_d

In order to better understand the effectiveness of retrofit strategies, the fragility curves of the existing and the retrofitted buildings for each damage state were drawn separately in Figure 4.17 through Figure 4.20 by using only PGA as the seismic intensity parameter. As seen from the figures, the effectiveness of passive viscous damper systems in enhancing the seismic performance of the building is greater for collapse and major damage levels than for slight and moderate damage levels. It can be also noted that the effect of retrofit by addition of shear walls have increasing effect with the increase in damage states.

From the results of the fragility analysis, it is noticed that the existing building has probability of having 3.0 per cent collapse, 6.0 per cent major, and 23.0 per cent moderate damage states under the probable scenario earthquake which is given in JICA (2002). In the JICA report, the ratio of heavily, moderately, and partly damaged buildings are reported as 3.2 per cent, 8.3 per cent, and 23.9 per cent, respectively. Therefore, the results found in this study are in line with previous estimates and expert estimations given in JICA report (2002). According to DIE, there are approximately 2160 high-rise buildings in Şişli

region. From the results of this study, the total number of heavily, moderately and partly damaged buildings was estimated as 65, 130, and 497, respectively.

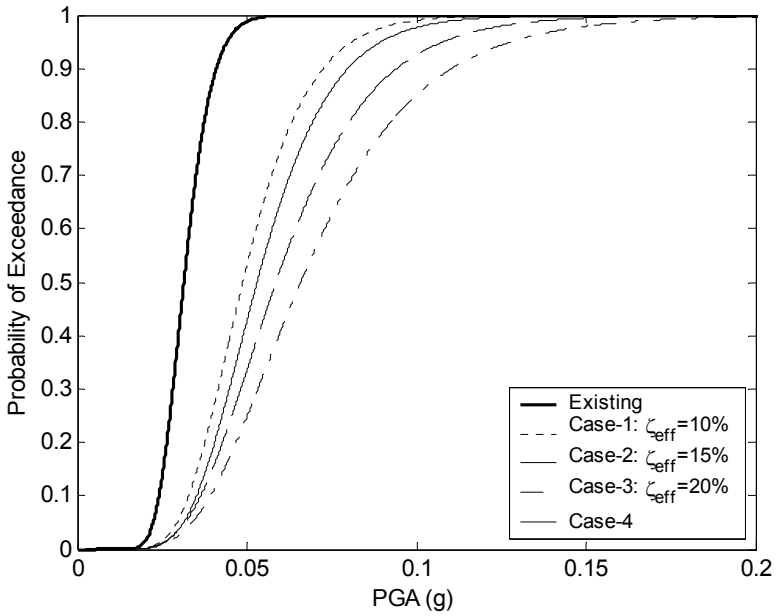

Figure 4.17. Fragility curves of existing and retrofitted buildings for slight damage level in terms of PGA

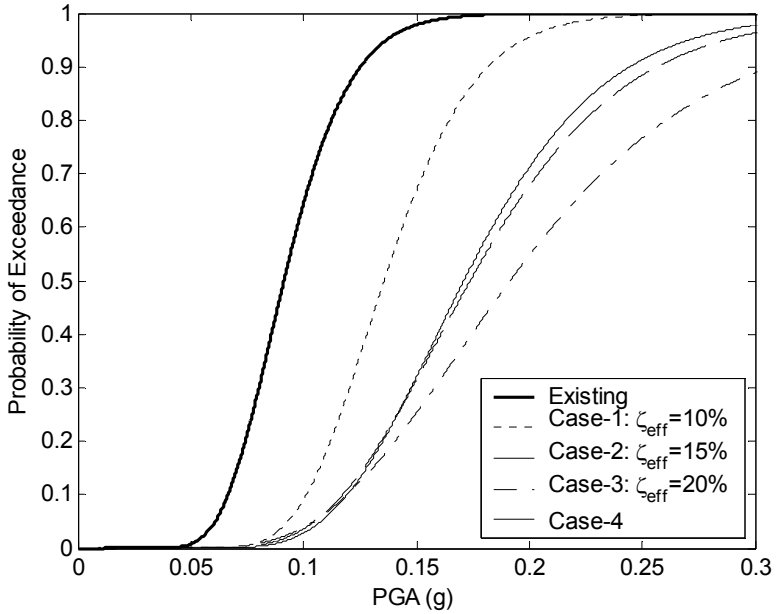

Figure 4.18. Fragility curves of existing and retrofitted buildings for moderate damage level in terms of PGA

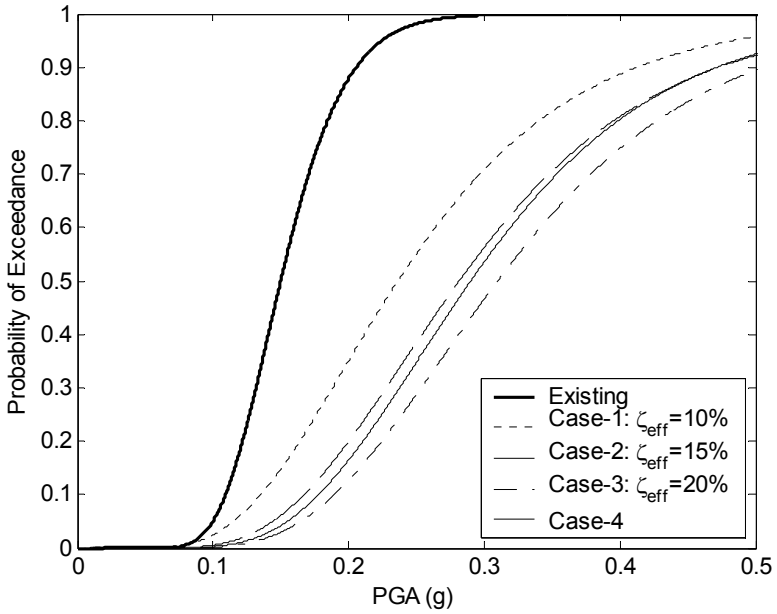

Figure 4.19. Fragility curves of existing and retrofitted buildings for major damage level in terms of PGA

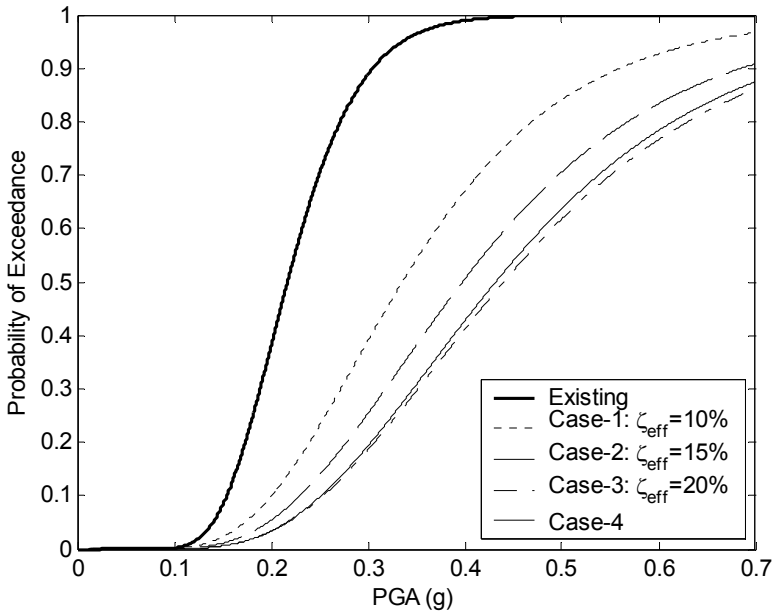

Figure 4.20. Fragility curves of existing and retrofitted buildings for collapse damage level in terms of PGA

Figure 4.21, in the form of a histogram, presents the relationship between the median values of probability of damage states in terms of PGA. The simulated fragility curves in this study demonstrate that, for all levels of damage states, the median fragility values after retrofit are larger than the corresponding values before retrofit. It is clearly observed from the figure that as the effective damping in the structure provided by the viscous dampers increases, the median value also increases. This implies that the effect of retrofit by addition of viscous dampers on the seismic performance is excellent in explaining, for example that the retrofitted building by viscous dampers providing 20 per cent effective damping is up to 2.1 times less fragile compared to the case of existing building in terms of the median values of the damage states. However, it is found that the seismic improvement provided by Case-4 is less than Case-2 for slight damage state, nearly the same with Case-2 for moderate damage state, greater than Case-2 for major damage state, and close to Case-3 for collapse damage state.

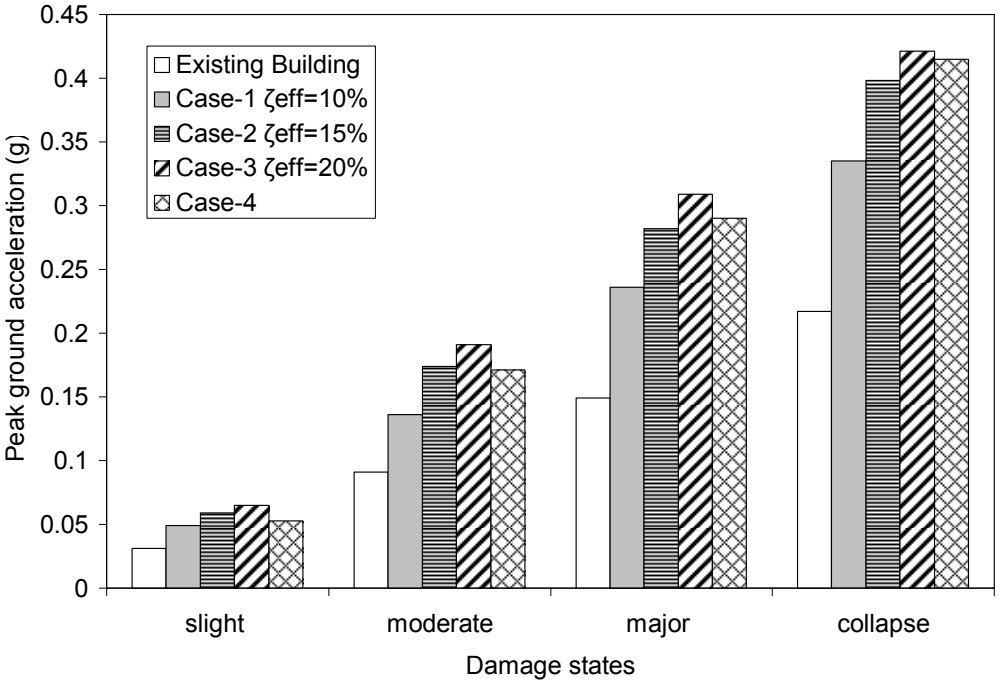

Figure 4.21. Comparison of the median values of PGA for the existing and retrofitted buildings

Considering 10, 15 and 20 per cent effective damping ratios provided by incorporation of viscous dampers in each retrofitting case, the average fragility

enhancement for damage states is computed and plotted as a function of effective damping ratio. An analytical function is interpolated and the enhancement curve is plotted through curve fitting as shown in Figure 4.22. Regression analysis performed between the effective damping ratio in the structure by viscous dampers and the corresponding average percent increase in median values indicates that these two parameters are strongly interdependent with each other. It is evident that percent increase in median values increases logarithmically with increasing effective damping ratio. The relevant function parameters (a and b), Pearson correlation coefficient (R^2), and analysis of variance, F statistics are also summarized in Table 4.3. The proposed function appears to fit the data with a considerably high R^2 value as observed in the figure. In addition, the analysis of variance, F statistics, showed that the relationship was significant at a 0.05 level.

Table 4.3. Parameters of the correlation studied and statistical test results

Model parameters	Average percent increase in median values vs. Effective damping ratio
Trend/Regression type	Logarithmic, f(x)=aLn(x)+b
a	73.05
b	-112
Number of case, n	12
Correlation coefficient, R^2	0.94
F statistics	169.0
P level	0.000
Significance at 0.05 level	Yes

From Figure 4.22, it is also clear that on average 55, 88 and 105 per cent improvement in median values may be achieved for the retrofitted cases having 10, 15 and 20 per cent effective damping ratios with respect to existing case, respectively. This indicates that the fragility enhancement is more significant with the increase in the effective damping ratio. There is a general trend that irrespective of the magnitudes of effective damping ratio provided by viscous dampers used, the addition of PFVD systems

to the structure resulted in less vulnerable structure, which has been shown to have better seismic behavior.

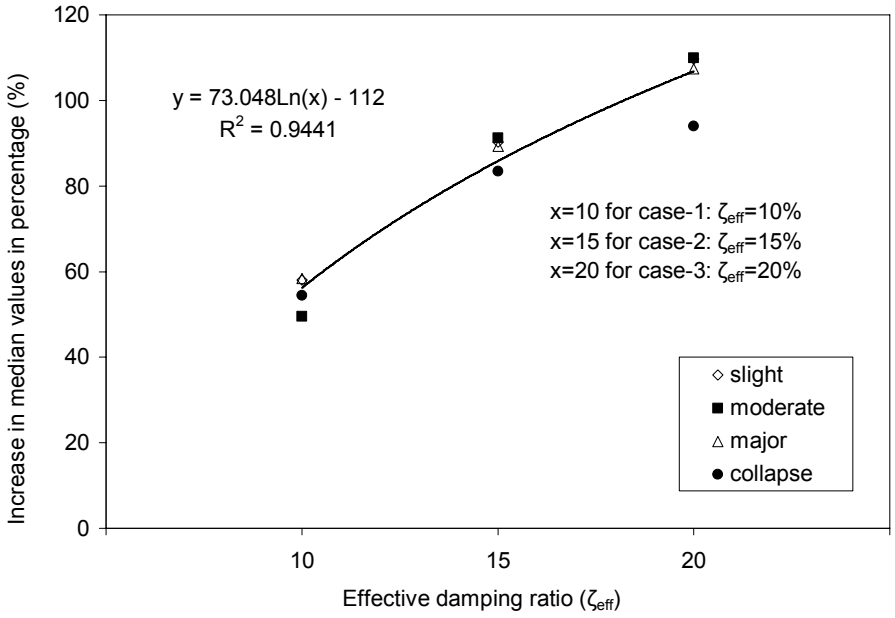

Figure 4.22. Enhancement curve with respect to ζ ratio provided by PFVD systems

5. SEISMIC RISK ANALYSIS

Seismic risk represents the expectancy of damage or losses which are expressed in probabilistic terms in relation to the performance of the built system, as a function of duration. The risk analysis recognizes basically the impossibility of deterministic prediction of events of interest, like future earthquakes, exposure of elements at risk, or chain effects occurring as a consequence of the earthquake-induced damage. Since the expectancy of losses represents the outcome of a more or less explicit and accurate predictive analysis, a prediction must be made somehow in probabilistic terms, by extrapolating or projecting into the future the present experience or know-how. Therefore, in this study, firstly the fragility analyses were combined with the seismic hazard data, in order to determine the seismic risk of the buildings under consideration.

The cost of damage caused by earthquakes to governments, businesses and families are very high. The large economic losses following the earthquakes have shown the need to investigate possible easily applicable mitigation measures that reduce the cost of disasters by minimizing property damage, injuries, and the potential for loss of life, and by reducing emergency response costs, which would otherwise be incurred. The decision to invest in measures that can protect property and life against possible seismic damage is primarily an economic decision. It should therefore be taken in the framework of the cost benefit analysis (CBA) to show if the benefits to life and property protected through mitigation measures exceeds the cost of the measure. Thus, secondly the seismic risks of the existing and retrofitted buildings were further investigated from the economic point of view.

5.1. Seismic Hazard

To examine the effects of the mitigation measures on the seismic performance of the representative structure, the seismic hazard data for the Mecidiyeköy region is used in the seismic risk analysis. The seismic hazard data expressed in terms of PGA values and their probabilities of annual occurrence for the Mecidiyeköy region are given in Figure 5.1 (Sarı, 2003).

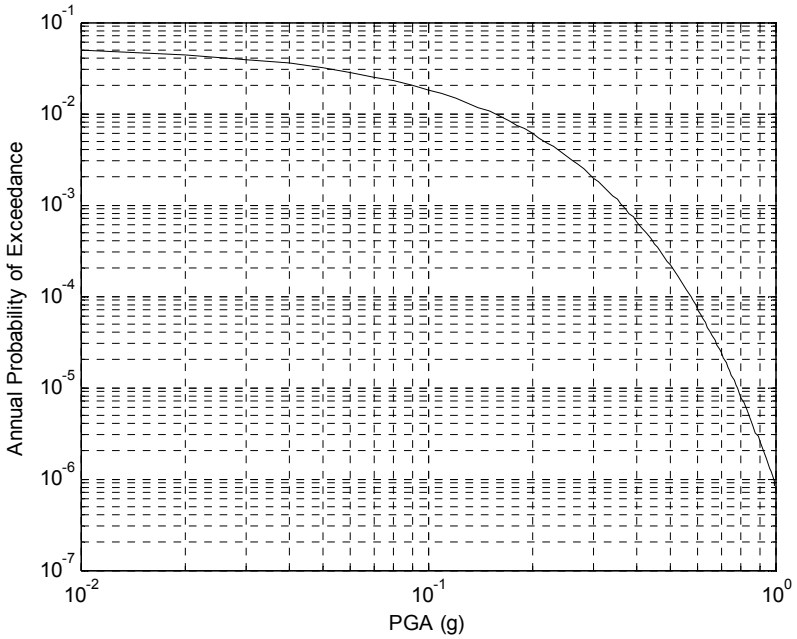

Figure 5.1. Seismic hazard curve: annual probability for exceeding various PGA levels for Mecidiyeköy region (Sarı, 2003)

5.2. Risk Analysis

The probabilistic risk assessment is not a straightforward matter and involves a high computational effort. The probabilistic risk assessment is aiming at computing the annual probability of exceedance of various damage states for a given structural system. The consistent probabilistic approach is based on the idea of Cornell and Krawinkler (2000) using the total probability formula applied in a form that suits the specific needs of seismic risk analysis:

$$P(\ \geq D) = \int_{PGA_{\min}}^{PGA_{\max}} \Phi\left(\geq D \middle| PGA\right) f\left(PGA\right)\ d\left(PGA\right) \tag{5.1}$$

where $P(\ \geq D)$ represents the annual probability of exceedance of damage state D, $\Phi(\ \geq D \middle| PGA)$ is the standard normal cumulative distribution function of damage state function D conditional upon PGA, and $f(PGA)$ is the probability density function of PGA.

This equation can be modified in order to obtain the mean annual rate of exceedance of various damage states:

$$\lambda(\geq D) = \int_{PGA_{\min}}^{PGA_{\max}} P(\geq D|PGA)\ \lambda(PGA)\, d(PGA) \tag{5.2}$$

where $\lambda(PGA)$ is the mean annual rate of occurrence of PGA, $P(\geq D|PGA)$ is the probability of exceedance of damage state D conditional upon PGA.

By using the results of the probabilistic seismic hazard assessment data, $\lambda(PGA)$, and the probabilistic assessment of seismic structural vulnerability, $P(\geq D|PGA)$; the risk was aggregated via summation (or integration) over all levels of the variables of interest using the equation given above. The exceedance probability of various damage states ($P_{exc}(D,T)$) in 1 year, 30 years, 50 years and 100 years assuming that the damage states follows a Poisson distribution were calculated as given in (5.3). The results on risk which were presented as mean annual rate of exceedance of damage state D: $P(\ \geq D|PGA)$; and exceedance probability based on time: $P_{exc}(D,T)$ are given in Table 5.1.

$$P_{exc}(D,T) = \sum_{t=1}^{T} \int_{PGA_{\min}}^{PGA_{\max}} P(\ \geq D|PGA)\ \lambda(PGA)\, e^{-\lambda(PGA_{\min})(t-1)}\, d(PGA) \tag{5.3}$$

The probability of exceedance of damage states in the following 1, 2, 3, 4, 5, 10, 15, 30, 50, and 100 years for the existing buildings is given in Figure 5.2. In order to see the effect of retrofitting measure more clearly, from Figure 5.3 through Figure 5.6, for each damage state the probability of exceedance of the existing and the retrofitted buildings are given, separately. As it is seen from the figures, annual probability of exceedance of slight damage for the existing building is 1.22, 1.36, 1.47 and 1.34 times greater than the annual probability of exceedance of slight damage for retrofitted Case-1, Case-2, Case-3 and Case-4, respectively. For the moderate damage state, annual probability of exceedance for existing building is 1.61, 2.31, 2.65 and 1.95 times greater than the retrofitted Case-1,

Case-2, Case-3 and Case-4 respectively. For the major damage state, the ratio of annual probability of exceedance for the existing building to the retrofitted cases becomes 2.00, 2.99, 3.90 and 3.64. Furthermore, as it is seen from the figure, when the collapse damage states are compared, exceedance probability of the existing building is 2.37, 3.55, 4.74 and 4.04 times greater than that of the retrofitted Case-1, Case-2, Case-3, and Case-4 respectively.

Table 5.1. Summary of the results of seismic risk analysis for the existing building

Damage State	Annual exceedance rate $\lambda(\geq D)$	Exceedance probability $P_{exc}(D,T)$			
		T=1	T=30	T=50	T=100
Slight	3.66E-02	0.0366	0.5877	0.6966	0.7561
Moderate	1.89E-02	0.0189	0.3042	0.3606	0.3913
Major	1.02E-02	0.0102	0.1639	0.1942	0.2108
Collapse	5.23E-03	0.0052	0.0840	0.0996	0.1081

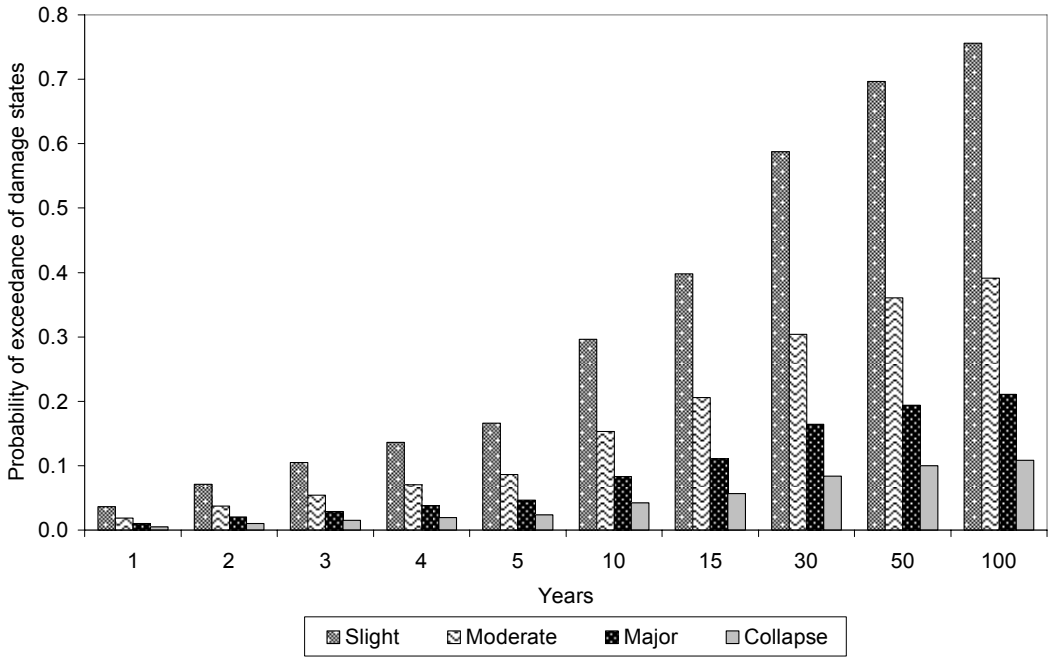

Figure 5.2. Probability of exceedance of each damage state based on time elapsed for the existing building

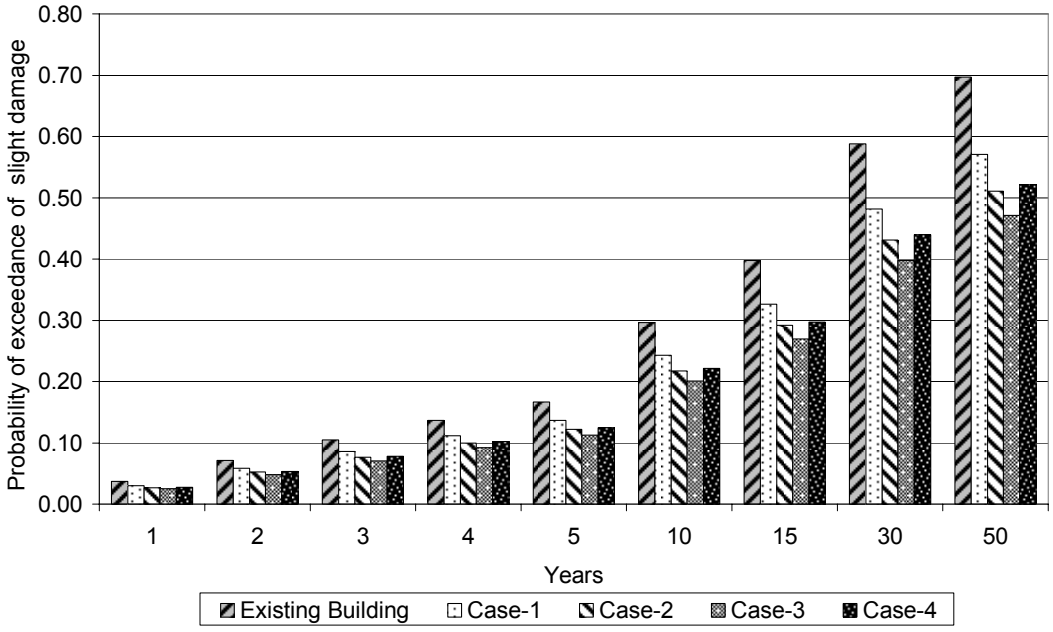

Figure 5.3. Probability of exceedance of slight damage state based on time elapsed for the existing and retrofitted buildings

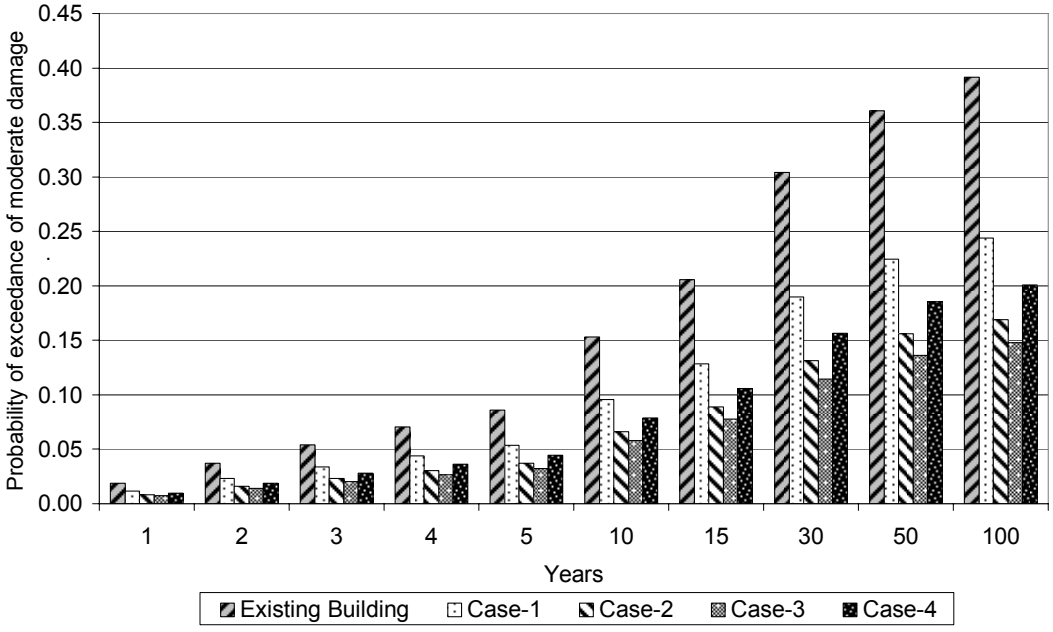

Figure 5.4. Probability of exceedance of moderate damage state based on time elapsed for the existing and retrofitted buildings

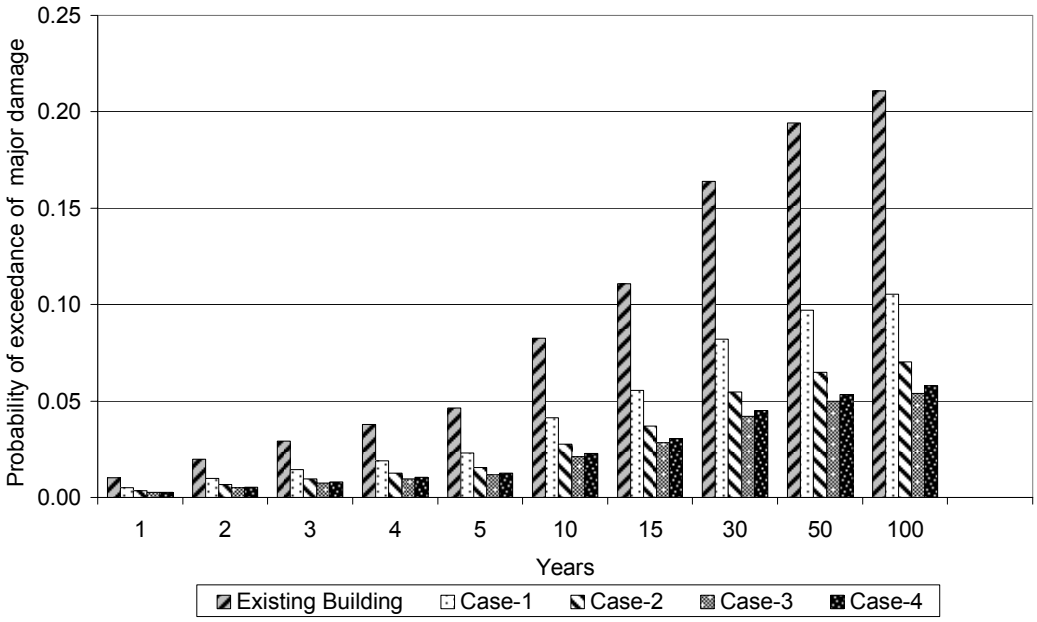

Figure 5.5. Probability of exceedance of major damage state based on time elapsed for the existing and retrofitted buildings

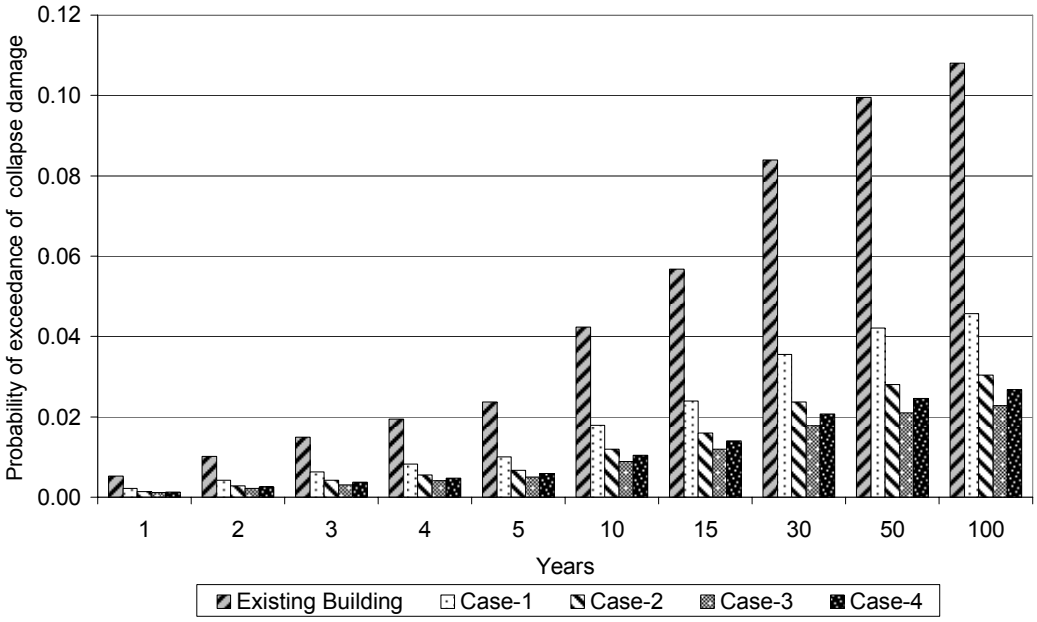

Figure 5.6. Probability of exceedance of collapse damage state based on time elapsed for the existing and retrofitted buildings

5.3. Cost-Benefit Analysis

In order to perform a basic cost-benefit analysis, the expected losses for arbitrary time periods are able to be computed. The basic equation to calculate the present value of losses using a real (social) discount rate d is given by the following equation (Smyth *et al*., 2004):

Total loss in present value for a given time horizon T (in years) =

$$EDC = \sum_{t=1}^{T} \sum_{k=1}^{4} \int_{PGA_{\min}}^{PGA_{\max}} \lambda(PGA)\, e^{-\lambda(PGA_{\min})(t-1)}\, P(D_k \mid PGA)\, \frac{CD_k}{(1+d)^{T-1}}\, d(PGA) \qquad (5.4)$$

in which EDC is the expected discounted cost of losses, $\lambda(PGA)$ is the annual probability of exceeding the PGA value given; $e^{-\lambda(PGA_{\min})(t-1)}$ is the probability that no earthquake has occurred in the previous $(t-1)$ years based on the assumption of a Poisson distribution of earthquake occurrence; $P(D_k \mid PGA)$ is the probability of only kth damage occurring for a PGA value; CD_k is the cost in present dollar value of kth damage limit state being reached and d is the discount rate.

5.3.1. Determination of Discount Rate

A discount rate was used to calculate the value of benefits or costs that will occur in the future. Increasing the discount rate lowered the present value of future benefits. Conversely, assuming a lower discount rate raised the present value of future benefits or costs. The choice of an appropriate discount rate is one of the most difficult aspects of benefit-cost analysis (Wen and Kang, 2001). The various approaches yielded values in the range of three to six per cent. Also, according to FEMA 227 (1992), for public sector considerations, a discount rate of three or four per cent is reasonable; for private sector considerations, a slightly higher rate of four to six per cent is reasonable. In this study, five per cent was used.

5.3.2. Determination of Damage-State Cost Functions

Every one the four discrete damage states D_k has an associated cost CD_k consisting of structural repair and replacement cost, loss of contents, relocation cost, economic (income) loss, and cost of human fatality. It is formulated as follows:

$$CD_k = CD_k^{rep} + CD_k^{con} + CD_k^{rel} + CD_k^{eco} + CD_k^{fat} \tag{5.5}$$

in which CD_k = cost due to kth damage state; CD_k^{rep} =building repair and replacement cost; CD_k^{con} =building content losses; CD_k^{rel} =relocation expenses; CD_k^{eco} =loss of proprietors' income and rental costs; and CD_k^{fat} =cost of human fatality.

Costs suggested by HAZUS for high-rise office buildings used for commercial, professional, technical, and business services were utilized. Repair and replacement cost was evaluated as a function of the limit state-dependent damage, floor area, and replacement cost. For example, for the collapse damage state, values of 170\$/m^2 and 600\$/m^2 were used for the structural damage cost and nonstructural damage cost, respectively, based on the typical replacement value for high rise reinforced concrete office buildings. Loss of contents was evaluated as a function of the damage state, floor area, and unit contents cost, depending on the social function classification of the building.

Relocation costs may be incurred when building damage requires repairs and the post-earthquake function of the facility is partially or fully lost. Total relocation costs depend on gross leasable area and estimated loss of function time. A relocation cost of 1.47\$/m^2 was considered for the fully damage state as suggested by HAZUS (1997).

Economic loss was divided into mainly four parts, income, wages, employees, and output loss. Income loss occurs when the building damage disrupts commercial activity. The two critical parameters to be estimated were the level of income generated by the enterprise and the time of length of disruption. Like rental income and relocation costs, income losses were expected to be proportional to the duration of complete or partial loss of function.

Estimating the economic value of human life and the expected number of fatalities from earthquakes of different magnitudes are important and difficult issues. The estimated value of human life varies widely, ranging from $1.1 million per life to $8 million per life. A review of 25 updated studies (Keech *et al*., 1998) suggested that the loss due to early death consist of foregone taxes and medical, emergency, legal, court, and public assistance administration costs. The summaries of these approaches and the estimated values of human life are presented in FEMA 228 (1992). It is unclear to us how one converts this value into estimates of value of life for Turkey; therefore we have arbitrarily chosen the lower limit of $1 million for our CBA analysis. The fact that most of the people would typically occupy the commercial building for eight hours of the day was also factored into the calculation. Therefore in the loss calculations, the assumed number of lives lost is actually 0.33 (8/24) of the actual lives lost in the event of collapse.

In HAZUS (1997) methodology, a direct relationship is established between structural damage and casualties. The definition of four levels of injury severity and the cost for the injury levels, which were used in the calculation of cost of fatality, according to the guidelines of HAZUS (1997) were given in Table 5.2.

The results of cost calculations for each damage state are given in Table 5.3. It is seen that the cost of damage and contents loss were dominant up to major damage state, but overshadowed by the cost of fatality at collapse damage state.

5.3.3. Determination of Direct Costs of Retrofitting

Also, the realistic estimates of the costs of the retrofitting measures C_i as well as the losses CD_k for each damage state must be established in order to perform cost benefit analysis.

The recent cost of each retrofitting measure designed by using passive viscous damper systems was taken from Taylor Devices Inclination (The company located in USA). Since the initial cost of the construction of passive viscous damper system which doesn't change much according to the properties of the damper system, the costs of each retrofit measure considered were estimated close to each other as given in Table 5.4.

Table 5.2. Casualty rates for RC structures according to guidelines of HAZUS

Injury Severity	Casualty Rates for RC Structures				Injury Description	Cost of Severity ($1000)
	Slight	Moderate	Major	Collapse		
Severity 1	0.0005	0.002	0.01	0.5	Injuries requiring basic medical aid without requiring hospitalization	0.1
Severity 2	0.00005	0.0002	0.001	0.1	Injuries requiring medical care and hospitalization, but not expected to progress into a life threatening status	1
Severity 3	0	0	0.00001	0.02	Injuries that pose an immediate life threatening condition if not treated adequately and expeditiously. The majority of these injuries result because of structural collapse and subsequent collapse or impairment of the occupants.	10
Severity 4	0	0	0.00001	0.02	Instantaneously killed or mortally injured	1000

Table 5.3. Cost calculation for each damage state (CD_k , $)

Damage State	CD^{rep}	CD^{con}	CD^{rel}	CD^{eco}	CD^{fat}
Slight	186.35	2.46	0	614	0.02
Moderate	985.14	66.47	3,688.36	3,682	0.07
Major	4,925.72	1,572.67	11,561.27	23,564	19.8
Collapse	9,554.71	6,646.75	17,465.96	51,546	18,722.00

5.3.4. Determination of Expected Discounted Benefits

The benefit of retrofitting measures applied were calculated by simply taking the difference in expected losses with and without retrofitting measure applied i.e.,

$$EDB_z = EDC_{existing} - \left(EDC_z + Cost\ of\ retrofit_z\right) \tag{5.6}$$

where EDB is the expected discounted benefits, EDC is the expected discounted costs and the subscript j represents the retrofitting case number. The calculated expected discounted costs for the existing and retrofitted buildings were given in Table 5.5. The expected discounted benefits in terms of net present values were calculated for each retrofitting case as given in Table 5.6 .

Table 5.4. Direct costs of retrofitting cases: C_z (\$1000)

Retrofitting Cases	C_z
Case-1: PFVD system providing $\varsigma_{eff} = 10\%$	475
Case-2: PFVD system providing $\varsigma_{eff} = 15\%$	500
Case-3: PFVD system providing $\varsigma_{eff} = 20\%$	550
Case-4: Shear Walls	350

Table 5.5. Expected discounted costs (EDCs) (\$1000)

Years	Expected Costs (\$1000)				
	Existing Building	Retrofitted Buildings			
		Case-1	Case-2	Case-3	Case-4
1	228.15	106.79	72.82	56.64	69.13
2	435.00	203.61	138.83	107.98	131.80
3	622.53	291.39	198.68	154.54	188.62
4	792.55	370.98	252.95	196.75	240.14
5	946.70	443.13	302.15	235.01	286.84
10	1526.60	714.58	487.23	378.97	462.56
25	2232.70	1045.10	712.60	554.26	676.50
50	2425.30	1135.20	774.06	602.07	734.85

Table 5.6. Expected discounted benefits in terms of net present value

Years	Expected Benefits in NPV ($1000)			
	Case-1	Case-2	Case-3	Case-4
1	-353.84	-391.87	-375.69	-190.98
2	-243.81	-251.03	-220.18	-46.80
3	-144.06	-123.35	-79.21	83.91
4	-53.63	-7.60	48.60	202.42
5	28.37	97.35	164.49	309.86
10	336.82	492.17	600.43	714.04
25	712.40	972.90	1131.24	1206.20
50	814.90	1104.04	1276.03	1340.45

5.3.5. Determination of Benefit-Cost Ratio

The criterion that is used for choosing between retrofitting measures considered is to maximize the benefit-cost ratio. The benefit cost ratio is defined as the ratio of benefit of retrofitting measure to the certain initial cost of retrofitting measure i.e.:

$$BCR_z = \frac{EDB_z}{Cost\ of\ retrofit_z} = \frac{EDC_{existing} - \left(EDC_z + Cost\ of\ retrofit_z\right)}{Cost\ of\ retrofit_z} \tag{5.7}$$

Based on the costs of alternative retrofitting measures and the data presented in Table 5.5 and Table 5.6; the relative attractiveness of the three retrofitting alternatives in terms of expected discounted benefits and costs for various time horizons (T, years) were able to be compared. For this purpose, the benefit cost ratios of each retrofitting case for the following 1, 2, 3, 4, 5, 10, 25 and 50 years were determined as shown in Figure 5.7. From the Figure 5.7, among the retrofitting measures by viscous dampers, it is seen that retrofit Case-3 is the most economically attractive option if the relevant time horizon is three years or more and the benefit-cost ratio of the retrofitting Case-3 is higher than the other two cases for all the relevant time horizons considered. It is also seen that it would be cost effective to retrofit the existing building with any of the retrofit alternatives after five years

or more. Although their improvements in seismic performance of the existing structure are different; since the initial certain cost of the retrofitting alternatives by PFVD systems are so close to each other, their benefit cost ratio is close to each other.

Although the seismic performance provided by Case-3 is higher than the other retrofitting measures applied, Case-4 has greater benefit cost ratio than Case-3. This is due to the fact that the initial cost of Case-4 is lower than the initial cost of Case-3. However, in the calculation of the direct costs of retrofitting measures, the costs related to the construction time, disruption of the commercial activity are neglected.

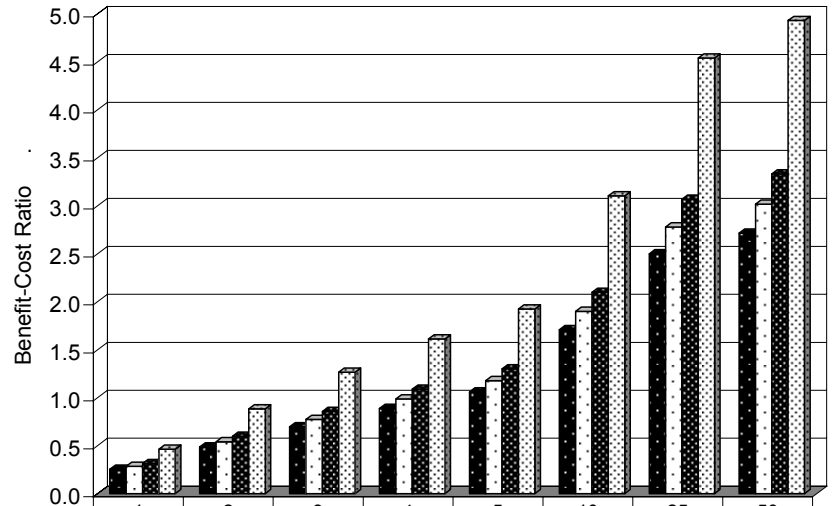

	1	2	3	4	5	10	25	50
Case-1	0.26	0.49	0.70	0.89	1.06	1.71	2.50	2.71
Case-2	0.28	0.54	0.77	0.99	1.18	1.90	2.78	3.02
Case-3	0.31	0.60	0.86	1.09	1.30	2.10	3.07	3.33
Case-4	0.46	0.88	1.27	1.61	1.92	3.10	4.54	4.93

Figure 5.7. Benefit-cost ratio of the existing and retrofitted buildings based on time elapsed.

6. SUMMARY AND CONCLUSIONS

In this study, an application of fragility analysis method to high rise R/C office building with either conventional strengthening techniques such as additional shear walls or innovative strengthening techniques such as additional viscous damping through a device placed as a brace has been investigated through the developed fragility curves. Furthermore, the effectiveness of fluid viscous damper systems in seismic retrofitting was also studied through seismic risk analysis and cost-benefit analysis.

In order to achieve this objective, a systematic approach consisting of deterministic and probabilistic analytical studies for fragility analysis is followed. The fragility curves have been developed for the comparative seismic evaluation of several retrofitting measures by incorporation of fluid viscous dampers applied to a representative high-rise R/C office building selected from Mecidiyeköy region. In the retrofitting strategies, the same type of viscous dampers was used and designed to provide the structure with three different effective damping ratios of 10, 15, and 20 per cent as retrofitting cases: Case-1, Case-2, and Case-3, respectively. In order to compare effectiveness of the innovative technique with conventional technique, the building was also retrofitted by using shear walls as a retrofitting case: Case-4. In the fragility analysis, a set of 240 artificially generated earthquake ground motions compatible with the design spectrum selected to represent the variability in ground motion were used to study nonlinear dynamic responses of the structures before and after retrofit. Four damage states: slight, moderate, major, and collapse were defined to express the condition of damage. Analytical fragility curves are represented by lognormal distribution functions developed as a function of PGA, S_a, and S_d. Since the decision to invest in retrofitting measures that can protect property and life against possible seismic damage is primarily an economic decision; the effectiveness of damper systems in the retrofit of the high rise building is further investigated based on economic point of view by performing seismic risk analysis and cost-benefit analysis.

The following concluding remarks can be made based on the present research:

- The fragility curves developed for the existing and the retrofitted buildings by viscous dampers for four damage states show that the fragility curves for the existing and retrofitted buildings having similar shapes, but with varying values for the different damage states. For all damage states, the physical improvement of the seismic vulnerability due to addition of fluid viscous dampers with increasing effective damping ratio becomes evident in terms of enhanced fragility curves shifting those associated with the existing building to the right when plotted as a function of PGA, S_a, or S_d.
- From the developed fragility curves, the median peak ground acceleration for a 50 per cent probability of exceeding slight, moderate, major, and collapse damage state for the existing building are obtained as 0.031, 0.091, 0.149, and 0.217, respectively. The median PGAs obtained for the retrofitted building Case-1 for the damage states of slight, moderate, major and collapse are 0.049, 0.136, 0.236, and 0.335, respectively. The retrofitted building Case-2 have a median PGA for 50 per cent probability of exceeding slight, moderate, major and collapse damage of 0.059, 0.174, 0.282, and 0.398, respectively. For the retrofitted building Case-3, the values obtained are 0.065, 0.191, 0.309, 0.421 PGA for the slight, moderate, major and collapse damage states, respectively. These results also confirm with the results of the fragility curves constructed in terms of S_a and S_d, which show the similar trend with the fragility curves in terms of PGA. It is clearly observed that as the effective damping in the structure provided by the viscous dampers increases, the median values are also increases. This implies that the effect of retrofit by addition of viscous dampers on the seismic performance is excellent in explaining, for example that the simulated fragility curves for retrofitting cases with viscous dampers show excellent improvement (less fragile) compared to those before retrofit, by as much as two times based on median PGA, S_a and S_d values simulated.
- The retrofitted building Case-4 (by conventional technique) has a median PGA value of 0.053, 0.171, 0.290 and 0.415 for slight, moderate, major and collapse damage states, respectively. Different from the behavior of the retrofitted buildings by PFVD systems, when the median PGA values of the retrofitted Case-4 are compared with the existing building, it is seen that the effectiveness of the retrofitting in enhancing seismic performance increases with the increase in damage states of the building.

- The results of the fragility analysis also indicate that supplemental damping is effective in reducing both structural deformations and internal forces, and hence improving the fragility curves. However, these enhancements are depended mainly on the design values of the viscous dampers used. It is found that the fragility enhancement is more pronounced with the increase in the effective damping ratio. It is also observed that there is a marked difference in the fragility curves of the original and retrofitted buildings, especially for that is designed to provide 20 per cent effective damping.
- Considering 10, 15 and 20 per cent effective damping ratios provided by incorporation of viscous dampers in each retrofitting case, the average fragility enhancement for damage states was computed and an analytical function between the effective damping ratios provided in the structure by viscous dampers and the corresponding average percent increase in median values was interpolated. The proposed function appears to fit the data with a considerably high R^2 value of 0.94. The analysis of variance, F statistics, also showed that the relationship was significant at a 0.05 level.
- The fragility curves developed in this study are used in determining the potential losses resulting from earthquakes based on seismic risk analysis for the existing and retrofitted buildings. The probability of exceedance of damage states in the following 1, 30, 50, and 100 years were calculated. When the annual probability of exceedance of damage states are compared, the maximum improvement is obtained in collapse damage state. It is observed that annual probability of exceedance of collapse damage for the existing building is 2.37, 3.55, 4.74, and 4.04 times greater than the annual probability of exceedance of collapse damage for retrofitted Case-1, Case-2, Case-3, and Case-4 respectively. This also implies that increasing the effective damping ratio of the structures results in remarkably lower seismic probability of damage. When the retrofit by shear walls are compared with the PFVD systems, it is seen that it has lower seismic probability of collapse damage state than Case-1 and Case-2, but greater seismic probability of collapse damage state than Case-3.
- In the cost-benefit analysis, the criterion that is used for comparing the retrofitting cases is to maximize the benefit-cost ratio. It is seen that retrofit Case-4 is the most economically attractive option. When the retrofitted cases by PFVD systems are compared, the benefit-cost ratio of the retrofitting Case-3 is higher than the other two

retrofitted cases for all the relevant time horizons considered. It is also observed that it would be cost effective to retrofit the existing building with any of the retrofit alternatives after five years or more.

- From the results of the fragility analysis, it is noticed that the existing building has probability of having 3.0 per cent collapse, 6.0 per cent major, and 23.0 per cent moderate damage states under the probable scenario earthquake which is given in JICA report. In the JICA report, the ratio of heavily, moderately, and partly damaged buildings are reported as 3.2 per cent, 8.3 per cent, and 23.9 per cent, respectively. Therefore, the results found in this study are in line with previous estimates and expert estimations given in JICA report. According to DIE, there are approximately 2160 high-rise buildings in Şişli region. From the result of this study, the total number of heavily, moderately and partly damaged buildings was estimated as 65, 130, and 497, respectively.

7. RECOMMENDATION FOR FUTURE RESEARCH

In this study, the fact that the building affects the buildings close to it, is neglected. For example, a building collapse or cause a fire also gives harm to the buildings near to it and cause losses. Further work would be useful to understand the effect of those cases.

In order to generalize the fragility curves to all buildings located in İstanbul, different soil considerations and randomness in structural properties can be considered in order to determine the confidence intervals on fragility curves.

Furthermore, a research on the effectiveness of other dampers such as frictional or metallic yield dampers on enhancing the seismic vulnerability of the office type buildings can be investigated and compared with the results of this study.

Different assumptions regarding the appropriate discount rate in the CBA can be examined. Generally in CBA, a constant discount rate over time is chosen. However, recently some economists have suggested the use of declining discount rates for impacts that occur further in the future and some philosophers have suggested the use of discount rate as zero (non-discounting) so that future events are given the same weight as current events.

APPENDIX A: COMPARISON OF DYNAMIC ANALYSIS RESULTS OBTAINED FROM IDARC-2D PROGRAM WITH HAND CALCULATION

A.1. Hand Calculation of a sample R/C Building

The natural period of vibration and the mode shapes of a sample three storey one bay R/C building were found by hand calculation. The elevation view of the sample building is given in Figure A.1. The concrete of the structure has a characteristic yield limit of 30 MPa while the corresponding Young's Modulus is 31800 MPa. The total load of each storey is taken as 17328 kN and assumed to lumped at the centroid of the each storey.

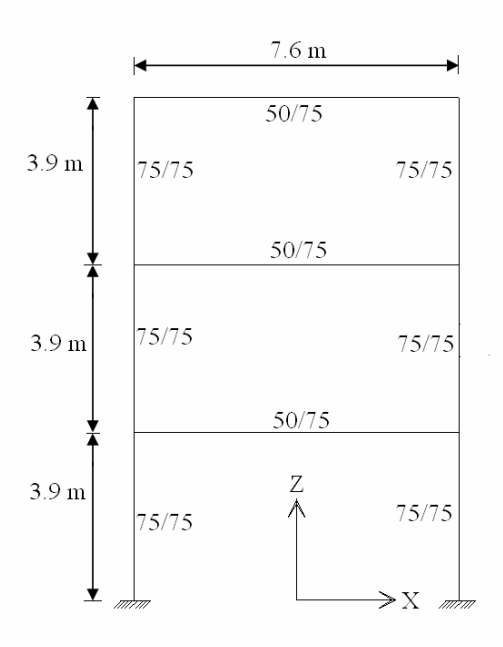

Figure A.1. Three storey R/C sample structure

Firstly, the differential equations of the motion and the frequency equation are written as given below in the equations (A.1) through (A.26).

Mass of the each storey was found:

$$m_1 = m_2 = m_3 = 1766.361 \text{ kNs}^2/\text{m} \qquad \text{(A.1)}$$

Differential equation of motion:

$$[M]\{\ddot{u}\}+[K]\{u\}=\{f\} \tag{A.2}$$

Inertia Matrix:

$$[M]=\begin{bmatrix}1766.361 & 0 & 0\\ 0 & 1766.361 & 0\\ 0 & 0 & 1766.361\end{bmatrix} \tag{A.3}$$

Stiffness Matrix:

$$[K]=\begin{bmatrix}522146 & -300623 & 74389\\ -300623 & 345238 & -144482\\ 74389 & -144482 & 85164\end{bmatrix} \tag{A.4}$$

$$\{f\}=-\ddot{y}_s\begin{Bmatrix}m_1\\ m_2\\ m_3\end{Bmatrix} \tag{A.5}$$

$$[M]\{\ddot{u}\}+[K]\{u\}=\{f\} \tag{A.6}$$

$$\begin{bmatrix}1766.361 & 0 & 0\\ 0 & 1766.361 & 0\\ 0 & 0 & 1766.361\end{bmatrix}\begin{Bmatrix}\ddot{u}_1\\ \ddot{u}_2\\ \ddot{u}_3\end{Bmatrix}+\begin{bmatrix}522146 & -300623 & 74389\\ -300623 & 345238 & -144482\\ 74389 & -144482 & 85164\end{bmatrix}\begin{Bmatrix}u_1\\ u_2\\ u_3\end{Bmatrix}=-\ddot{y}_s\begin{Bmatrix}1766.361\\ 1766.361\\ 1766.361\end{Bmatrix} \tag{A.7}$$

$$\left|[K]-w^2[M]\right|=0 \tag{A.8}$$

$$\left|\begin{bmatrix}522146 & -300623 & 74389\\ -300623 & 345238 & -144482\\ 74389 & -144482 & 85164\end{bmatrix}-w^2\begin{bmatrix}1766.361 & 0 & 0\\ 0 & 1766.361 & 0\\ 0 & 0 & 1766.361\end{bmatrix}\right|=0 \tag{A.9}$$

$$\left|[K]-w^2[M]\right| = \begin{bmatrix} 7.02-\lambda & -4.04 & 1.0 \\ -4.04 & 4.64-\lambda & -1.94 \\ 1.0 & -1.94 & 1.14-\lambda \end{bmatrix} = 0 \qquad \text{(A.10)}$$

For $\lambda = \dfrac{w^2 1766.361}{74389.38}$, by solving the equation we obtain :

$$3.13-\lambda^3-24.78\lambda+12.8\lambda^2 = 0 \qquad \text{(A.11)}$$

$$\lambda_1 = 0.13573 \quad \Rightarrow \quad w_1 = 2.3908 \text{ rad/s} \qquad \text{(A.12)}$$

$$\lambda_2 = 2.2048 \quad \Rightarrow \quad w_2 = 9.6361 \text{ rad/s} \qquad \text{(A.13)}$$

$$\lambda_3 = 10.459 \quad \Rightarrow \quad w_3 = 20.9875 \text{ rad/s} \qquad \text{(A.14)}$$

Natural period of each mode:

$$T_1 = \frac{2\pi}{w_1} = \frac{2\pi}{2.3908} = 2.628 \ \text{ sec.} \qquad \text{(A.15)}$$

$$T_2 = \frac{2\pi}{w_2} = \frac{2\pi}{9.6361} = 0.652 \ \text{ sec.} \qquad \text{(A.16)}$$

$$T_3 = \frac{2\pi}{w_3} = \frac{2\pi}{20.9875} = 0.299 \ \text{ sec.} \qquad \text{(A.17)}$$

Mode shapes:

$$\left|[K]-w^2[M]\right|\{\varphi\} = 0 \qquad \text{(A.18)}$$

$$\begin{bmatrix} 522146 & -300623 & 74389 \\ -300623 & 345238 & -144482 \\ 74389 & -144482 & 85164 \end{bmatrix} - 2.3908^2 \begin{bmatrix} 1766.361 & 0 & 0 \\ 0 & 1766.361 & 0 \\ 0 & 0 & 1766.361 \end{bmatrix} \begin{Bmatrix} \varphi_{11} \\ \varphi_{21} \\ \varphi_{31} \end{Bmatrix} = 0 \quad \text{(A.19)}$$

Assume $\varphi_{31} = 1$, solve the matrix $\Rightarrow \quad \varphi_{11} = 0.2284 \quad \varphi_{21} = 0.6337$

$$\{\varphi\}_1 = \begin{Bmatrix} 0.2284 \\ 0.6337 \\ 1 \end{Bmatrix} \quad \text{(A.20)}$$

For the second mode:

$$\begin{bmatrix} 522146 & -300623 & 74389 \\ -300623 & 345238 & -144482 \\ 74389 & -144482 & 85164 \end{bmatrix} - 9.6361^2 \begin{bmatrix} 1766.361 & 0 & 0 \\ 0 & 1766.361 & 0 \\ 0 & 0 & 1766.361 \end{bmatrix} \begin{Bmatrix} \varphi_{12} \\ \varphi_{22} \\ \varphi_{32} \end{Bmatrix} = 0 \quad \text{(A.21)}$$

Assume $\varphi_{12} = 1$, solve the matrix $\Rightarrow \quad \varphi_{22} = 0.9801 \quad \varphi_{32} = -0.8504$

$$\{\varphi\}_2 = \begin{Bmatrix} 1 \\ 0.9801 \\ -0.8504 \end{Bmatrix} \quad \text{(A.22)}$$

For the third mode:

$$\begin{bmatrix} 522146 & -300623 & 74389 \\ -300623 & 345238 & -144482 \\ 74389 & -144482 & 85164 \end{bmatrix} - 20.9875^2 \begin{bmatrix} 1766.361 & 0 & 0 \\ 0 & 1766.361 & 0 \\ 0 & 0 & 1766.361 \end{bmatrix} \begin{Bmatrix} \varphi_{13} \\ \varphi_{23} \\ \varphi_{33} \end{Bmatrix} = 0 \quad \text{(A.23)}$$

Assume $\varphi_{23} = 1$, solve the matrix $\Rightarrow \quad \varphi_{13} = 0.9801 \quad \varphi_{33} = -0.8504$

$$\{\varphi\}_3 = \begin{Bmatrix} -1.2748 \\ 1 \\ -0.3453 \end{Bmatrix} \tag{A.24}$$

$$[\phi] = \begin{bmatrix} 0.2284 & 1 & -1.2748 \\ 0.6337 & 0.9801 & 1 \\ 1 & -0.8539 & -0.3453 \end{bmatrix} \tag{A.25}$$

When the mode shapes are maximum normalized we obtain:

$$[\phi] = \begin{bmatrix} 0.2284 & 1 & -1 \\ 0.6337 & 0.9801 & 0.7844 \\ 1 & -0.8539 & -0.2708 \end{bmatrix} \tag{A.26}$$

A.2. Linear Dynamic Analysis of a sample R/C Building by IDARC Program

Initial dynamic characteristics of the sample structure are obtained by using IDARC structural analysis program. The natural period of vibration of each mode and the mode shape of the structure is given in Tables A.1 and A.2. It is seen that the results obtained are in compliance with the results of hand calculations.

Table A.0.1. Modes of structure

Mode	Period
1	2.61
2	0.6519
3	0.2993

Table A.0.2. Mode shape of the structure (Eigen vectors maximum normalized)

	Mode 1	Mode 2	Mode 3
Story 1	0.228	1	-1
Story 2	0.636	0.980	0.784
Story 3	1	-0.852	-0.271

APPENDIX B: IDARC INPUT CODES

B.1. IDARC Input Code for the Existing Building (Time History Analysis)

CASE STUDY : Typical Office Building in Turkey (Halkbank)
Control Data
12,1,1,1,0,0,0,1,1
Element Types
6,1,0,0,0,0,0,0,0,0
Element Data
48,35,0,0,0,0,0,0,0
Units System : kN - mm
2
Floor Elevations
2750, 5500, 8250, 11000, 13750, 16500, 19250, 22000, 24750, 27500, 30250, 33000
Description of Identical Frames
1
Plan Configuration: No of Column Lines
4
Nodal Weights
1,1, 43.6, 43.6, 43.6, 43.6
2,1, 43.6, 43.6, 43.6, 43.6
3,1, 43.6, 43.6, 43.6, 43.6
4,1, 43.6, 43.6, 43.6, 43.6
5,1, 43.6, 43.6, 43.6, 43.6
6,1, 43.6, 43.6, 43.6, 43.6
7,1, 43.6, 43.6, 43.6, 43.6
8,1, 43.6, 43.6, 43.6, 43.6
9,1, 43.6, 43.6, 43.6, 43.6
10,1, 43.6, 43.6, 43.6, 43.6
11,1, 43.6, 43.6, 43.6, 43.6
12,1, 43.6, 43.6, 43.6, 43.6

Code for Specification of User Properties

0

Concrete Properties

1, 16e-3, 0.0, 0.0, 0.0, 0.0, 0.0

Reinforcement Properties

1, 2.2e-1, 0.0, 0.0, 0.0, 0.0

Hysteretic Modeling Rules

3

1, 1, 2, 0.1, 0.0, 1.0, 2

2, 1, 2, 0.1, 0.0, 1.0, 2

3, 1, 2, 0.1, 0.0, 0.1, 0

Moment Curvature Envelope Generation

0

Column Dimensions

1

1,1,1, 0.0, 2750.0, 0.0, 200.0,

1, 800.0, 800.0, 20.0, 1600.0, 10.0, 200.0, 0.5

1, 800.0, 800.0, 20.0, 1600.0, 10.0, 200.0, 0.5

1

2,1,1, 0.0, 2750.0, 0.0, 200.0,

1, 800.0, 950.0, 20.0, 1900.0, 10.0, 200.0, 0.5

1, 800.0, 950.0, 20.0, 1900.0, 10.0, 200.0, 0.5

1

3,1,1, 0.0, 2750.0, 200.0, 200.0,

1, 800.0, 550.0, 20.0, 1100.0, 10.0, 200.0, 0.5

1, 800.0, 550.0, 20.0, 1100.0, 10.0, 200.0, 0.5

1

4,1,1, 0.0, 2750.0, 200.0, 200.0,

1, 800.0, 650.0, 20.0, 1400.0, 10.0, 200.0, 0.5

1, 800.0, 650.0, 20.0, 1400.0, 10.0, 200.0, 0.5

1

5,1,1, 0.0, 2750.0, 200.0, 200.0,

1, 800.0, 450.0, 20.0, 900.0, 10.0, 200.0, 0.5

1, 800.0, 450.0, 20.0, 900.0, 10.0, 200.0, 0.5

1

6,1,1, 0.0, 2750.0, 200.0, 200.0,

1, 800.0, 450.0, 20.0, 900.0, 10.0, 200.0, 0.5

1, 800.0, 450.0, 20.0, 900.0, 10.0, 200.0, 0.5

Beam Moment Curvature Envelope Generation

0

Beam Dimensions

1

1,1,1, 7860.0, 375.0, 375.0

2, 600.0, 400.0, 300.0, 0.0, 25.0, 1200.0, 1556.0, 10.0, 200.0

2, 600.0, 400.0, 300.0, 0.0, 25.0, 1200.0, 1556.0, 10.0, 200.0

Column Connectivity

1,1,1,1,0,1

2,2,1,2,0,1

3,2,1,3,0,1

4,1,1,4,0,1

5,1,1,1,1,2

6,2,1,2,1,2

7,2,1,3,1,2

8,1,1,4,1,2

9,1,1,1,2,3

10,2,1,2,2,3

11,2,1,3,2,3

12,1,1,4,2,3

13,1,1,1,3,4

14,2,1,2,3,4

15,2,1,3,3,4

16,1,1,4,3,4

17,3,1,1,4,5

18,4,1,2,4,5

19,4,1,3,4,5

20,3,1,4,4,5

21,3,1,1,5,6

22,4,1,2,5,6

23,4,1,3,5,6

24,3,1,4,5,6

25,5,1,1,6,7

26,6,1,2,6,7

27,6,1,3,6,7

28,5,1,4,6,7

29,5,1,1,7,8

30,6,1,2,7,8

31,6,1,3,7,8

32,5,1,4,7,8

33,5,1,1,8,9

34,6,1,2,8,9

35,6,1,3,8,9

36,5,1,4,8,9

37,5,1,1,9,10

38,6,1,2,9,10

39,6,1,3,9,10

40,5,1,4,9,10

41,5,1,1,10,11

42,6,1,2,10,11

43,6,1,3,10,11

44,5,1,4,10,11

45,5,1,1,11,12

46,6,1,2,11,12

47,6,1,3,11,12

48,5,1,4,11,12

Beam Connectivity

1,1,1,1,1,2

2,1,1,1,2,3

3,1,1,1,3,4

4,1,2,1,1,2

5,1,2,1,2,3
6,1,2,1,3,4
7,1,3,1,1,2
8,1,3,1,2,3
9,1,3,1,3,4
10,1,4,1,1,2
11,1,4,1,2,3
12,1,4,1,3,4
13,1,5,1,1,2
14,1,5,1,2,3
15,1,5,1,3,4
16,1,6,1,1,2
17,1,6,1,2,3
18,1,6,1,3,4
19,1,7,1,1,2
20,1,7,1,2,3
21,1,7,1,3,4
22,1,8,1,1,2
23,1,8,1,2,3
24,1,8,1,3,4
25,1,9,1,1,2
26,1,9,1,2,3
27,1,9,1,3,4
28,1,10,1,1,2
29,1,10,1,2,3
30,1,10,1,3,4
31,1,11,1,1,2
32,1,11,1,2,3
33,1,11,1,3,4
34,1,12,1,1,2
35,1,12,1,2,3
36,1,12,1,3,4

Type of Analysis

3
Static loads
0,0,0,0
Dynamic Analysis Control Data
0.21659,0.0,0.005,30,5,3
Wave data
0,3000,0.01
Synthetic Earthquakes
acc61.dat
Output options
0
0 0 0 0 0
Story Output Control
1,0.02,10
floor10ex.out
Hys output
0,0,0,0,0,0

B.2. IDARC Input Code for the Retrofitted Building

Case Study: Typical Office Building (Retrofitted by Viscous Braces)
Control Data
12,1,1,1,0,0,0,1,1
Element Types
6,1,0,0,0,0,1,0,0,0
Element Data
48,36,0,0,0,0,0,12,0
Units System : KN - MM
2
Floor Elevations
2750, 5500, 8250, 11000, 13750, 16500, 19250, 22000, 24750, 27500, 30250, 33000
Description of Identical Frames
1

Plan Configuration: No of Column Lines

4

Nodal Weights

1,1, 43.6, 43.6, 43.6, 43.6

2,1, 43.6, 43.6, 43.6, 43.6

3,1, 43.6, 43.6, 43.6, 43.6

4,1, 43.6, 43.6, 43.6, 43.6

5,1, 43.6, 43.6, 43.6, 43.6

6,1, 43.6, 43.6, 43.6, 43.6

7,1, 43.6, 43.6, 43.6, 43.6

8,1, 43.6, 43.6, 43.6, 43.6

9,1, 43.6, 43.6, 43.6, 43.6

10,1, 43.6, 43.6, 43.6, 43.6

11,1, 43.6, 43.6, 43.6, 43.6

12,1, 43.6, 43.6, 43.6, 43.6

Code for Specification of User Properties

0

Concrete Properties

1, 16e-3, 0.0, 0.0, 0.0, 0.0, 0.0

Reinforcement Properties

1, 2.2e-1, 0.0, 0.0, 0.0, 0.0

Hysteretic Modeling Rules

3

1, 1, 2, 0.1, 0.0, 1.0, 2

2, 1, 2, 0.1, 0.0, 1.0, 2

3, 1, 2, 0.1, 0.0, 0.1, 0

Moment Curvature Envelope Generation

0

Column Dimensions

1

1,1,1, 0.0, 2750.0, 0.0, 200.0,

1, 800.0, 800.0, 20.0, 1600.0, 10.0, 200.0, 0.5

1, 800.0, 800.0, 20.0, 1600.0, 10.0, 200.0, 0.5

1

2,1,1, 0.0, 2750.0, 0.0, 200.0,

1, 800.0, 950.0, 20.0, 1900.0, 10.0, 200.0, 0.5

1, 800.0, 950.0, 20.0, 1900.0, 10.0, 200.0, 0.5

1

3,1,1, 0.0, 2750.0, 200.0, 200.0,

1, 800.0, 550.0, 20.0, 1100.0, 10.0, 200.0, 0.5

1, 800.0, 550.0, 20.0, 1100.0, 10.0, 200.0, 0.5

1

4,1,1, 0.0, 2750.0, 200.0, 200.0,

1, 800.0, 650.0, 20.0, 1400.0, 10.0, 200.0, 0.5

1, 800.0, 650.0, 20.0, 1400.0, 10.0, 200.0, 0.5

1

5,1,1, 0.0, 2750.0, 200.0, 200.0,

1, 800.0, 450.0, 20.0, 900.0, 10.0, 200.0, 0.5

1, 800.0, 450.0, 20.0, 900.0, 10.0, 200.0, 0.5

1

6,1,1, 0.0, 2750.0, 200.0, 200.0,

1, 800.0, 450.0, 20.0, 900.0, 10.0, 200.0, 0.5

1, 800.0, 450.0, 20.0, 900.0, 10.0, 200.0, 0.5

Beam Moment Curvature Envelope Generation

0

Beam Dimensions

1

1,1,1, 7860.0, 375.0, 375.0

2, 600.0, 400.0, 300.0, 0.0, 25.0, 1556.0, 1556.0, 10.0, 200.0

2, 600.0, 400.0, 300.0, 0.0, 25.0, 1556.0, 1556.0, 10.0, 200.0

Viscous Brace Properties (Kelvin Model)

0, 0

1, 0.36, 381, 1.0

Column Connectivity

1,1,1,1,0,1

2,2,1,2,0,1

3,2,1,3,0,1
4,1,1,4,0,1
5,1,1,1,1,2
6,2,1,2,1,2
7,2,1,3,1,2
8,1,1,4,1,2
9,1,1,1,2,3
10,2,1,2,2,3
11,2,1,3,2,3
12,1,1,4,2,3
13,1,1,1,3,4
14,2,1,2,3,4
15,2,1,3,3,4
16,1,1,4,3,4
17,3,1,1,4,5
18,4,1,2,4,5
19,4,1,3,4,5
20,3,1,4,4,5
21,3,1,1,5,6
22,4,1,2,5,6
23,4,1,3,5,6
24,3,1,4,5,6
25,5,1,1,6,7
26,6,1,2,6,7
27,6,1,3,6,7
28,5,1,4,6,7
29,5,1,1,7,8
30,6,1,2,7,8
31,6,1,3,7,8
32,5,1,4,7,8
33,5,1,1,8,9
34,6,1,2,8,9
35,6,1,3,8,9

36,5,1,4,8,9
37,5,1,1,9,10
38,6,1,2,9,10
39,6,1,3,9,10
40,5,1,4,9,10
41,5,1,1,10,11
42,6,1,2,10,11
43,6,1,3,10,11
44,5,1,4,10,11
45,5,1,1,11,12
46,6,1,2,11,12
47,6,1,3,11,12
48,5,1,4,11,12
Beam Connectivity
1,1,1,1,1,2
2,1,1,1,2,3
3,1,1,1,3,4
4,1,2,1,1,2
5,1,2,1,2,3
6,1,2,1,3,4
7,1,3,1,1,2
8,1,3,1,2,3
9,1,3,1,3,4
10,1,4,1,1,2
11,1,4,1,2,3
12,1,4,1,3,4
13,1,5,1,1,2
14,1,5,1,2,3
15,1,5,1,3,4
16,1,6,1,1,2
17,1,6,1,2,3
18,1,6,1,3,4
19,1,7,1,1,2

20,1,7,1,2,3

21,1,7,1,3,4

22,1,8,1,1,2

23,1,8,1,2,3

24,1,8,1,3,4

25,1,9,1,1,2

26,1,9,1,2,3

27,1,9,1,3,4

28,1,10,1,1,2

29,1,10,1,2,3

30,1,10,1,3,4

31,1,11,1,1,2

32,1,11,1,2,3

33,1,11,1,3,4

34,1,12,1,1,2

35,1,12,1,2,3

36,1,12,1,3,4

VS Brace Connectivity

1,1,1,1,1,0,3,2,8327

2,1,1,1,2,1,2,3,8327

3,1,1,1,3,2,3,2,8327

4,1,1,1,4,3,2,3,8327

5,1,1,1,5,4,3,2,8327

6,1,1,1,6,5,2,3,8327

7,1,1,1,7,6,3,2,8327

8,1,1,1,8,7,2,3,8327

9,1,1,1,9,8,3,2,8327

10,1,1,1,10,9,2,3,8327

11,1,1,1,11,10,3,2,8327

12,1,1,1,12,11,2,3,8327

Type of Analysis

3

Static loads

0,0,0,0

Dynamic Analysis Control Data

0.37337, 0.0,0.005,30,10,3

Wave data

0,3000,0.01

Synthetic Earthquakes

acc85.dat

Output options

0

0 0 0 0 0

APPENDIX C: MATLAB CODES

C.1. Time History Generation Code

% First Part

```
% Earthquake Acceleration Generation Code for Time History Analysis
% 240 Artificially Generated Accelerations Based on Response Spectrum between 0&1
% PGA
function Timehistory(nofth,seconds)
% Time history generation function for 240 time histories required between 0 and 1 pga.
% Seconds: Duration of the time history (the time interval is taken as 0.01 seconds)
% nofth: Number of Time Histories needed to be generated
damp=0.05;
wu=15*2*pi;
N=512;
dw=wu/N;
seconds=30;
dt=0.01;
t=0:dt:seconds;
n=1:1:N;
w=dw.*n;
nofth=240;
if nargin<1;
  nofth=-1;
end
%Determination of target peak ground accelerations
accdiff=1/(nofth-1);
for i=1:nofth
   if i==1; pga(i)=0.00001;
   elseif i==2; pga(i)=pga(i-1)+accdiff-0.00001;
   else pga(i)=pga(i-1)+accdiff;
```

```
  end
end;

f(1:length(t))=0;
for thno=1:nofth;
clear f;
filename=['Acc',num2str(thno),'.dat'];
[f,SRS]=timehistforpga(pga(thno),damp,w,seconds,thno);

 %In order to decrease the effect of random phase angles, the number of iterations are
%decreased and the time history satisfies the convergence limit (at most five tries) from
%these are selected.

if abs(max(abs(f))-pga(thno))<=0.05;
disp(['Generation is within the limits']);
else [f,SRS]=timehistforpga(pga(thno),damp,w,seconds,thno);
   if abs(max(abs(f))-pga(thno))<=0.05;
     disp(['Generation is within the limits']);
   else [f,SRS]=timehistforpga(pga(thno),damp,w,seconds,thno);
       if  abs(max(abs(f))-pga(thno))<=0.05;
          disp(['Generation is within the limits']);
       else [f,SRS]=timehistforpga(pga(thno),damp,w,seconds,thno);
           if  abs(max(abs(f))-pga(thno))<=0.05;
              disp(['Generation is within the limits']);
           else [f,SRS]=timehistforpga(pga(thno),damp,w,seconds,thno);
               if  abs(max(abs(f))-pga(thno))<=0.05;
                  disp(['Generation is within the limits']);
               else disp(['PGA Obtained: ',num2str(max(abs(f))),' g']);
                  save(filename,'f','-ascii'); disp(['Error']);
             end;
          end;
       end;
   end;
```

```
end;
end;
```

%Second Part

```
%Time History Earthquake Acceleration Generation Code Accelerations based on
%Response Spectrum are generated.

function [f,SRS,a] = timehistforpga(pga,damp,w,seconds,thno)
filename=['Acc',num2str(thno),'.dat'];
[M,N]=size(w);
dw=w(1,N)./N;
phase=rand(1,N)*2*pi;
dt=0.01;
t=0:dt:seconds;
f(1:length(t))=0;

% Modulating Function
t1=1.5;
t2=8.5;
c=0.18;

for i=1:length(t);
   if t(i)<t1
      MOD(i)=(t(i)/t1)^2;
   elseif t(i)<=t2
      MOD(i)=1;
   else
      MOD(i)=exp(-c*(t(i)-t2));
   end
end

 % Elastic Response Spectra
```

```
T1=0.15;
T2=0.40;
r=2.5;

T=[(2*pi)./w];
TRS=zeros(1,length(T));

for i=1:length(T);
   if T(i)<=T1;
      TRS(1,i)=pga + ((pga*(r-1)/T1)*T(i));
   elseif T(i)>=T1 & T(i)<=T2;
      TRS(1,i)=pga*r;
   else
      TRS(1,i)=(pga*r)*((T2/T(i))^(0.8));
   end
end

psdfconstant=(pga*10)^2/4/dw/(N^2);

psdf(1:(N))=psdfconstant;
A=(2.*psdf.*dw).^0.5;

 %The iteration is limited to eight, and at each iteration the spectral density function
 %is smoothed by a rectangular 9 point window. The loop provides 8 iterations, the first
 %one is the original time history.

for iteration=1:(7+1);

      clear f;
      f(1:length(t))=0;
      for i=1:1:(N);
      f=f+A(i).*cos(w(i).*t+phase(1,i));
      end;
```

```
        f=(2^0.5).*f;
        f=f.*MOD;

        for i=1:length(w);
           a=[0 1;-w(i)^2 -2*w(i)*damp];
           b=[0;-1];
           c=[-w(i)^2 -2*w(i)*damp];
           d=[0];
           cs=ss(a,b,c,d);
           ds=c2d(cs,dt);
           y=lsim(ds,f);
           SRS(i)=max(abs(y));
        end;

 %Upgrading Power Spectral Density Matrix
psdf=psdf.*((TRS./SRS).^2);

% Smoothing power spectral density function at each iteration with a 9 point window
if iteration==1
psdf=smoothts(psdf,'g',9);
end;
A=(2.*psdf.*dw).^0.5;

end ;

f=f';
if abs(max(abs(f))-pga)<=0.05
      disp(['PGA Obtained: ',num2str(max(abs(f))),' g']);
      save(filename,'f','-ascii');
end;
```

C.2. Fragility Curve Generation Code

```
%The results of the time history analysis, and damage limits obtained from the results
%of the pushover analysis are used in the construction of Fragility Curves.

clear all;
close all;
filepga=['pga.dat'];
pga=load(filepga);
filedisp=['disp.dat'];
disp=load(filedisp);
[m,n]=size(pga);

for i=1:m
   if disp(i,1)<=12.79
     slight(i,2)=disp(i,1);
     slight(i,1)=pga(i,1);
     else if disp(i,1)<=23.24
         moderate(i,2)=disp(i,1);
         moderate(i,1)=pga(i,1);
         else if disp(i,1)<=37.73
                major(i,2)=disp(i,1);
                major(i,1)=pga(i,1);
                else if disp(i,1)>37.73
                   collapse(i,2)=disp(i,1);
                   collapse(i,1)=pga(i,1);
                end;
             end;
         end;
      end;
   end;
```

```
[t,z]=size(slight);
j=1;
for i=1:t;
   if slight(i,1)>0;
      for k=1:j
         slightson(j,2)=0;
         slightson(j,1)=0;
         if k==1 & slightson(1,1)==0
         slightson(1,1)=slight(i,1);
         slightson(1,2)=slight(i,2);
         else
         slightson(j,1)=slight(i,1);
         slightson(j,2)=slight(i,2);
      end;
     end;
     j=j+1;
   end;
end;


[t,z]=size(moderate);
j=1;
for i=1:t;
   if moderate(i,1)>0;
      for k=1:j
         moderateson(j,2)=0;
         moderateson(j,1)=0;
         if k==1 & moderateson(1,1)==0
         moderateson(1,1)=moderate(i,1);
         moderateson(1,2)=moderate(i,2);
         else
         moderateson(j,1)=moderate(i,1);
```

```
        moderateson(j,2)=moderate(i,2);
      end;
     end;
     j=j+1;
   end;
end;


[t,z]=size(major);
j=1;
for i=1:t;
   if major(i,1)>0;
     for k=1:j
        majorson(j,2)=0;
        majorson(j,1)=0;
        if k==1 & majorson(1,1)==0
        majorson(1,1)=major(i,1);
        majorson(1,2)=major(i,2);
        else
        majorson(j,1)=major(i,1);
        majorson(j,2)=major(i,2);
      end;
     end;
     j=j+1;
   end;
end;


[t,z]=size(collapse);
j=1;
for i=1:t;
   if collapse(i,1)>0;
     for k=1:j
```

```
        collapseson(j,2)=0;
        collapseson(j,1)=0;
        if k==1 & collapseson(1,1)==0
        collapseson(1,1)=collapse(i,1);
        collapseson(1,2)=collapse(i,2);
        else
        collapseson(j,1)=collapse(i,1);
        collapseson(j,2)=collapse(i,2);
      end;
     end;
     j=j+1;
   end;
end;

[MUslight,SIGMAslight,mucislight,sigmacislight] = normfit(slightson(:,1));
[MUmoderate,SIGMAmoderate,mucimoderat,sigmacmoderat]=normfit(moderateson(:,1));
[MUmajor,SIGMAmajor,mucimajor,sigmacimajor] = normfit(majorson(:,1));
[MUcollapse,SIGMAcollapse,mucicollapse,sigmacicollapse] = normfit(collapseson(:,1));

x=0.00000001:0.001:1;

yslightex = normcdf(log(x), log(MUslight), SIGMAslight);
ymoderateex = normcdf(log(x), log(MUmoderate), SIGMAmoderate);
ymajorex = normcdf(log(x), log(MUmajor), SIGMAmajor);
ycollapseex = normcdf(log(x), log(MUcollapse), SIGMAcollapse);

figure;
plot (x,yslightex,'k-',x,ymoderateex,'k:',x,ymajorex,'k-.',x, ycollapseex,'k--');
legend ('slight','moderate','major','collapse',4);
title ('Fragility Curves of Existing Building');
xlabel (' PGA (g) ');
ylabel (' Probability of Exceeding Damage ');
```

REFERENCES

ABYYHY, 1975, *Specification for Structures to be Built in Disaster Areas,* Ministry of Public Works and Settlement, Ankara.

ABYYHY, 1998, *Specification for Structures to be Built in Disaster Areas,* Ministry of Public Works and Settlement, Ankara.

Aki, K. and P. Richards, 1980, *Quantitative Seismology: Theory and Methods*, *Volume I, II*, W. H. Freeman and Company, San Francisco.

Aki, K., 1968, "Seismic Displacements Near a Fault," *Journal of Geophysical Research*, Vol. 73, No. 6, pp. 5359-5376.

Aleskerov, F., A. İ. Say, A. Toker, H. L. Akin and G. Altay, 2005, "Cluster Based Decision Support System for Estimating Earthquake Damage and Causalities", *Disasters,* Vol. 29, No. 3, pp. 255-276.

ATC 13, 1985, *Earthquake Damage Evaluation Data for California, Palo Alto*, Applied Technology Council, Redwood City, California.

ATC 40, 1996, *Seismic Evaluation and Retrofit of Concrete Buildings,* Applied Technology Council, Redwood City, California.

Atkinson, G. and P. Somerville, 1994, "Calibration of Time History Simulation Methods," *Bulletin of Seismological Society of America*, Vol. 84, pp. 400-414.

Beresnev, I. A. and G. M. Atkinson, 1997, "Modelling Finite-Fault Radiation From the W_n Spectrum," *Bulletin of Seismological Society of America*, Vol. 87, No. 1, pp. 67-84.

Bolt, B. A., 1995, "Intraplate Seismicity and Zonation," *Proceedings of the Fifth Pacific Conference on Earthquake Engineering*, Melbourne, Australia, pp. 1-11.

Bracci, J. M., A. M. Reinhorn and J. B. Mander, 1992a, *Seismic Resistance of Reinforced Concrete Frame Structures Designed only for Gravity Loads: Part I - Design and Properties of One-Third Scale Model Structure*, Technical Report: NCEER 92-0027, State University of New York at Buffalo, NY.

Bracci, J. M., A. M. Reinhorn and J. B. Mander, 1992b, *Seismic Resistance of Reinforced Concrete Frame Structures Designed only for Gravity Loads: Part II – Experimental Performance and Analytical Study of Structural Model*, Technical Report: NCEER 92-0029, State University of New York at Buffalo, NY.

Bracci, J. M., A. M. Reinhorn and J. B. Mander, 1992c, *Seismic Resistance of Reinforced Concrete Frame Structures Designed only for Gravity Loads: Part III – Experimental Performance and Analytical Study of Retrofitted Model Structure*, Technical Report: NCEER 92-0031, State University of New York at Buffalo, NY.

Bracewell, R. N., 1986, *The Fourier Transform and Its Applications*, McGraw-Hill, New York.

Bruno, S. and C. Valente, 2002, "Comparative Response Analysis of Conventional and Innovative Seismic Protection Strategies", *Earthquake Engineering and Structural Dynamics*; Vol. 31, No. 5, pp. 1067–1092.

Butterworth, J. W., 1999, "Seismic Damage Limitation in Steel Frames Using Friction Energy Dissipators", *Sixth International Conference on Steel and Space Structures*, Singapore.

Choi, E., 2002, *Seismic analysis and retrofit of mid-America bridges*, Ph.D. Dissertation, Georgia Institute of Technology.

Choi, E., R. DesRoches and B. Nielson, 2004, "Seismic Fragility of Typical Bridges in Moderate Seismic Zones", *Engineering Structures,* Vol. 26, No. 2, pp. 187-199.

Chopra, A. K., 2000, *Dynamics of Structures*, Prentice-Hall, New Jersey.

Christis, Z. and T. D. M. P. A. S Chrysostomou, 2005, "Retrofit of a Church with Linear Viscous Dampers", *Structural Control and Health Monitoring*, Vol. 12, No. 2, pp. 197-212.

Constantinou, M. C. and M. D. Symans, 1992, *Experimental and Analytical Investigation of Seismic Response of Structures with Supplemental Fluid Viscous Dampers*, Technical Report: NCEER-92-0032, National Center for Earthquake Engineering Research, Buffalo, NY.

Cornell, C. A. and H. Krawinkler, 2000, "Progress and Challenges in Seismic Performance Assessment", *PEER Center News*, Vol. 4, No. 1, pp.1-3.

Deodatis, G., 1996, "Non-Stationary Stochastic Vector Processes: Seismic Ground motion Applications", *Probabilistic Engineering Mechanics*, Vol. 11, No. 3, pp.149-167.

Dumova-Jovanoska, E., 2000, "Fragility Curves For Reinforced Concrete Structures in Skopje (Macedonia) Regions", *Soil Dynamics and Earthquake Engineering,* Vol. 19, No. 6, pp. 455–466.

Elenas, A. and K. Meskouris, 2001, "Correlation Study Between Seismic Acceleration Parameters and Damage Indices of Structures", Engineering Structures, Vol. 23, pp.698-704.

Elnashai, A. and R. Pinho, 1998, "Repair and Retrofitting of RC Walls Using Selective Techniques", *Journal of Earthquake Engineering,* Vol. 2, No. 4, pp. 525–568.

Elnashai, A., B. Borzi and S. Vlachos, 2004, "Deformation-Based Vulnerability Functions for RC Bridges", *Structural Engineering and Mechanics*; Vol. 17, No. 2, pp. 215-244.

Erberik, M. A. and A. Elnashai, 2004, "Fragility Analysis of Flat-Slab Structures", *Engineering Structures*, Vol. 26, No. 7, pp. 937-948.

Erdik, M. and N. Aydınoğlu, 2002, *Earthquake Performance and Vulnerability of Buildings in Turkey*, The World Bank Group Disaster Management Facility.

FEMA 154, 1988, *Rapid Visual Screening of Buildings for Potential Seismic Hazards: A Handbook*, Federal Emergency Management Agency, Washington, D.C.

FEMA 227, 1992, *A Benefit-Cost Model For The Seismic Rehabilitation of Buildings: Volume 1*, Federal Emergency Management Agency, Washington, D.C.

FEMA 228, 1992, *A Benefit-Cost Model For The Seismic Rehabilitation of Buildings: Volume 2*, Federal Emergency Management Agency, Washington, D.C.

FEMA 273, 1997, *Guidelines for Seismic Rehabilitation of Buildings*, Federal Emergency Management Agency, Washington, D.C.

FEMA 274, 1997, *Commentary on the Guidelines for the Seismic Rehabilitation of Buildings,* Federal Emergency Management Agency, Washington, D.C.

FEMA 310, 1998, *Handbook for the Seismic Evaluation of Buildings—A Prestandard*, Federal Emergency Management Agency, Washington, D.C.

Ghobarah, A., M. El-Attar and N. M. Aly, 2000, "Evaluation of Retrofit Strategies for Reinforced Concrete Columns: A Case Study", *Engineering Structures*, Vol. 22, No. 5, pp. 490-501.

Grigoriu, M., 1995, *Applied Non-Gaussian Processes*, Prentice Hall, New Jersey.

Güneyisi, E. M. and G. Altay, 2005, "A Study on the Seismic Behavior of a Retrofitted Building Based on Nonlinear Static and Dynamic Analyses", *Earthquake Engineering and Engineering Vibration*, Vol. 4, No. 1, pp. 173-180.

HAZUS, 1997, *Earthquake loss estimation methodology-Technical Manual*, Federal Emergency Management Agency, Washington, D.C.

Hubert-Ferrari, A., A. A Barka, E. Jacques, S. S. Nalbant, B. Meyer, R. Armijo, P. Tapponnier and G. C. P. King, 2000, Seismic Hazard in The Marmara Sea Region Following the 17 August 1999 İzmit Earthquake, *Nature,* Vol. 404, No. 6775, pp. 269–273.

Hwang, H., J. B. Jernigan and Y. W. Lin, 2000, "Evaluation of Seismic Damage to Memphis Bridges and Highway Systems", *Journal of Bridge Engineering*, Vol. 5, No. 4, pp. 322-330.

Irikura, K. and K. Kamae, 1994, "Simulation of Strong Ground Motion Based On Fractal Composite Faulting Model and Empirical Green's Function," *Proceedings of the 9th Japan Earthquake Engineering Symposium*, Tokyo.

Jennings, P. C., G. W. Housner and N. C. Tsai, 1968, *Simulated Earthquake Motions*, Technical Report, Earthquake Engineering Laboratory, California Institute of Technology.

JICA, 2002, *The Study on A Disaster Prevention / Mitigation Basic Plan in Istanbul including Seismic Microzonation in the Republic of Turkey*, Japan International Cooperation Agency and Istanbul Metropolitan Municipality.

Karim, K. R. and F. Yamazaki, 2000, "Comparison of Empirical and Analytical Fragility Curves for RC Bridge Piers in Japan" *Proceedings of eight ASCE Speciality Conference on Probabilistic Mechanics and Structural Reliability*; Notre Dame, Indiana, pp.205–212.

Karim, K. R. and F. Yamazaki, 2001, "Effect of Earthquake Ground Motions on Fragility Curves of Highway Bridge Piers Based on Numerical Simulation", *Earthquake Engineering and Structural Dynamics*, Vol. 30, No. 12, pp. 1839–1856.

Karim, K. R. and F. Yamazaki, 2003, "A Simplified Method of Constructing Fragility Curves for Highway Bridges", *Earthquake Engineering Structural Dynamics,* Vol. 32, No. 10, pp. 1603–1626.

Keech, W., S. Hoffer, C. Timmerman, and F. Beradino, 1998, *Economic Values of Federal Aviation Administration Investment and Regulatory Programs*, Office of Aviation Policy and Plans, Federal Aviation Administration, Washington, D.C.

Kircher, C. A., A. A. Nassar, O. Kustu and W. T. Holmes, 1997, "Development of Building Damage Functions for Earthquake Loss Estimation", *Earthquake Spectra*, Vol. 13, No. 4, pp. 663–680.

Kırçıl, M. S: and Z. Polat, 2006, "Fragility Analysis of Mid-Rise R/C Frame Buildings", *Engineering Structures*, Vol. 28, No. 9, pp.1135-1345.

Kunnath, S. K., A. M. Reinhorn and R. F. Lobo, 1992, *IDARC Version 3.0: A Program for the Inelastic Damage Analysis of Reinforced Concrete Structures*, Technical Report: NCEER 92-0022, State University of New York at Buffalo, NY.

Lee, D. and D. P. Taylor, 2001, "Viscous Damper Development and Future Trends", *The Structural Design of Tall Buildings,* Vol. 10, No. 5, pp. 311-320.

Li, C. and A. M. Reinhorn, 1995, *Experimental and Analytical Investigation of Seismic Retrofit with Supplemental Damping, PART II: Friction Devices*, Technical Report: NCEER-95-0009, State University of New York at Buffalo, NY.

Mackie, K. and B. Stojadinovic, 2004, "Fragility Curves for Reinforced Concrete Highway Overpass Bridges" *Proceedings of 13th World Conference on Earthquake Engineering*, Vancouver, B.C., Canada.

Mander, J. B. and N. Basoz, 1999, "Seismic Fragility Curve Theory for Highway Bridges", *Proceedings of 5th US Conference on Lifeline Earthquake Engineering*, New York, Vol. 16, pp. 31–40.

Martinez-Rodrigo, M. and M. L. Romero, 2003, "An Optimum Retrofit Strategy for Moment Resisting Frames With Nonlinear Viscous Dampers for Seismic Applications", *Engineering Structures,* Vol. 25, No. 7, pp. 913-925.

Moayyad, P. and B. Mohraz, 1982, *A study of Power Spectral Density of Earthquake Accelograms*, Research Report, Civil and Mechanical Engineering Department, Southern Methodist University.

Mosalam, K. M., G. Ayala, R. N. White and C. Roth, 1997, "Seismic Fragility of LRC Frames With and Without Masonry Infill Walls", *Journal of Earthquake Engineering,* Vol. 1, No. 4, pp. 693–719.

Orsini, G. A, 1999, "Model for Buildings' Vulnerability Assessment Using the Parameterless Scale of Seismic Intensity (PSI)", *Earthquake Spectra*, Vol. 15, No. 3, pp. 463–483.

Parsons, T., S. Toda, R. S. Stein, A. A. Barka, and J. H. Dieterich, 2000, "Heightened Odds of Large Earthquakes near Istanbul: An Interaction-Based Probability Calculation", *Science,* Vol. 288, No. 5466, pp. 661–665.

Perera, R., S. Gomez and E. Alarcon, 2004, "Experimental and Analytical Study of Masonry Infill Reinforced Concrete Frames Retrofitted with Steel Braces", *Journal of Structural Engineering*, Vol. 130, No. 12, pp.2032-2039.

Pincheira, J. A. and J. O. Jirsa, 1995, "Seismic Response of RC Frames Retrofitted with Steel Braces or Walls", *Journal of Structural Engineering*, Vol. 121, No. 8, pp. 1225–1235.

Priestley, M. J. N., 1998, "Displacement-Based Approaches to Rational Limit States Design of New Structures", *Proceedings of the 11th European Conference on Earthquake Engineering*, Rotterdam, AA Balkema.

Reinhorn, A. M., C. Li and M. Constantinou, 1995, *Experimental and Analytical Investigation of Seismic Retrofit with Supplemental Damping, PART I: Fluid Viscous Damping Devices*, Technical Report: NCEER-95-0001, State University of New York at Buffalo, NY.

Reinhorn, A. M., R. E. Valles, S. K. Kunnath, A. Madan, Y. Reichmen, A. Vladesscu, C. Li and C. Özer, 2006, *IDARC 2D version 6.1: Users Manual*, State University of New York at Buffalo, Buffalo, NY.

Rosetto, T. and A. S. Elnashai, 2003, "Derivation of Vulnerability Functions for European-Type RC Structures Based on Observational Data", *Engineering Structures*, Vol. 25, No.10, pp. 1241-1263.

Sarı, A., 2003, *Energy Considerations in Ground Motion Attenuation and Probabilistic Seismic Hazard Studies*, Ph.D. Dissertation, The University of Texas at Austin.

Saxena, V., G. Deodatis, M. Shinozuka and M. Q. Feng, 2000, "Development of Fragility Curves for Multi-Span Reinforced Concrete Bridges", *Proceedings of International Conference on Monte Carlo Simulation*, pp. 499–504.

Shinozuka, M. and C. Jan, 1972, "Digital Simulation of Random Processes and Its Applications," *Journal of Sound and Vibration*, Vol. 25, pp. 111–128.

Shinozuka, M. and G. Deodatis, 1991, "Simulation of Stochastic Processes by Spectral Representation", *Applied Mechanics Review*, Vol. 44, No. 4, pp. 191-204.

Shinozuka, M. and J. N. Yang, 1971, "Peak Structural Response to Non-stationary Random Excitations," *Journal of Sound and Vibration,* Vol. 16, pp. 505–517.

Shinozuka, M., M. Q. Feng, H. K. Kim and S. H. Kim, 2000a, "Nonlinear Static Procedure for Fragility Curve Development", *Journal of Engineering Mechanics*, Vol. 126, No. 12, pp. 1287–1295.

Shinozuka, M., M. Q. Feng, J. Lee and T. Naganuma, 2000b, "Statistical Analysis Of Fragility Curves", *Journal of Engineering Mechanics,* Vol. 126, No. 12, pp. 1224–1231.

Singhal, A. and A. S. Kiremidjian, 1997, *A Method For Earthquake Motion Damage Relationships with Application To Reinforced Concrete Frames,* Technical Report: NCEER-97-0008, National Center for Earthquake Engineering Research, Buffalo, NY.

Smyth, A., G. Altay, G. Deodatis, M. Erdik, G. Franco, P. Gülkan, H. Kunreuther, H. Luş, E. Mete, N. Seeber and O. Yüzügüllü, 2004, "Probabilistic Benefit-Cost Analysis for Earthquake Damage Mitigation: Evaluating Measures for Apartment Houses in Turkey", *Earthquake Spectra,* Vol. 20, No. 1, pp. 171–203.

Soong, T. T. and G. F. Dargush, 1997, *Passive Energy Dissipation Systems in Structural Engineering*, John Wiley & Sons, Chichester.

Soong, T. T. and M. Grigoriu, 1993, *Random Vibration of Mechanical and Structural Systems*, Prentice-Hall, New Jersey.

Sues, R. H., Y. K. Wen and A. H. S. Ang, 1985, "Stochastic Evaluation of Seismic Structural Performance", *Journal of Structural Engineering*, Vol. 111, No. 6, pp. 1204–1218.

TS 498, 1997, *Design Loads for Buildings*, Turkish Standards Institution, Ankara.

Uriz, P. and A. S. Whittaker, 2001, "Retrofit of Pre-Northridge Steel Moment-Resisting Frames Using Fluid Viscous Dampers", *The Structural Design of Tall Buildings,* Vol. 10, No. 5, pp. 371-390.

USGS, 2000, *Implication for earthquake risk reduction in the United States from the Kocaeli, Turkey, earthquake of August 17, 1999*, U.S. Geological Survey Circular, 1193, pp. 64.

Valles, R. E., A. M. Reinhorn, S. K. Kunnath, C. Li and A. Madan, 1996, *IDARC-2D Version 4.0: A Computer Program for the Inelastic Damage Analysis of Buildings*,

Technical Report: NCEER-96-0010, National Center for Earthquake Engineering Research, Buffalo, NY.

Vanmarcke, E. H., and P. S. Lai, 1980, "Strong Motion Duration and RMS Amplitude of Earthquake Records," *Bulletin of Seismological Society of America*, Vol. 70, No. 4, pp. 1293-1307.

Wen, Y. K. and Y. J. Kang, 2001, "Minimum Building Life-Cycle Cost Design Criteria, II: Applications", *Journal of Structural Engineering,* Vol. 127, No. 3, pp. 338-346.